AUS DEM ADOLF-BUTENANDT-INSTITUT, LEHRSTUHL: MOLEKULARBIOLOGIE IM BIOMEDIZINISCHEN CENTRUM DER LMU
VORSTAND: PROF. DR. PETER BECKER

STAGE-SPECIFIC HISTONE MODIFICATION PROFILES ARE SHAPED BY MITOTIC ACTIVITY DURING *XENOPUS* DEVELOPMENT

DISSERTATION ZUM ERWERB DES DOKTORGRADES DER NATURWISSENSCHAFTEN AN DER MEDIZINISCHEN FAKULTÄT DER LUDWIG-MAXIMILIANS-UNIVERSITÄT ZU MÜNCHEN

vorgelegt von Daniil Pokrovskii
aus Sankt-Petersburg, Russland
2019

Mit Genehmigung der Medizinischen Fakultät der Universität München

Betreuer: Prof. Dr. Ralph A.W. Rupp

Zweitgutachter: Prof. Dr. André Brändli

Dekan: Prof. Dr. med. dent. Reinhard Hickel

Tag der mündlichen Prüfung: 09.07.2019

EIDESSTATTLICHE VERSICHERUNG

Pokrovskii, Daniil

Ich erkläre hiermit an Eides statt, dass ich die vorliegende Dissertation mit dem Thema:

Stage-specific histone modification profiles are shaped by mitotic activity during *Xenopus* development

selbständig verfasst, mich außer der angegebenen keiner weiteren Hilfsmittel bedient und alle Erkenntnisse, die aus dem Schrifttum ganz oder annähernd übernommen sind, als solche kenntlich gemacht und nach ihrer Herkunft unter Bezeichnung der Fundstelle einzeln nachgewiesen habe.

Ich erkläre des Weiteren, dass die hier vorgelegte Dissertation nicht in gleicher oder in ähnlicher Form bei einer anderen Stelle zur Erlangung eines akademischen Grades eingereicht wurde.

Munich, 26.03.2019

Daniil Pokrovskii

Ort, Datum Unterschrift
Doktorandin/Doktorand

Eidesstattliche Versicherung Stand: 31.01.2013

Contents

Zusammenfassung

Die Embryonalentwicklung von Wirbeltieren ist ein komplexer Prozess, bei dem mehrere Regulationsebenen zeitlich und räumlich zusammenarbeiten müssen. Epigenetische Merkmale wie die kovalenten Modifikationen von Histonproteinen auf dem chromosomalen Chromatin liefern dabei einen wichtigen Beitrag zur Genregulation, deren Dynamik und Bedeutung für das Entwicklungsgeschehen wir gegenwärtig nur ansatzweise verstehen. Der allgemeine Antagonismus von Zellproliferation und Zelldifferenzierung veranschaulicht die Bedeutung einer zweiten regulatorischen Ebene - der entwicklungsspezifischen Kontrolle des Zellzyklusgeschehens. In dieser Arbeit habe ich ein mögliches Zusammenspiel dieser beiden Regulationsebenen während der Embryonalentwicklung von *X. laevis* untersucht. Dazu wurden Embryonen im Gastrulastadium einem systemischen Zellzyklusblock unterworfen und ihre Entwicklung bis zum Kaulquappenstadium verfolgt. Die Auswirkungen des Zellzyklus-Arrests wurden sowohl morphologisch als auch hinsichtlich regionaler Genexpressions-muster analysiert. Um Informationen über die mit der Behandlung einhergehenden Veränderungen im embryonalen Chromatin zu erhalten, wurde eine Massenspektrometrie-Pipeline erfolgreich etabliert und zur Quantifizierung der Histonmodifikationen verwendet, die zu vier wichtigen Entwicklungsstadien aus embryonalem Chromatin extrahiert wurden.

Die Ergebnisse dieser Arbeit zeigen, dass ein systemischer Zellzyklusblock am G1/S-Phasenübergang ab dem Stadium der Gastrula grundsätzlich mit dem Überleben des Embryos und der morphologischen Differenzierung vereinbar ist, obwohl unter diesen Bedingungen einige Organe und Gewebe nicht gebildet werden können. Die nichtproliferierenden Embryonen weisen zudem eine epigenetische Fehlentwicklung auf, deren Merkmale sich in selektiven Veränderungen der stadienspezifischen Histonmodifikationsprofile widerspiegeln. Insbesondere sind transkriptionell repressiv wirkende Histonmodifikationen im Zellzyklus-arretierten Chromatin gegenüber Kontrollembryonen überrepräsentiert. Wie Embryonen belegen, die zum Zeitpunkt der Neurulation aus dem Zellzyklusblock wieder entlassen wurden, sind die auf morphologischer, molekularer und epigenetischer Ebene beobachteten Veränderungen prinzipiell revertierbar. Insgesamt zeigen diese Ergebnisse, dass die Etablierung und Aufrechterhaltung der stadienspezifischen Histonmodifikationsprofile vom Zellzyklus beeinflusst wird.

Summary

Vertebrate embryogenesis is a complex process, in which multiple regulatory layers have to cooperate in time and space. Epigenetic information, specifically the unfolding pattern of covalent posttranslational histone modifications, represents a major mechanism for gene regulation, whose impact on development is underinvestigated. The general antagonism of cell proliferation and differentiation illustrates the importance of another regulatory layer, i.e. the proper control of the cell cycle. In this work I have investigated a possible interplay between these two regulatory layers during *Xenopus* embryogenesis. To address this hypothesis, I have applied a systemic cell cycle block to Xenopus gastrula embryos and followed their development until the tadpole stage. Developmental consequences of the cell cycle arrest were analysed morphologically and molecularly. To obtain information on consequential changes in the embryonic epigenome, a mass spectrometry pipeline was successfully established and used to quantify histone post-translational modifications extracted from bulk chromatin at four key developmental stages.

The results of this work indicate that a systemic G1/S-phase arrest from the gastrula stage on is principally compatible with embryonic survival and morphological differentiation, although some organs and tissues cannot be formed under the cell cycle block. The arrested embryos develop a perturbed chromatin landscape, whose features are illustrated in abnormal stage-specific histone modification profiles. Transcriptionally repressive histone modifications are overrepresented in the chromatin of arrested embryos, compared to controls. Embryos released from the cell cycle block during neurulation revert towards normal-like on morphological, molecular and epigenetic levels. Altogether the results indicate that the cell cycle plays a role in establishment and maintenance of stage-specific histone modification profiles during *Xenopus* development.

Introduction

Epigenesis

While the genetic information is stored in DNA, making use of this information is invariably connected in eukaryotes to the functional organization of chromatin. The chromatin fiber itself is organized by nucleosomes, consisting of an octamer of histone proteins, around which 147 bp of the chromosomal DNA are wrapped in two turns (Kornberg, 1974, Luger *et al.*, 1997). This packaging regulates the accessibility of DNA in multiple ways, including low and higher order levels of folding, its intranuclear localization, nucleosomal positioning and phasing, and incorporation of histone variants (Hake and Allis, 2006, Van Steensel, 2011, Bickmore and van Steensel, 2013) and, most importantly in the context of this thesis, the existence of a plethora of covalent modifications attached to the core histone proteins themselves (Turner, 1993, Freitas *et al.*, 2004, Cosgrove, 2007, Kebede *et al.*, 2015). Epigenetic information is also stored on DNA in form of Cytosine methylation at CpG dinucleotides (Smith and Meissner, 2013). Although there is evidence for crosstalk between DNA methylation and chromatin (Cedar and Bergman, 2009, Castillo-Aguilera *et al.*, 2017), DNA methylation lies outside the experimental scope of this thesis and will not be reviewed further.

Some forty years after the initial finding of histone acetylation (Allfrey *et al.*, 1964) and of DNAse I hypersensitive sites, indicating specialized nucleosomal patterns associated with gene activity (Wu *et al.*, 1979, Stalder *et al.*, 1980), we have now a fairly detailed understanding, how important chromatin structure is for every aspect of DNA metabolism. Notably, the regulation of transcription, which is very often associated with specific cell types or differentiation states, depends on information provided by local chromatin cues. As of today, we know at least 6 amino acid residues on core nucleosome histones that can be modified by enzymes, called “writers” of potential epigenetic information. The activity of these enzymes is antagonized by other enzymes called “erasers”, which can remove these modifications. Their combined activities regulate the half-life and abundance of histone post-translational modifications (PTMs), which can vary extensively both locally and globally. Although the list is still growing, there are at least 14 different molecules/moieties that can be attached to specific amino acid residues (Sadakierska-Chudy and Filip, 2014). Most, but not all of them, are found on the exposed amino-terminal histone tail domains (Kebede *et al.*,

2015). Some of the more common modifications, in particular acetylation, methylation and phosphorylation (see below), have been studied in great detail and their regulatory quality is now firmly established, even though mechanistically it is not fully understood. Histone PTMs localize to specific chromosomal regions, are associated with hetero- or euchromatin, and some of them can be even enriched discretely on small regulatory regions such as enhancers and promoters, resulting in a chromatin landscapes rich in regulatory information (Lee and Mahadevan, 2009). This scenario has been predicted by the "Histone Code" hypothesis (Turner, 1993, Strahl and Allis, 2000), which postulates that nuclear proteins with specialized "reader" domains are binding to specific histone modifications and influence the outcome of DNA-based processes.

Through numerous studies on chromatin structure and the correlation between gene activity and local histone PTM decoration, it has become textbook knowledge that different cell types are functionally connotated with unique epigenome states to accommodate "multidimensional layers of DNA readout" (Allis *et al.*, 2006). This model connects the field of epigenetics with the central question in developmental biology: how does a single cell, i.e. the fertilized egg, turn into an adult organism with over 200 cell types? Vertebrate model systems, notably the African clawed frog *Xenopus*, have provided information on developmental programs, some of which have been conserved since the Urbilateria, the last common ancestors of flies, nematodes and humans. These programs use peptide growth factor signaling cascades to pattern the early embryo into domains of selective gene expression, ultimately leading to the formation of all necessary cell types, tissues and organs (Benazeraf and Pourquie, 2013, Drost *et al.*, 2017, De Robertis, 2008). These findings imply that the single epigenome of the zygote needs to become diversified in the course of development. For example, the chromatin of embryonic stem cells has to provide for the transcriptional competence that is needed for cell-type-specific gene induction during cell fate determination. At the same time, the cellular plasticity must be limited to maintain the acquired cell identities in differentiated cells (Waddington, 1957).

The remarkable stability of developmentally acquired epigenome states is revealed by the general resistance of cells against trans-differentiation. Even powerful systems, such as the trans-differentiation of fibroblasts to skeletal muscle by forced expression of myoD1, is no exception (Manandhar *et al.*, 2017). Finally, the full reprogramming of somatic cells to an

embryonic stem cell state (Takahashi and Yamanaka, 2006), first accomplished in 1962 in *X. laevis* (Gurdon, 1962), is notoriously incomplete. Induced pluripotent stem (iPS) cells are prone to maintain megabase-long chromosomal stretches, which retain either DNA or histone methylation marks of the original somatic epigenome (Doi *et al.*, 2009, Becker *et al.*, 2016, Hormanseder *et al.*, 2017). A deeper understanding of the mechanisms, controlling establishment and maintenance of epigenetic states during development, is therefore an important goal in biomedical research. Before introducing our current state of knowledge on epigenetic diversification, the following chapter will provide biochemical and functional information on important histone post-translational modifications.

Post-translational histone modifications

In the scope of this work we will be dealing exclusively with the most well studied histone modifications, i.e. methylation (m), acetylation (ac) and phosphorylation (Ph) on core histones H3 and H4. They can be typically found on side chains of Lysine (K), Arginine (R), Serine (S) and Threonine (T) amino acid residues. For technical reasons and its low abundance, Arginine methylation is ignored here, although it comes in different states and some biological functions have been reported (Di Lorenzo and Bedford, 2011). Nevertheless, the epigenetic complexity generated by the remaining modifications is enormous. This has to do with several facts. First, while only single acetate and phosphoryl groups can be added per residue, up to three methyl groups can be attached per Lysine side chain. As outlined below, mono-, di- or tri-methylated states occur in different functional contexts. Second, some positions on histone tails can be either acetylated or methylated. Finally, it has become obvious that histone modifications act in concert and they influence each other. Crosstalk between neighbouring amino acids has been reported, e.g. for phosphorylation of Ser10 or Ser28 with methylation of Lys9 and Lys27 of Histone H3, respectively. In total, this limited set of modification states accounts for a major part of the existing epigenetic information (Jenuwein and Allis, 2001).

Histone acetylation

Histone acetylation is catalyzed by a class of enzymes called histone acetyl-transferases (HATs). For transcription, acetylation is considered as a positive histone mark. As an acid, the DNA backbone is negatively charged, while the aminoterminal tail domains of the histone proteins are positively charged, allowing them to engage in stable, electrostatic interactions.

The acetylation of histone Lysines neutralizes the positive charge and therefore weakens the interaction between DNA and histones. This makes it easier to mobilize histone octamers, generate access to the DNA binding motifs of transcription factors, and to lift DNA off the nucleosome during transcription. The typical Lysine residues which become acetylated on the histone H3 are in positions K9, K14, K18, K23, K27. The histone H4 can carry acetylation also on the Lysine residues in position K5, K8, K12, K16. Regardless of the exact acetylated Lysine residue position on the histone, acetylation is associated with actively transcribed part of the DNA. Let us have a look at the biological connotations for histone acetylation.

On histone H3, acetyl marks are found at the amino acids K9, K14, K18, K23, and K27. H3K9ac is highly correlated with active promoters. H3K14ac is frequently found around transcription start sites (TSS) and facilitates efficient activation of nearby licensed replication origins in the S phase of cell cycle (Feng *et al.*, 2016). H3K9ac has a high co-occurrence with H3K14ac. These two marks are the hallmark of active gene promoters (Karmodiya *et al.*, 2012). When found together, the two modifications support binding of the general transcription factor TFIID, which is a subunit of the RNA polymerase II preinitiation complex (Agalioti *et al.*, 2002). In contrast, H3K18 is tightly involved in cell cycle regulation, cell proliferation and apoptosis. It also correlates with transcription activation. Hypoacetylation of H3K18 is considered to be essential for the maintenance of oncogenic transformation (Barber *et al.*, 2012). H3K27 is mostly famous for its methylated states, we will talk about this shortly. The acetylated version of H3K27 is associated with active transcription and may protect promoters from becoming decorated with repressive H3K27 trimethylation (Tie *et al.*, 2009). Additionally, H3K27ac defines active enhancers (Creyghton *et al.*, 2010).

On histone H4, Lysine residues in the positions K5, K8, K12 and K16 can be acetylated. Acetylation on these sites is involved in the regulation of the chromatin structure. For example, H4K16ac modification loosens chromatin compaction by interfering with interactions of adjacent nucleosomes, making the underlying DNA more accessible to transcription factors (Zhang *et al.*, 2017). Additionally, acetylated histone H4 is enriched on the male X chromosome in *D. melanogaster*. By this mechanism, male flies produce a transcriptional output that is comparable to the two X chromosomes found in female flies (Bone *et al.*, 1994).

Histone methylation

As mentioned above, methylation of core histones is more diverse than acetylation. Due to its biochemical features, it does not act through charge neutralization. Instead, it is recognized by reader proteins, which can discriminate between sites and numbers of methyl groups attached to histone tails. Overall, some specific methylation states upregulate transcription by either promoting the binding of positive transcription factors and/or interfering with the binding of repressors. Depending on the amount of methyl groups attached to Lysine residues (mono-, di- or tri-methylated) and its positions on the histones, it can be either active or repressive marks. Lysine methylation is written by the so-called histone methyltransferases (HMTs). The most functionally well understood methylated Lysine amino residues on the histone H3 are in positions K4, K9, K27, K36, K79. Histone H4 is famous for its Lysine residue in position K20 which is consecutively methylated be several HMTs in a cell cycle regulated manner. Let us have a look at the functions associated with the methylated states of specific Lysine residues.

Methylation of the Lysine in position K4 of histone H3 is considered to be an active mark, regardless of how many methyl groups are attached to it. In general, K4 methylation is tightly associated with the promoters of active genes. However, mono-, di-, or tri-methylated states of H3K4 have slightly different chromosomal distributions. H3K4me3 is associated with the transcriptional start site (TSS) of actively transcribed genes (Barski *et al.*, 2007). It is a good example to consider how methylation contributes to active transcription. H3K4me3 recruits the chromatin remodeling factors CHD1 (Flanagan *et al.*, 2005) and BPTF (Li *et al.*, 2006), which open chromatin, while preventing the binding of the repressive protein complexes NuRD (Nishioka *et al.*, 2002) and INHAT (Schneider *et al.*, 2004). A very interesting case of chromatin-mediated gene control is represented by so-called “bivalent domains”, where a TSS carries both H3K4me3 (active) and H3K27me3 (repressive) marks, often at important developmental genes (Bernstein *et al.*, 2006). Bivalent domains are believed to play a role in keeping promoters of developmental genes inactive, yet “poised” to be transcribed when the time comes (Voigt *et al.*, 2013). In fact, H3K4 methylation happens to be important in development, because H3K4 HMTs were initially identified as regulators of *Hox* genes. A group of proteins called Trithorax which specifically methylate H3K4 along the *Hox* gene bodies, inducing gene activation by trimethylation of H3K4. This modification attracts

chromatin remodelers which activate transcription and prevent binding of repressive complexes, in particular from the Polycomb group (Schuettengruber *et al.*, 2017).

The other well-known methylation happens on Lysine 9 on histone H3. As discussed before, H3K9 acetylation invariably stimulates transcription, however, methylated K9 can either activate or silence genes. As with other methylation states, mono-, di-, and tri-methylations of H3K9 have distinct distributions. Monomethylated H3K9 is found enriched at the TSS of active genes, while H3K9m2 and H3K9m3 are found enriched on silenced genes (Barski *et al.*, 2007). H3K9me2 is a characteristic mark of the inactivated X chromosome (Xi) (Rougeulle *et al.*, 2004). H3K9m3 binds heterochromatin protein 1 (HP1) and is considered the main constitutive heterochromatin mark (Lehnertz *et al.*, 2003). This chromatin is full of repetitive regions which have to be silenced. Otherwise transcription of them can give rise to transposable elements (TE or transposons), which are DNA sequences that can change its position within a genome, sometimes creating or reversing mutations and altering the cell's genetic identity and genome size (Bourque *et al.*, 2018, Saksouk *et al.*, 2015).

The Lysine in position 27 of H3 is best known in its trimethylated state, which is associated with inactive gene promoters and thought to shut down transcription (Wang *et al.*, 2018). Most methylated histone sites are served by more than one enzyme. H3K27me3 is unique in this sense, because it has only one known methyltransferase. The Polycomb repressive complex 2 (PRC2) methylates K27 via its catalytic subunit EZH2 (Kuzmichev *et al.*, 2002, Schuettengruber *et al.*, 2017). The PRC2 complex was initially discovered as a repressor of *Hox* genes, acting in an antagonistic fashion to gene products of the Trithorax group. It is responsible for the repression of many genes involved in development and cell differentiation and therefore acts in opposition to H3K4me3 (Boyer *et al.*, 2006, Bracken *et al.*, 2006). H3K27m3 is also an important mark of the inactive X chromosome (Xi) (Rougeulle *et al.*, 2004). The mono- and di-methylation states of K27 are less studied. H3K27m2 shows a similar distribution to H3K27m3, while H3K27m1 is associated with active promoters and positively affects transcription (Barski *et al.*, 2007). Their role remains a bit elusive. Recently it has been shown that H3K27m1 positively affects transcription, while H3K27m2 has a broad distribution and a role in silencing of non-cell-type-specific enhancers (Ferrari *et al.*, 2014). Interestingly, during embryonic stem cells (ESCs) differentiation, the H3K27m2 levels are declining by conversion into H3K27m3. It has been proposed that these change in the ratio of the two

modifications is sufficient for both acquisition and repression of defined cell lineage transcriptional programs and phenotypes (Juan *et al.*, 2016).

In addition, methylation of the Lysine 36 of histone H3 needs to be discussed, whose implications are still under investigation. The mono-, di-, and tri-methylation of H3K36 differ from each other in their distribution and functional roles. Higher methylated states of K36 increase from the promoter to the 3' end of active genes (Barski *et al.*, 2007). Particular role of H3K36m1 remains unclear; however, H3K36me2 is relatively well characterized in the context of DNA repair, where it is deposited near double-strand breaks early, and then serves to recruit repair factors such as NBS1 and Ku70 (Fnu *et al.*, 2011). H3K36me3 may be involved in defining exons and influencing alternative splicing, by signalling effector proteins to mark particular exons for inclusion in the final transcript as they exit the RNAPII complex (Luco *et al.*, 2010).

The Lysine residue in position 79 on histone H3 is located in the globular domain of the histone, unlike the other sites, which are part of the exposed amino terminal tail domain of H3. Despite its position in the globular domain, K79 is exposed on the nucleosomal surface, where it can be methylated by DOT1 (Lacoste *et al.*, 2002). Methylation of H3K79 has very diverse functions. It is involved in the regulation of telomeric silencing, cellular development, cell-cycle checkpoint, DNA repair, and regulation of transcription (Farooq *et al.*, 2016). Intergenic H3K79m1 is enriched at enhancer regions and provides unique binding surfaces along the chromatin fiber to stabilize interactions between enhancers and their target promoters. H3K79m2 and H3K79m3 are also widespread histone modifications and are associated with transcriptionally active genes (Steger *et al.*, 2008). With this Lysine residue I would like to finish with the histone H3 and shift to the histone H4.

While many Lysines on Histone H4 can be acetylated, there is only one in position 20, which gets methylated (Jorgensen *et al.*, 2013). Indeed, there is only one report using antibody-mediated precipitation, which suggests that K20 could also be acetylated (Hayashi-Takanaka *et al.*, 2015). Since antibodies are prone to false-positive cross-reactions, in particular with modified nucleosomes (Egelhofer *et al.*, 2011), the existence of H4K20ac is doubtful. In contrast, the methylation states of K20 are very well characterized. Methylated K20 plays many roles in genome regulation. It is involved in transcriptional control, DNA replication licensing, DNA damage response and chromosome segregation. There is one

dedicated enzyme, PR-Set7, which methylates H4K20 (Beck *et al.*, 2012). PR-Set7 levels oscillate during the cell cycle and monomethylates new histone H4 proteins, incorporated in S-phase, on K20. This modification is essential for chromosome condensation and maintenance of genome integrity during M-phase (Wu and Rice, 2011, Beck *et al.*, 2012). Dimethylation of H4K20 represents the most abundant histone modification genome-wide in fibroblasts and HeLa cells (Pesavento *et al.*, 2008, Schotta *et al.*, 2008). H4K20m2 is shown to play a role in DNA damage repair signaling (Botuyan *et al.*, 2006, Greeson *et al.*, 2008) and to be important for cell cycle control, in particular for marking points of origin for DNA replication (Kuo *et al.*, 2012). Trimethylation of H4K20 is involved in heterochromatin formation and associated with transcription repression when present at gene promoters (Wang *et al.*, 2008, Nicetto *et al.*, 2013). Another important feature of H4K20m3 is silencing repetitive DNA and transposons (Schotta *et al.*, 2004, van Kruijsbergen *et al.*, 2017). This notion has been validated in *Xenopus*, where H4K20m3 preferentially accumulates at evolutionarily young DNA transposons (van Kruijsbergen *et al.*, 2017).

Histone phosphorylation

There are a few phosphorylated sites on core histones, which have been functionally very well characterized. For instance, Serine 139 on histone H2AX becomes phosphorylated by ATM in the context of DNA double strand repair. Phosphorylation of gammaH2AX on Tyrosine 142 decides, whether the DSB response leads to apoptosis or repair. Phosphorylation of Serine 10 and 28 on histone H3 has multiple functions. H3S28Ph plays role in transcription activation, and defines a phospho-methyl switch with H3K9m3 during interphase. During mitosis, H3S10Ph leads to release/relocalization of HP1, the chromosomal passenger complex CPC and of TAF3 from H3K4m3 (Sawicka and Seiser, 2014).

The phospho-methyl switch requires only low levels of this modification at discrete sites in the genome. In contrast, cells in late G2 phase, preparing for mitosis, accumulate much higher levels of H3S10Ph, which has been described initially as a major mitotic mark. Phosphorylation of S10 is mediated by Aurora kinase B (AURKB) and is involved in mitotic chromatin condensation. Indeed, this modification is essential for cell cycle progression (Hendzel *et al.*, 1997, Van Hooser *et al.*, 1998). The mechanism, by which H3S10Ph initiates chromosome condensation, has been unraveled recently in *S. cerevisiae*. Here it was found, that its abundant appearance in the G2-phase recruits the Histone deacetylase HST2 to

chromosomes. This enzyme deacetylates H4K16, which allows the H4 histone tail domain to interact with the acidic patch on H2A as a prerequisite of condensation. In the scope of this work we will be frequently dealing with cell cycle progression and mitotic activity. The cell-cycle phase dependent accumulation of the H3S10Ph mark allows us to identify mitotically active cells.

Developmental chromatin maturation

The functional connotation of histone PTMs, laid out in the previous chapters, provides the necessary background to discuss a sequence of global epigenetic transitions known to accompany vertebrate development. While the formation of cell types and tissues requires the induction of regulatory transcription factor genes that install region-specific gene regulatory networks, some global changes in chromatin composition and structure can be suspected to set the frame for developmental genome usage. Remarkably, some of these changes occur independently from the activities of newly induced transcriptional regulators. We refer to this phenomenon as “developmental chromatin maturation”.

Zygotic gene expression starts in embryos at the midblastula transition (MBT) (Biechele *et al.*, 2015, Tadros and Lipshitz, 2009). At this time, many developmental regulatory genes are decorated exclusively by predeposited H3K4m3 and H3K9ac marks in both *Xenopus* and zebrafish embryos (Akkers *et al.*, 2009, Vastenhouw *et al.*, 2010). Repressive histone PTMs, such as H3K27m3 and H4K9m3, appear from gastrula stages on and contribute to regionalized gene expression and the epigenetic stability of lineage commitment and differentiation (Akkers *et al.*, 2009). These findings have led to the conclusions that in these non-mammalian models i) distinct chromatin marks are acquired in a hierarchical manner with active marks being followed by repressive PTMs, and ii) the onset of embryonic transcription is heavily influenced by maternal factors that constitute an environment called maternally acquired domain (Hontelez *et al.*, 2015). This suggests that embryonic chromatin at blastula stage is mostly permissive and receptive to inducing signals, while being guided by maternal signatures. Repressive chromatin features follow later in these models. This situation could be special, since in mice removal of H3K9m3 has been shown recently as prerequisite for cell lineage programming (Nicetto *et al.*, 2019).

In general, the intrauterine development and small litter size has hampered the *in vivo* analysis of chromatin states at comparable depth in mice , however, embryonic stem cells (ESCs) have provided an alternative resource (Hemberger *et al.*, 2009). Undifferentiated ES cells contain fewer heterochromatic foci than their differentiated progeny (Meshorer and Misteli, 2006, Bhattacharya *et al.*, 2009). In addition, highly disperse chromatin fibers were detected in mouse ES cells, 8-cell embryos and pluripotent epiblast cells, in contrast to lineage-committed cells, which demonstrated a higher degree of chromatin compaction (Ahmed *et al.*, 2010). In addition, both H3K9m3 and heterochromatin protein 1 (HP1) are distributed diffusely in ESCs, while in differentiated neural progenitors they form well-defined foci (Meshorer and Misteli, 2006).

Another discrepancy in early chromatin states seems to exist for "bivalent chromatin domains", in which nucleosomes are co-decorated with positive H3K4m3 and repressive H3K27m3 modifications (Azuara *et al.*, 2006, Bernstein *et al.*, 2006, Boyer *et al.*, 2006, Mikkelsen *et al.*, 2007). As mentioned earlier, bivalent domains are believed to repress genes, yet keeping them poised for activation until a later time point. Indeed, it was shown that differentiation causes many bivalent regions to be resolved to monovalent states by loss of one of the two modifications (Mikkelsen *et al.*, 2007). In *Xenopus*, ChIP experiments detected an increase in H3K27m3 positive regions during gastrulation or differentiation (Akkers *et al.*, 2009, Lim *et al.*, 2011). However, while ChIP-Seq experiments identify a large and partly conserved number of bivalent domains in pluripotent mouse ES cells and zebrafish blastulae, bivalent domains were hardly found in *Xenopus* at this stage. In fact, the acquisition of H3K27m3 was delayed until the gastrula stage in the frog. The results of re-ChIP experiments indicate that suspected bivalent domains in *Xenopus* correspond instead to monovalently marked nucleosomes from different cells with differential gene activity (Akkers *et al.*, 2009). The differences in bivalent chromatin may be influenced by culture conditions and assay sensitivities. Indeed, quantitative mass spectrometry analysis has indicated that bulk chromatin of mouse ES cells contains under serum culture conditions about 100-fold more H3K27m3 than uncommitted *Xenopus* blastula embryos (Schneider *et al.*, 2011). It is also possible that the kinetics of resolving bivalent domains differs between model systems.

The relative abundancies of histone modifications in early *Xenopus* embryos has been the topic of several studies (Nicklay *et al.*, 2009, Shechter *et al.*, 2009), but only one study

from our group has managed so far to directly assess by mass spectrometry histone PTMs from frog embryos (Schneider *et al.*, 2011). This study identified the relative abundance of about forty modification states on tryptic peptides from histones H3 and H4 at four key stages of frog development: blastula, gastrula, neurula and tadpole stage. It independently confirmed the relative absence of repressive histone modifications from pluripotent embryonic cells, notably H3K27m2/m3 and H4K20m3, and their gradual accumulation during development. In contrast, both acetylated and monomethylated states of H3K56 were abundant early on, but decreased by more than an order of magnitude over the same time period. Subjecting this data to hierarchical clustering analysis revealed a unique quantitative combination of histone PTMs for each developmental stage. These patterns have been called "stage-specific histone modification profiles" (HMPs) (Schneider *et al.*, 2011). The disproportionate change in the steady state of these PTMs suggests that their abundance is regulated by unknown developmental cues.

Altogether, this data indicates that in the three model organisms *Xenopus*, zebrafish and mouse, development starts out from a relaxed, derepressed epigenome state (Surani *et al.*, 2007, Hemberger *et al.*, 2009, Perino and Veenstra, 2016). In line with embryonic pattern formation, early chromatin comes under repressive control, in particular by the accumulation of heterochromatic PTMs (H3K9m3, H3K27m3 and H4K20m3). The developmentally regulated histone modification profiles represent a first vector of the postulated chromatin maturation.

A second example of developmental chromatin maturation is related to its 3-dimentional organization. All higher-order folding of the chromatin fiber requires H1 linker histones (Izzo and Schneider, 2016, Roque *et al.*, 2016). The H1 proteins are not included in the core nucleosome, but bind to the linker DNA near the entry/exit site of the nucleosome. Binding of H1 regulates nucleosome compaction and represses nucleosome unwrapping, thereby limiting the accessibility of the underlying DNA. Interestingly, there are multiple levels of crosstalk between H1 linker histones and core histone modifications. For instance, acetylation of H3K56 abolishes H1 binding and leaves DNA binding motifs open (Bernier *et al.*, 2015). On the other hand, binding of H1 to nucleosomes supports local H3K9 methylation (Boija and Mannervik, 2015). Finally, while linker histones are generally depleted from active promoters, H3K27m3-decorated nucleosomes promote the incorporation of a specific linker

histone variant, thus contributing to heterochromatin formation (Kim *et al.*, 2015). Interestingly, the chromatin of undifferentiated ES cells has about two-fold less H1 linker histone proteins incorporated than any other cell type (Fan *et al.*, 2003). This unique feature is compatible with the general notion of an open, relaxed chromatin in undifferentiated embryonic cells.

H1 linker histones constitute a family of protein variants with evolutionarily conserved origins (Pan and Fan, 2016). While none of the individual somatic H1 genes is essential *per se*, reducing in compound mutant mice the total H1 amount to about 50% of the normal level is embryonic lethal (Fan *et al.*, 2005). Interestingly, metazoan oocytes contain in their chromatin not the typical "somatic" H1 proteins, but a specialized, maternal variant that is called csH1 (sea urchin), B4/H1M (*Xenopus*) or H1FOO (mouse) (Clarke *et al.*, 1998, Yang *et al.*, 2015). Since genes encoding maternal H1 proteins are usually transcribed only during oogenesis, production of somatic H1 subtypes in embryos triggers a global transition in chromatin composition. In *Xenopus*, both oocyte and somatic 5S RNA genes become activated at the MBT. The incorporation of newly synthesized somatic H1 protein silences the oocyte-type 5S RNA genes, while being compatible with persistent transcription of the somatic genes (Bouvet *et al.*, 1994, Kandolf, 1994). Subsequent gain- and loss-of-function analyses in *Xenopus* have revealed that the global H1 linker histone transition is rate-limiting for the loss of cellular competence for skeletal muscle formation. Loss of competence is achieved by silencing the transcriptional responsiveness of the muscle master regulatory gene *myoD1* to mesoderm inducing growth factors (Steinbach *et al.*, 1997a). Interestingly, this function depends on the globular domain of somatic H1 variants, but not their N- or C-terminal tails, indicating a local role for H1 in making myoD refractory to induction (Vermaak *et al.*, 1998). Consistent with this model, the linker histone H1b was found to repress a key enhancer element of the mouse *myoD1* gene in the C2C12 myoblast cell line (Lee *et al.*, 2004).

The findings in *Xenopus* have helped to establish the paradigm for H1 linker histones as gene-specific regulators, which is now widely accepted (Hergeth and Schneider, 2015, Pan and Fan, 2016). Most importantly, the transition from maternal to somatic H1 linker histone proteins represents a global and irreversible change in chromatin composition, which occurs independently from cell-type-specific differentiation programs. Therefore, it constitutes a

second example for chromatin maturation with possible far-reaching impact on developmental programs.

The cell cycle as a potential regulator of the epigenome

Turning the zygote into an embryo requires extensive cell proliferation. Every time a cell enters S-phase to replicate its DNA, it will dilute the epigenetic information, which it has acquired. Restoring the methylated DNA status poses one major problem: hemimethylated CpG motifs are sequestered to the daughter chromosomes and are reverted to the fully methylated state by maintenance DNA methyltransferases. How the parental histone PTMs are segregated between the two DNA molecules and how the local histone modifications are restored to the original level is much less clear and a matter of intense research (Serra-Cardona and Zhang, 2018, Almouzni and Cedar, 2016). Furthermore, SILAC-labelling of synchronized tissue culture cells has identified at least two different modes to propagate histone PTMs across the cell cycle. Some modifications, including acetyl marks and H3K4m3 are quantitatively restored within one cell cycle, while repressive histone modifications take several generations to reach the original density (Alabert *et al.*, 2015). This would predict a qualitative difference between dividing and non-dividing cells with regard to writing and maintaining histone PTMs.

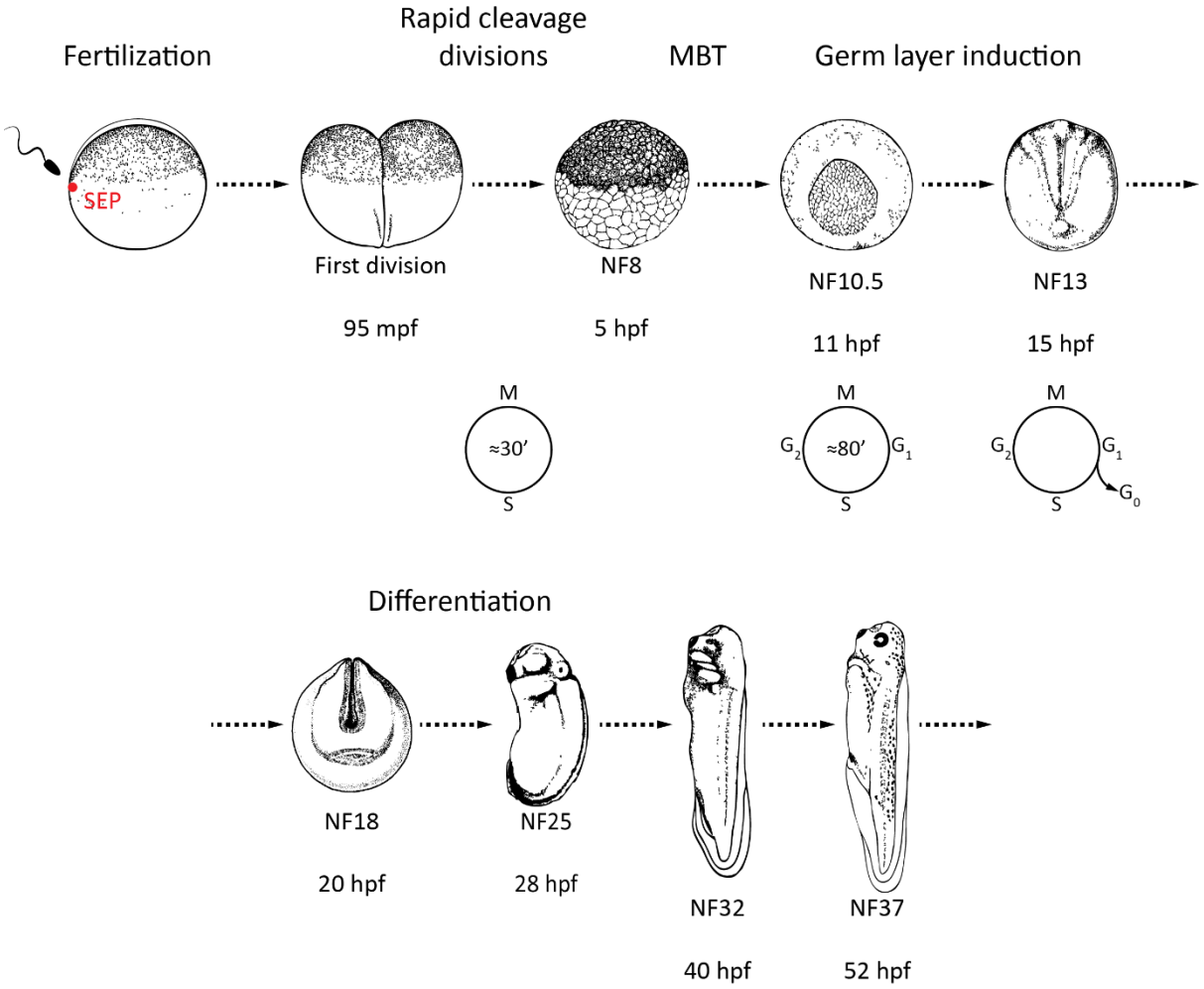

Figure 1. A schematic representation of the early *Xenopus* embryo development. Fertilization is followed by rapid, synchronous cleavage divisions. During this time the cell cycle takes approximately 30 minutes. After the midblastula transition (MBT), when zygotic genome becomes active, the cell cycle slows down until it becomes asynchronous, and first post-mitotic cells appear at the neurula stage. On the scheme: SEP - sperm entry point, m/hpf - minutes/hours post fertilization, NF - embryo stages according to the Nieuwkoop and Faber (1994) Normal Table of *Xenopus laevis* development.

The cell cycle of *Xenopus* embryos is known to undergo massive changes and rearrangements. Compared to mammals, cell divisions occur in much faster sequence. A timescale of the early frog development is provided in Figure 1. From fertilization to the first division it takes around 95 minutes. In this time, the fertilized egg completes meiosis, maternal and paternal pronuclei fuse, and the zygote enters its first mitosis. From the second until the 12th cleavage division, cells divide synchronously every 30 minutes. At this stage, there are no Gap phases and cells alternate between M- and S-phases (Newport and Kirschner, 1984, Kimelman *et al.*, 1987). During this period, the cell cycle is driven by a cell-autonomous, biochemical oscillator that is unaffected by developmental signals or checkpoints (Ikegami *et al.*, 1997, Kane and Kimmel, 1993, Kimelman *et al.*, 1987, Newport

and Kirschner, 1982, Newport and Kirschner, 1984). After twelve divisions, the embryo approaches the midblastula transition (MBT), when bulk zygotic transcription is initiated (Tadros and Lipshitz, 2009). MBT is triggered by a critical nuclear to cytoplasmic (N/C) ratio as a consequence of rapid cell divisions in the virtual absence of cell growth and zygotic transcription (Jevtic and Levy, 2015). This leads to the activation of the Chk1 kinase that in turn causes proteasome-mediated degradation of the replication-initiation factor DRF1 (Collart *et al.*, 2017). The cell cycle lengthens, becomes asynchronous and the G1/G2 gap phases are established. For the prospective endoderm in tail bud embryos, kinetics of thymidine-labelling of DNA have been used to estimate the cell cycle length at about eleven hours, achieved by lengthening of G1-, S- and G2-phases (Graham and Morgan, 1966). As soon as the early neurula stage, the first non-replicative cells can be observed in *Xenopus* (Hartenstein, 1989). They are located in neural plate and paraxial mesoderm, i.e. territories that contain a significant portion of the total embryonic cell number (Briggs *et al.*, 2018). Although their quiescence is probably transient (Lange and Calegari, 2010, Leise and Mueller, 2004).

Overall, these observations provide evidence for a dramatic cell cycle slow down and reduced mitotic activity in large parts of the embryo, which could affect the writing and maintenance of histone PTMs. We consider these cell cycles changes as a third potential mechanism involved in developmental chromatin maturation.

Objectives

This thesis aims to provide experimental evidence for a coupling between cell cycle dynamics and stage-specific histone modification profiles during *Xenopus* development. Such coupling would demonstrate that HMPs are regulated by a physiological process. Furthermore, it should give an insight into selectivity and direction, by which mitotic activity impacts the epigenome and how HMPs are interpreted by the developmental program.

To address these questions, it was necessary to master the following goals:

- establish a method, by which the cell cycle can be systemically manipulated in *Xenopus* embryos
- develop a pipeline for the absolute quantification of covalent histone post-translational modifications from bulk chromatin of *Xenopus* embryos
- investigate the developmental consequences of a systemic cell cycle manipulation by morphological and molecular analyses.

Materials and methods

Method ethics statement

In this study, embryos from African clawed frog *Xenopus laevis* were used. Animal work has been conducted in accordance with Deutsches Tierschutzgesetz; experimental use of *Xenopus* embryos has been licensed by the Government of Oberbayern (AZ: 55.2.1.54–2532.6-7-12).

Frog handling and in vitro fertilization

Xenopus laevis females were injected with about 500 units of human Chorionic gonadotropin (Ovogest, MSD animal health) into the dorsal lymphatic sac and put in incubator overnight. *Xenopus laevis* males were anesthetized in 5g/L solution of Tricaine for 40min, sacrificed by cutting cervical spine, and the testes were excised for the following fertilization. The testes were stored in the testis solution. When female frogs started ovulating, the eggs were collected in Petri dish by gentle squeezing of the frog, the excess of water was removed, and eggs were covered with 1x MBS solution containing a homogenized piece of testis. After 5 minutes, the dish with fertilized eggs was filled with 0.1x MBS and stored in incubator until the embryos reached desirable stage of development. The staging was done according to Nieukoop and Faber (Nieuwkoop and Faber, 1994).

Solutions:

- Testis solution: 20% Chicken serum, 200U/ml Penicillin, 200U/ml Streptomycin in 0.8x MBS
- MBS (1x): 880mM NaCl, 10mM KCl, 24mM $NaHCO_3$, 8.2mM $MgSO_4$, 3.3mM $Ca(NO_3)_2$, 4.1mM $CaCl_2$, 100mM Hepes

HUA treatment

When embryos reached the desired stage, they were transferred into HUA solution: 20mM Hydroxyurea (USBiological, H9120) and 150µM Aphidicolin (BioViotica, BVT-0307), made from a frozen stock at 10mg/ml in dimethyl sulfoxide (DMSO), in 0.1x MBS solution. Hydroxyurea, dissolved in water, is stable for 9 months (at room temperature) with a drop of its activity not more than 30%, while Aphidicolin, dissolved in DMSO, is stable for at least 4 weeks (at -20°C). This combination of DNA synthesis inhibitors was used because hydroxyurea alone works quickly (within 2hr), but does not inhibit synthesis completely, while aphidicolin works more slowly (within 4-6hr) and blocks DNA synthesis more completely and irreversibly

(Harris and Hartenstein, 1991). Controls in all cases were embryos from the same batch that were treated identically, except they were incubated in 2% DMSO (dissolvent for Aphidicolin) in 0.1x MBS solution (Mock). In the Experiment type A, HUA and Mock treated embryos were kept continuously in the solutions until the end of the experiment. In the Experiment type B, HUA treated cohort of embryos at NF13 was split into two groups, one was left in HUA, another was placed in Mock solution. HUA treated embryos were staged accordingly to sibling Mock treated embryos.

Whole mount RNA in situ hybridization

Embryos collected at the proper stages were anesthetized in 0.05% benzocaine (N24), fixed in MEMFA and stored at -20°C in Ethanol to solubilize and remove cell membranes for at least 2h before *in situ*. Embryos were rehydrated by series of 5min incubations in 75%, 50% and 25% EtOH in PBSw and then washed in PBSw 3 times for 5min on a roller. Then the embryos were incubated in 10ug/ml of Proteinase K in PBSw for 20 minutes at room temperature to degrade proteins associated with RNAs. After embryos were washed with PBSw 2 times for 5min each to remove Proteinase K, with following refixation in 4% Paraformaldehyde in PBSw for 20min. The refixation was stopped by short rinse in PBSw followed by 5 washes in PBSw 5min each. Then embryos were washed for 3min with 50% hybridization solution in PBSw, followed by 3min 100% hybridization solution wash. Hybridization solution was replaced with 0.5ml of the fresh one and then the embryos were incubated in water bath at 65°C for 1h to inactivate endogenous alkaline phosphatases. The incubation continued for another 2 to 6 hours at 60°C for pre-hybridization. Then 3-5µl of dUTP dig-labelled RNA probe was added to 100µl of hybridization solution and heated to 95°C to release possible secondary structures. The solution with RNA probe was added to the embryos which were kept in water bath for overnight for hybridization. If using recycled RNA probe, then hybridization solution was replaced with the recycled RNA probe with the following overnight incubation in water bath at 60°C as well. Next day, the RNA dig probe was removed and kept at -20°C for recycling, and embryos were kept with fresh hybridization solution for 10min at 60°C in water bath. Embryos were shortly rinsed 2 times in 2x SSC, followed by 3 washes for 20min each in 2x SSC at 60°C in water bath. Then embryos were shortly rinsed in 0.2x SSC, followed by 2 washes for 30min each in 0.2x SSC at 60°C in water bath to remove not specifically bound RNA probe. After, embryos were removed from water

bath and washed 2 times in MAB for 15 at room temperature. The MAB buffer then was replaced with 1ml of antibody buffer and let incubating for 1h at room temperature with slight agitation. The antibody buffer was replaced with 0.5ml of new antibody buffer with 1:2000 dilution of anti-dig antibody (Anti digoxigenin-AP Fab fragment, Roche) and let incubating for at least 4h at room temperature. During this step anti-dig antibody was bound to the RNA dig-labelled probe. The antibody buffer was removed and after short rinse in MAB, embryos were left overnight in the fresh MAB solution at 4°C. On the following day, embryos were washed 4 times for 60min each with MAB buffer at room temperature. The last MAB wash was followed by a short rinse in AP buffer and subsequent 15min incubation in AP buffer. AP buffer was replaced with NBT/BCIP staining solution to start the color reaction. Embryos were kept in dark and the color reaction was checked by eye until staining emerges. The color reaction was stopped by incubating embryos in PBS with following refixation in MEMFA for at least 1h. To destroy endogenous melanin pigment granules, embryos were dehydrated in 75% EtOH in PBS for 15min and then incubated in bleaching solution on a bright visible-light source, followed by refixation in MEMFA again. Pictures of embryos were acquired using Leica M205FA stereomicroscope using Z-stack acquisition mode.

Solutions:

- MEMFA: 0.1M MOPS 2mM EGTA 1mM MgSO4 3.7% Formaldehyde)
- PBSw: PBS with 20% Tween
- Hybridization solution (50ml): 0.5g Boehringer Block, 25ml Formamide, 12.5ml 20xSSC, 6ml H_2O, 5ml torula yeast RNA (10mg/ml), 100µl Heparin, (50mg/ml), 250µl Tween-20 (20%), 500µl CHAPS (10%) and 500µl EDTA (0.5 M). Stored frozen at -20°C
- SSC (20X): 3M NaCl, 0.3M sodium citrate, pH adjusted to 7.0
- MAB: 11.61g Maleic acid, 8.76g NaCl, pH adjusted to pH 7.5 and filtered
- Antibody buffer: 2% Blocking reagent (Roche) in MAB
- AP buffer: 100mM Tris/HCl pH 9.5, 100mM NaCl, 50mM MgCl2, 0.1% Tween 20
- NBT/BCIP staining solution: 4.5µl NBT (100mg/ml nitro blue tetrazolium in 70% Dimethylformamide), 3.5µl BCIP (50mg/ml 5-bromo-4-chloro-3-indolyl-phosphate in 100% Dimethylformamide) in 1ml of AP buffer
- Bleaching solution: 1% Hydrogen peroxide, 5% Formamide in 0.5x SSC

Immunocytochemistry (ICC)

Harvested embryos were fixed in MEMFA for 2h and stored overnight in MetOH at -20°C to remove cell membranes. Embryos were rehydrated by series of 5min washes in 75%, 50% and 25% MetOH in PBS and then washed in PBS 1 time for 5min on a roller. After rehydration, embryos were washed with PBT 2 times for 15min each, followed by incubation in blocking buffer for 2h at room temperature. Then embryos were incubated with primary antibody diluted in blocking buffer overnight at 4°C. On the following day the primary antibody solution was removed, and embryos were washed 5-6 times in PBT for 30-60min each time at room temperature. Secondary antibody diluted in blocking buffer was added to embryos with following incubation overnight at 4°C. On the following day embryos were washed 5-6 times in PBT for 30-60min each time at room temperature and put in AP buffer for 20min with followed by color reaction. The color reaction was then stopped with 2-3 washes in PBS, embryos were refixed in MEMFA for 2-4h and then bleached on bright light course. Embryos were photographed with a Leica M205FA stereomicroscope using Z-stack acquisition mode. Signal from H3S10Ph positive cells was counted using ImageJ software. For the fluorescent detection embryos were photographed with Leica TCS SP5II confocal microscope, using Z-stack montage function.

Solutions:

- PBT: 2mg/ml BSA, 0.1% triton x-100 in PBS
- Blocking buffer: 10% heat inactivated lamb serum in PBT
- AP buffer: 100mM Tris/HCl pH 9.5, 100mM NaCl, 50mM $MgCl_2$, 0,1% Tween 20, 25.5mg/100ml Leavamisole
- Bleaching solution: 1% Hydrogen peroxide, 5% Formamide, 0.5% SSC

Antibody and DNA dye used for ICC and IF:

	name	**dilution**	**method**	**company**
primary	H3S10Ph (mouse)	1:500	ICC/IF	Active Motif
	x-β-catenin (rat)	1:100	IF	Elizabeth Kremmer
secondary	anti-mouse AP	1:2000	ICC	Chemicon
	anti-mouse (green)	1:500	IF	Jackson ImmunoResearch

	Cy3D anti-rat	1:500	IF	Jackson ImmunoResearch
DNA dye	DAPI	1:200	IF	Sigma

RNA extraction and qRT-PCR

Total RNA of 10 embryos was extracted using Trizol (Ambion) and phenol/chloroform. The RNA was precipitated with 70% Isopropanol and cleaned using the RNeasy Cleanup Kit (Qiagen) including DNAse-on-column digestion. For qPCR analysis 1µg of total RNA was transcribed with the DyNAmo CDNA Synthesis Kit (Bioenzym). For qRT-PCR 5–20ng cDNA was mixed with the Fast SYBR Green Master mix (Applied Biosystems) and primers and amplified using a Light-Cycler (Roche) in multi well plates 384/white (Roche). Primer sequences are given in the following table.

Gene		**5'-3' sequence**
pax6	for	ACCCCAGAAGTGGTGAACAA
	rev	GACTCCCTCAGACAGCAACC
actc1	for	ATCTGCCGGTATCCATGAAA
	rev	CCACCAGAGAGGACGTTGTT
twist1	for	AATGTCAGGGAGCGTCAGAG
	rev	CCAGTTTGAGCGTTTGGATT
myt1	for	TCCCCTGACCAATCTCAAAG
	rev	GGACCATCCCAATCATCTTG
tnni3	for	ACTGTCCGGCTTATCCCTCT
	rev	GTTCACTTCGGCTTCCATGT
pdx1	for	CCATTCCCAGATGACAACG
	rev	ACTGTCCTTTCCAGGTGTGG
fabp2	for	TGAAAGAATCCAGCACATTCC
	rev	GAACCAGGCACCATTGAGTT
ins	for	GTCAGTGGACCCCAGGATAA
	rev	CACAATCCCCCTCTTCATTTT
odc	for	ACAAAGAAACCCAAACCAGA
	rev	CAAACAACATCCAGTCTCCAA

Nuclear histone acid extraction

Around 50 to 200 embryos developed to desired stages (NF13, NF18, NF25 NF32) were harvested and washed 3 times in 1ml of E1-0.25 Sucrose-complete buffer. Washed embryos were homogenized in narrow 5ml Glass-Glass douncer (Braun, Melsungen) in 3ml of E1-0.25 Sucrose-complete buffer. The homogenate was transferred into 15ml falcon and centrifuged with 1000rpm (190RCF) for 10min at 4°C. The supernatant was removed, and the pellet was resuspended in 3ml of ice-cooled E1-0.25 Sucrose-complete buffer with 0.5% Triton and 0.5% NP-40 (nuclei suspension), and left on ice for 20min. Meanwhile, 50ml falcon was filled with 5ml of ice-cooled E1-1.25 Sucrose-complete buffer (E1-complete buffer with 1.25M Sucrose) to form a "cushion". The nuclei suspension was carefully overlaid on the cushion, then centrifuged with 1000rpm (190RCF) for 30min at 4°C (2000rpm or 380RCF for the stages >NF30). The supernatant was removed, and the pellet was resuspended in 1ml of ice-cooled E1-complete (without Sucrose) buffer, then transferred to low-binding 1.5ml eppi and centrifuged with 5000rpm for 5min at 4°C. The supernatant was removed, and the nuclear pellet of *Xenopus* embryos was resuspended in 1ml of 0.4M HCl, incubated on a rotating wheel overnight. The solution was transferred in molecularporous membrane tubes (Spectra/Por, 6-8 kDa) and then dialysed against 3l of 0.1M acetic acid/1mM DTT overnight. The dialysed histone solution was vacuum-dried, dissolved in Lämmli Buffer (Roti-Load 4x, Roth) in 1ml per 1 embryo ratio in each sample, and stored at -80°C (Schneider *et al.*, 2011).

Solutions:

- E1-0.25M or 1.25M Sucrose-complete buffer: 90mM KCl, 50mM Tris/HCl pH 7.4 at 23°C, 5mM $MgCl_2$, 0.1mM EDTA pH 8, 10mM Na-butyrate, 0.4mM PMSF, 0.1mM Leupeptin, 2mM DTT dissolved in 0.25M or 1.25M Sucrose

Heavy-labelled peptide (R10) library preparation

Once the histone PTMs of interest for mass spectrometry analysis were chosen, synthetic isotopically heavy-labelled peptides were ordered from JPT company (see table below). Individual R10 peptides were then mixed in the R10 library as following. R10 peptides were dissolved individually in RB buffer to reach concentration 1nmol/100µl. Then they were vortexed for 1min, sonicated for 3min and let on shaker for 15min, the whole procedure repeated twice. 50µl aliquot from each R10 peptide was taken and propionylated with 2.5µl Propionic anhydride in 22.5µl 1M Ammonium bicarbonate (as described in (Villar-Garea *et al.*,

2008)), so final concentration after propionylation was 5pmol/µl. Then 20µl aliquot was taken from each propionylated peptide, pooled together in a low-binding eppi and the solution was evaporated in SpeedVac up to approximately 50µl. 0.1M Ammonium bicarbonate was added to the evaporated R10 peptides to reach 200µl forming the R10 library with concentration of each peptide 500fmol/µl. To check propyonilation, 4µl from the R10 library were digested overnight at 37°C shaking with 2µl Trypsin [25ng/µl] (Promega) in 20µl 100mM Ammonium bicarbonate. Next day, digestion was stopped by adding into the Trypsin solution 10µl 0.1% TFA. Mixture with digested peptides was then desalted using C18 Stagetips (3M Empore) and porous carbon material (TipTop Carbon, Glygen) (as described in (Rappsilber *et al.*, 2007) and analysed using mass spectrometer. Initially R10 peptides come with a fluorescent tag (Q-tag) bound to the last isotopically heavy-labelled Arginine (R*). This tag is used to estimate the concentration after R10 synthesis. During trypsin digestion the tag is cleaved off, so it does not interfere with the following mass spectrometry analysis.

Solutions:

- RB buffer: 80% 100mM Ammonium bicarbonate, 18% ACN, 2% DMSO

Order No	**Index**	**Name**	**Peptide sequence**
#22466	44	H3.K122R128_noPTM	KRVTIMPKDIQLA-R*-Qtag
#22466	17	H3.K18R26_noPTM	PRKQLATKAA-R*-Qtag
#22466	19	H3.K23ac	PRKQLAT-Lys(Ac)-AA-R*-Qtag
#22466	18	H3.K18ac	PR-Lys(Ac)-QLATKAA-R*-Qtag
#22466	20	H3.K18acK23ac	PR-Lys(Ac)-QLAT-Lys(Ac)-AA-R*-Qtag
#25679	1	H3.K18acK23me1	PR-Lys(Ac)-QLAT-Lys(Me)-AA-R*-Qtag
#22466	7	H3.T3Ph	AR-Thr(Ph)-KQTA-R*-Qtag
#22466	5	H3.T6Ph	ARTKQ-Thr(Ph)-A-R*-Qtag
#22466	1	H3.T3R8_noPTM	ARTKQTA-R*-Qtag
#22466	6	H3.K4me1T6Ph	ART-Lys(Me)-Q-Thr(Ph)-A-R*-Qtag
#22466	2	H3.K4me1	ART-Lys(Me)-QTA-R*-Qtag
#22466	3	H3.K4me2	ART-Lys(Me2)-QTA-R*-Qtag
#22466	4	H3.K4me3	ART-Lys(Me3)-QTA-R*-Qtag
#13438	27	H3.K27me1K36me1	AR-Lys(Me)-SAPATGGV-Lys(Me)-KPH-R*-Qtag

#13438	28	H3.K27me1K36me2	AR-Lys(Me)-SAPATGGV-Lys(Me2)-KPH-R*-Qtag
#22466	21	H3.K27R40_noPTM	ARKSAPATGGVKKPH-R*-Qtag
#22466	29	H3.K37me1	ARKSAPATGGVK-Lys(Me)-PH-R*-Qtag
#22466	30	H3.K37me2	ARKSAPATGGVK-Lys(Me2)-PH-R*-Qtag
#22466	31	H3.K37me3	ARKSAPATGGVK-Lys(Me3)-PH-R*-Qtag
#22466	26	H3.K36me1	ARKSAPATGGV-Lys(Me)-KPH-R*-Qtag
#22466	27	H3.K36me2	ARKSAPATGGV-Lys(Me2)-KPH-R*-Qtag
#22466	28	H3.K36me3	ARKSAPATGGV-Lys(Me3)-KPH-R*-Qtag
#22466	25	H3.K27ac	AR-Lys(Ac)-SAPATGGVKKPH-R*-Qtag
#22466	22	H3.K27me1	AR-Lys(Me)-SAPATGGVKKPH-R*-Qtag
#22466	32	H3.K27me1K37me1	AR-Lys(Me)-SAPATGGVK-Lys(Me)-PH-R*-Qtag
#22466	23	H3.K27me2	AR-Lys(Me2)-SAPATGGVKKPH-R*-Qtag
#22466	34	H3.K27me2K36me1	AR-Lys(Me2)-SAPATGGV-Lys(Me)-KPH-R*-Qtag
#22466	24	H3.K27me3	AR-Lys(Me3)-SAPATGGVKKPH-R*-Qtag
#24656	8	H3.K37ac	ARKSAPATGGVK-Lys(Ac)-PH-R*-Qtag
#24656	7	H3.K36ac	ARKSAPATGGV-Lys(Ac)-KPH-R*-Qtag
#24656	11	H3.K27acK36me2	AR-Lys(Ac)-SAPATGGV-Lys(Me2)-KPH-R*-Qtag
#24656	9	H3.K27acK36me3	AR-Lys(Ac)-SAPATGGV-Lys(Me3)-KPH-R*-Qtag
#24656	10	H3.K27me2K36ac	AR-Lys(Me2)-SAPATGGV-Lys(Ac)-KPH-R*-Qtag
#25679	8	H3.K27acK36ac	AR-Lys(Ac)-SAPATGGV-Lys(Ac)-KPH-R*-Qtag
#22466	35	H33.K27R40_noPTM	ARKSAPSTGGVKKPH-R*-Qtag
#22466	36	H3.Y41R49_noPTM	HRYRPGTVAL-R*-Qtag
#22466	37	H3.Y54R63_noPTM	RRYQKSTELLI-R*-Qtag
#22466	38	H3.K56acS57Ph	RRYQ-Lys(Ac)-Ser(Ph)-TELLI-R*-Qtag
#22466	39	H3.K56ac	RRYQ-Lys(Ac)-STELLI-R*-Qtag
#25679	4	H3.K56me1S57Ph	RRYQ-Lys(Me)-Ser(Ph)-TELLI-R*-Qtag
#25679	2	H3.K56me2	RRYQ-Lys(Me2)-STELLI-R*-Qtag
#25679	3	H3.K56me3	RRYQ-Lys(Me3)-STELLI-R*-Qtag
#25679	5	H3.I63R69_noPTM	IRKLPFQ-R*-Qtag
#22466	13	H3.S10Ph	ARK-Ser(Ph)-TGGKAP-R*-Qtag
#22466	14	H3.S10PhK14ac	ARK-Ser(Ph)-TGG-Lys(Ac)-AP-R*-Qtag

#22466	8	H3.K9R17_noPTM	ARKSTGGKAP-R*-Qtag
#22466	12	H3.K14ac	ARKSTGG-Lys(Ac)-AP-R*-Qtag
#22466	15	H3.K9ac	AR-Lys(Ac)-STGGKAP-R*-Qtag
#22466	16	H3.K9acK14ac	AR-Lys(Ac)-STGG-Lys(Ac)-AP-R*-Qtag
#22466	9	H3.K9me1	AR-Lys(Me)-STGGKAP-R*-Qtag
#22466	10	H3.K9me2	AR-Lys(Me2)-STGGKAP-R*-Qtag
#22466	11	H3.K9me3	AR-Lys(Me3)-STGGKAP-R*-Qtag
#24656	4	H3.K9me1K14ac	AR-Lys(Me)-STGG-Lys(Ac)-AP-R*-Qtag
#24656	5	H3.K9me2K14ac	AR-Lys(Me2)-STGG-Lys(Ac)-AP-R*-Qtag
#24656	6	H3.K9me3K14ac	AR-Lys(Me3)-STGG-Lys(Ac)-AP-R*-Qtag
#22466	40	H3.E73R83_noPTM	VREIAQDFKTDL-R*-Qtag
#22466	41	H3.K79me1	VREIAQDF-Lys(Me)-TDL-R*-Qtag
#22466	42	H3.K79me2	VREIAQDF-Lys(Me2)-TDL-R*-Qtag
#22466	43	H3.K79me3	VREIAQDF-Lys(Me3)-TDL-R*-Qtag
#24656	1	H4.K20me1	HR-Lys(Me)-VL-R*-Qtag
#24656	2	H4.K20me2	HR-Lys(Me2)-VL-R*-Qtag
#24656	3	H4.K20me3	HR-Lys(Me3)-VL-R*-Qtag
#25679	6	H4.K20_noPTM	HRKVL-R*-Qtag
#25679	7	H4.K45R55_noPTM	KRISGLIYEET-R*-Qtag
#25679	9	H4.K79R92_noPTM	KRKTVTAMDVVYALK-R*-Qtag

Mass spectrometry sample preparation

15µL of the dissolved in Lämmli Buffer (Roti-Load 4x, Roth) nuclear histone solution were loaded on an 8-16% gradient SDS-PAGE gel (SERVA, V140115-1) and stained with Coomassie Blue to visualize the histone bands. Histone bands were excised as one block, cut in smaller pieces (3x3mm) to fit in an PCR eppi and incubated in 200µl 50% ACN in 50mM Ammonium bicarbonate 2 times for 30min at 37°C to destain. The gel pieces were washed with water and dehydrated with 100% ACN. The gel pieces were propionylated with 5µl of Propionic anhydrate (as described in (Villar-Garea *et al.*, 2008) and dehydrated with 100% ACN again. 1µl of isotope heavy-labelled peptides (product of JPT company, R10), merged within the R10 library with equimolar concentration of 500fmol of each R10 peptide, was

added in the samples before in-gel trypsin digestion (Villar-Garea *et al.*, 2012). Digested peptides were sequentially extracted from the gel pieces by sequential washes in 50mM Ammonium bicarbonate, 2 times in 50% ACN in 0.1% TFA and 2 times in 100% ACN, and desalted using C18 Stagetips (3M Empore) and porous carbon material (TipTop Carbon, Glygen) (as described in (Rappsilber *et al.*, 2007). Extracted peptides were resuspended in 15µl 0.1% TFA and stored at -80C for the following mass spectrometry analysis.

Mass spectrometry analysis with scheduled PRM method

The mass spectrometer (Q ExactiveHF, Thermo Fisher) was operated in the scheduled parallel reaction monitoring (PRM) mode to identify and quantify specific fragment ions of N-terminal peptides of histone proteins. PRM is based on Q-Orbitrap as the representative quadrupole-high resolution mass spectrum detector. It is more suitable for absolute quantification of multiple peptides in a complex mixture, where the peptides are derived from post-translational modifications of a protein. In case of histone post-translational modifications, PRM is especially useful, since there are a lot of isobaric peptides derived from histone PTMs. Isobaric peptides are tryptic peptides which share the same m/z ratio but have different modification states. For example, H3 aa 27-40 has 3 Lysine residues, which can be modified, and K27m1/K36p/K37p has the same m/z as K27p/K36m1/K37p or K27p/K36p/K37m1. Usually, isobaric peptides elute from liquid chromatography column at different distinguishable retention time, otherwise, they co-elute forming one MS peak and can be identified by distribution of the respective y- and b-fragments monitored by scheduled PRM. Using PRM method it is possible to detect and quantify peptides on an attomole-level. In this mode, mass spectrometer automatically switched between one full MS survey scan within 270-1600 m/z range, and 9 PRM MS/MS fragmentation acquisitions of the m/z values described in the inclusion list (see table below), which contained information of m/z of the precursor ions, corresponding fragments and retention time windows. Retention time windows were important to not overwhelm the machine and minimize the idle time. Full MS survey scan of MS spectra (from m/z 270–1600) were acquired with resolution 60,000, while PRM MS/MS fragmentation spectra were acquired with resolution 30,000. Maximum idle time of the machine was 60ms, isolation window 0.7 m/z and fragmentation collision energy (CE) was set to 27% or 30%. Typical mass spectrometric conditions were: spray voltage, 1.5kV; no sheath and auxiliary gas flow; heated capillary temperature, 250°C.

Each developmental stage in the Experiment type A was measured with 3 biological replicates, while 1 biological replicate was acquired for the Experiment type B. The reason being, in the Experiment type B (HUAwo) recovery of the histone PTMs was assessed, thus, Mock values were compared to HUAwo values for the similarity. However, there is no statistical test which tests for similarities, therefore 1 biological replicate was enough. Each biological replicate derived from a different mating pair.

Mass [m/z]	Charge [z]	Start [min]	End [min]	CE [%]	Comment
392.7317	2	15	20	27	H3_3-8_K4m1 R10
387.7276	2	15	20	27	H3_3-8_K4m1
371.7265	2	13.91	18.91	27	H3_3-8_K4m2 R10
366.7223	2	13.91	18.91	27	H3_3-8_K4m2
378.7343	2	13.89	18.89	27	H3_3-8_K4m3 R10
373.7301	2	13.89	18.89	27	H3_3-8_K4m3
425.7071	2	14.62	19.7	27	H3_3-8_T3Ph/K4p and K4p/T6Ph R10
420.703	2	14.62	19.7	27	H3_3-8_T3Ph/K4p and K4p/T6Ph
432.715	2	15.37	20.37	27	H3_3-8_K4m1/T6Ph R10
427.7108	2	15.37	20.37	27	H3_3-8_K4m1/T6Ph
512.2952	2	16.06	22.18	27	H3_9-17_K9m1/K14ac and K9p/K14p R10
507.2911	2	16.06	22.18	27	H3_9-17_K9m1/K14ac and K9p/K14p
519.3031	2	20.04	25.04	27	H3_9-17_K9m1/K14p R10
514.2989	2	20.04	25.04	27	H3_9-17_K9m1/K14p
498.2978	2	14.41	19.53	27	H3_9-17_K9m2/K14p and K9m3/K14ac R10
493.2936	2	14.41	19.53	27	H3_9-17_K9m2/K14p and K9m3/K14ac
505.3056	2	14.53	19.53	27	H3_9-17_K9m3/K14p R10
500.3015	2	14.53	19.53	27	H3_9-17_K9m3/K14p
505.2874	2	15.48	20.48	27	H3_9-17_K9ac/K14p and K9p/K14ac R10
500.2833	2	15.48	20.48	27	H3_9-17_K9ac/K14p and K9p/K14ac
498.2796	2	14.99	19.99	27	H3_9-17_K9ac/K14ac R10
493.2754	2	14.99	19.99	27	H3_9-17_K9ac/K14ac
552.2784	2	19.31	24.31	27	H3_9-17_K9p/S10Ph/K14p R10
547.2743	2	19.31	24.31	27	H3_9-17_K9p/S10Ph/K14p
545.2706	2	16.68	21.68	27	H3_9-17_K9p/S10Ph/K14ac R10
540.2665	2	16.68	21.68	27	H3_9-17_K9p/S10Ph/K14ac
491.29	2	14.51	19.51	27	H3_9-17_K9m2/K14ac R10
486.2859	2	14.51	19.51	27	H3_9-17_K9m2/K14ac
554.8398	2	28.16	34.37	27	H3_18-26_K18p/K23p and K18ac/K23m1 R10
549.8357	2	28.16	34.37	27	H3_18-26_K18p/K23p and K18ac/K23m1
547.832	2	25.56	30.87	27	H3_18-26_K18ac/K23p and K18p/K23ac R10
542.8278	2	25.56	30.87	27	H3_18-26_K18ac/K23p and K18p/K23ac
540.8242	2	21.72	26.72	27	H3_18-26_K18ac/K23ac R10
535.82	2	21.72	26.72	27	H3_18-26_K18ac/K23ac

542.6508	3	31.06	36.46	30	H3_27-40_m1pp; pm1p; ppm1 R10
539.3147	3	31.06	36.46	30	H3_27-40_m1pp; pm1p; ppm1
528.6473	3	20.45	30.28	30	H3_27-40_m2pp; pm2p; ppm2; acm3p R10
525.3112	3	20.45	30.28	30	H3_27-40_m2pp; pm2p; ppm2; acm3p
533.3191	3	19.73	32.5	30	H3_27-40_m3pp; pm3p; ppm3; m2m1p; m1m2p R10
529.983	3	19.73	32.5	30	H3_27-40_m3pp; pm3p; ppm3; m2m1p; m1m2p
547.3227	3	32.69	38.06	30	H3_27-40_m1m1p; m1pm1 R10
543.9866	3	32.69	38.06	30	H3_27-40_m1m1p; m1pm1
533.3071	3	28.07	33.49	30	H3_27-40_acpp; pacp; ppac R10
529.971	3	28.07	33.49	30	H3_27-40_acpp; pacp; ppac
523.9754	3	18.2	27.17	30	H3_27-40_m2acp; acm2p R10
520.6393	3	18.2	27.17	30	H3_27-40_m2acp; acm2p

Histone PTM quantification

The raw data analysis was performed with the Skyline (version 3.7) (MacLean *et al.*, 2010) by using doubly and triply charged peptide masses for extracted ion chromatograms (XICs). Selection of respective peaks was identified based on the retention time and fragmentation spectra of the spiked in heavy-labelled peptides. Integrated peak values (Total Area MS1) were exported as ".csv" file for further calculations. Total area MS1 from endogenous peptides was normalized to the respective area of heavy-labelled peptides. The sum of all normalized total area MS1 values of the same isotopically modified peptide in one sample resembled the amount of total peptide. The relative abundance of an observed modified peptide was calculated as percentage of the overall peptide.

Statistical analysis

For embryonic quantitative analysis (morphological phenotype, qRT/PCR, quantitative MS analysis) SEM are displayed and the statistical analysis was performed using two-tailed, paired Student's t-test. For boxplots, "ggplo2" R package was used. Principal Component Analyses (PCA) were performed using R, without scaling ().

Heatmap generation

Mass spectrometry absolute intensity values of the spiketides were Log2-transformed and missing values imputed using two nearest neighbours (library "knnImputation" in R). Endogenous peptides intensities were Log2-transformed after adding 1 to all values. For heatmap display the normalized log ratios were quantile normalized across all samples and subsequently averaged per condition (N=3 biological replicates per stage per condition for Experiment type A, and N=1 biological replicate per stage per condition for Experiment type

B). The values were scaled row-wise per peptide and hierarchically clustered using the "complete" method on Euclidean distances.

Results

A systemic cell cycle arrest in Xenopus embryos

The cell cycle is a multistep continuous process, lacking by definition a start or end-point. Although it has been studied in extent, new insight about its regulatory mechanisms still emerges in the field (Garcia-Blanco and Moreno, 2019). Most of the cell cycle studies are performed on cells in culture. Using different methods, cells could be synchronized at different cell cycle stages. Treatment with nocodazole, which is an inhibitor of microtubule formation, synchronizes cells at G2/M phase (Davis *et al.,* 2001), while hydroxyurea, a dNTP synthesis inhibitor, synchronizes cells at early S phase (Koc *et al.,* 2004). Thymidine as an Inhibitor of DNA synthesis (Schvartzman *et al.,* 1984) can arrest cells at G1/S boundary (Chen and Deng, 2018), and serum starvation results in a reversible cell cycle arrest and synchronous progress through G0/G1 (Tong *et al.,* 2016). Additionally, an acceleration of the cell cycle in *Xenopus* embryos has been reported. This can be achieved by overexpression of the CyclinA/CDK2 compounds (Richard-Parpaillon *et al.,* 2004).

Early *Xenopus* embryos rely on the consumption of maternally supplied molecules, which restricts the available repertoire of cell cycle manipulations. Considering the options that can be applied to *Xenopus* embryos I have focused on a systemic cell cycle arrest, achieved by the two small molecule inhibitors Hydroxyurea and Aphidicolin (HUA). When added to the cell culture medium, both drugs effectively block DNA replication, and consequently cell division, without obvious side effects on cell viability or differentiation capacity (Jensen, 1987, Maurer-Schultze *et al.,* 1988). This effectively leads to a cell cycle arrest at the G1/S-transition. The applicability of this strategy to *Xenopus* embryos has been demonstrated previously by Harris and Hartenstein (Fig. 2). The authors reported that incubation of embryos in the HUA solution earlier than stage NF9 led to defective gastrulation and aborted development. HUA treatment started shortly after NF10 allowed embryo development until stage NF37/38 (Harris and Hartenstein, 1991, Newport and Dasso, 1989).

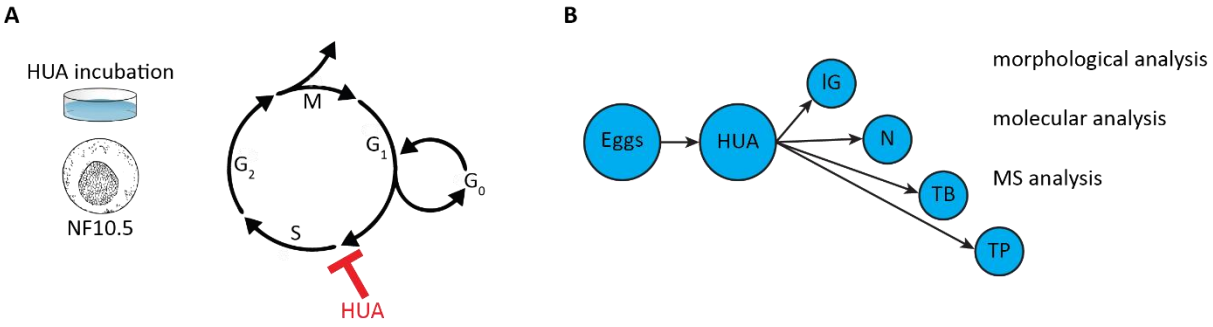

Figure 2. Manipulation of the cell cycle during early embryo development. A) Incubation of embryos in the Hydroxyurea and Aphidicolin solution (HUA) leads to a cell cycle arrest at the G1/S-transition. B) A general overview of the experimental pipeline, embryos are incubated in HUA, then harvested at the indicated stages (lG - late gastrula, N - neurula, TB - tail bud, TP - tadpole stages) with following morphological, molecular and mass spectrometry analyses.

To estimate an involvement of the cell cycle into the process of chromatin maturation, we performed three types of analyses (Fig. 2B). First, a morphological examination of the treated embryos with a focus on the developmental hallmarks; second, an examination of the tissue-specific marker gene expression and establishment of the "molecular age"; and third, an analysis of the histone post-translational modifications (PTMs), that builds up in the stage-specific histone modification profiles (HMPs). The latter is done by liquid chromatography based tandem mass spectrometry (LC-MS/MS), using parallel reaction monitoring method (PRM).

Experimental setup for the HUA treatment

The embryos were immersed and incubated in the solution containing the two inhibitors (HUA). The first inhibitor Hydroxyurea blocks ribonucleotide diphosphate reductase, an enzyme that catalyzes the reductive conversion of ribonucleotides to deoxyribonucleotides, a crucial step in the biosynthesis of DNA; the second inhibitor is Aphidicolin. Aphidicolin blocks eukaryotic DNA Pol-alpha (Ikegami *et al.,* 1978, Harris and Hartenstein, 1991).

In this study we performed two types of experiments (Fig. 3). Experiment type A (G1/S block) implies a continuous HUA and Mock treatment in parallel from NF10.5 until NF32. Mock solution is a 2% DMSO, which is a dissolvent for Aphidicolin, in 0.1x MBS (standard incubation solution). In Experiment type B (Reversal of G1/S block) additionally to the continuous HUA and Mock treatments, HUA washout (HUAwo) condition is introduced. Under the HUAwo condition embryos are temporarily incubated in the HUA solution from NF10.5

until NF13 and then returned to Mock treatment. This tests for reversibility of the standard HUA treatment and should allow me to assess potential toxic effects of the treatment.

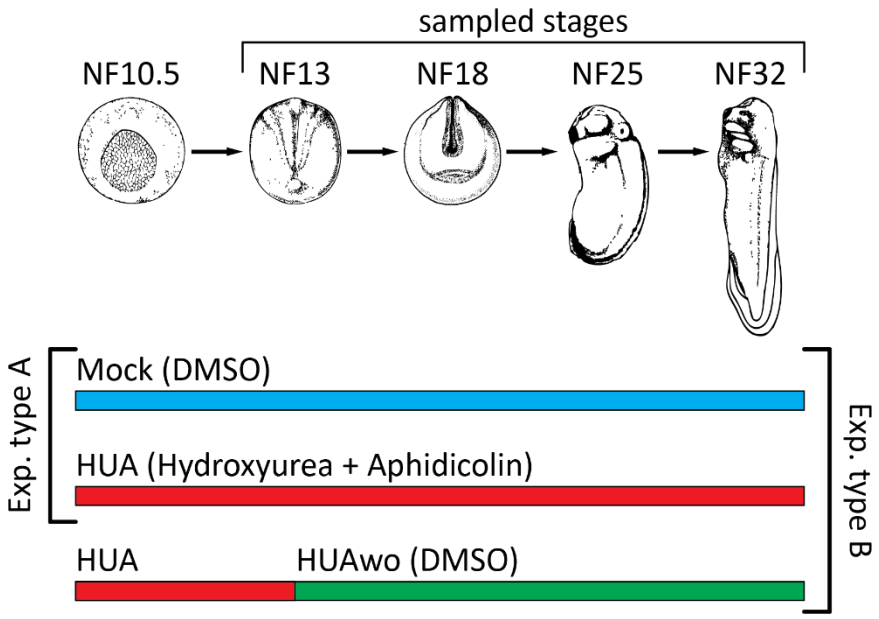

Figure 3. Experimental conditions for investigation consequences of the cell cycle block. Top part - timeline of *Xenopus laevis* embryonic development. Developmental stages (NF) according to Nieuwkoop and Faber, 1994. Stages used for mass spectrometry of histone modifications and embryonic analyses are characterized by the following features: NF13 – late gastrula, germ layer specified; NF18 – neurula, germ layer patterning and differentiation; NF25 – tail bud stage, start of organogenesis; NF32 – early tadpole, body plan established. Bottom part – we perform two types of experiments: Experiment type A (G1/S block) – embryos are split in two groups, which from NF10.5 on are continuously incubated in HUA solution (Hydroxyurea and Aphidicolin) or Mock solution (DMSO). Experiment type B (HUAwo) – embryos are split in three groups – continuous Mock, continuous HUA and transient HUA. In the last group, HUA solution is replaced at NF13 with DMSO solution.

Continuous HUA treatment reduces embryos survival

Titration of the HUA starting point

The planned mass spectrometry analysis of bulk histone modifications is demanding with regard to required embryos numbers, each of which consisting only between some 10^4-10^5 cells. Given that HUA treatment reduces embryo vitality, we expected this to be a bottle neck for the experiment and so decided to determine the earliest possible starting point (Fig. 4). We tested four different embryo stages: midblastula (NF8), late blastula (NF9), blastopore lip formation (NF10), and early gastrula (NF10.5). The concentration of the drugs remained constant throughout all experiments presented in this work.

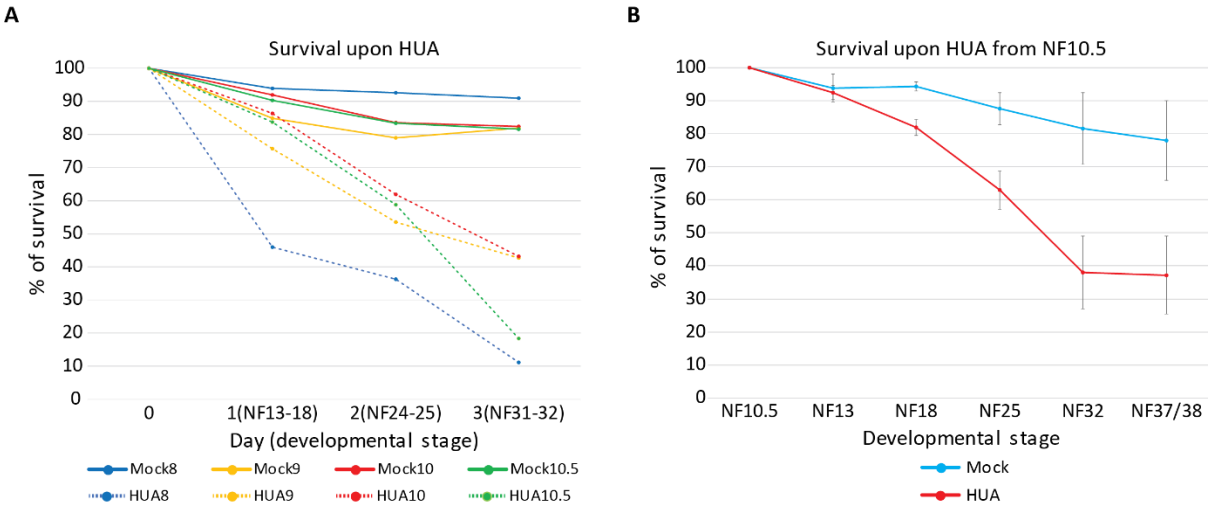

Figure 4. HUA treatment reduces survival of embryos. A) Survival curves under HUA and Mock treatment starting from different developmental stages. Solid lines indicate Mock treatment, dashed lines - HUA treatment. B) Survival curves under HUA and Mock treatment starting from NF10.5 stage. A major drop in survival upon HUA happened from stage NF18, however, it still allowed collecting enough material for the following experiments.

The treatment starting at MBT (NF8) invariably led to severe gastrulation failure (data not shown) and left less than 10% of embryos alive at tadpole stage, consistent with the findings of Harris and Hartenstein (1991). Applying the HUA starting from NF9 allowed for slightly better survival, which would be reasonably not enough for the following tests (Fig. 4A). Applying the inhibitors at stage NF10.5 was compatible with survival of about 40% of the arrested embryos, only two-fold less than under mock treatment with the solvent DMSO. Stage NF10.5 was selected as the optimal compromise between early inhibition and survival for subsequent experiments.

Since the drugs were known to establish a full cell cycle arrest about 6h after their application (Harris and Hartenstein, 1991), this allowed us to investigate embryos from stage NF13 on as cell cycle arrested. Based on the previous studies from Harris and Hartenstein, a permanent HUA treatment starting at NF10.5 is compatible with survival beyond the end of embryogenesis (NF36). Most importantly, the drop in the HUA embryos survival at the earlier stages was considerable but still acceptable in terms of the material amount, in contrast to the later stages, when it was very difficult to harvest enough of the embryos. Therefore, the limits of the HUA treatment were set from the stage NF13 to NF32.

A permanent HUA treatment, starting from NF10.5, gradually reduced embryo viability from NF18 onwards, however, at NF13, the first sampled stage, there was no change in viability compare to Mock (Fig. 4B). At the later stages NF25 and NF32 embryo viability

dropped dramatically. This phenomenon may be explained by the nuclear to cytoplasmic ratio, which diminishes as treatment starts earlier. An embryo with fewer nuclei in its body can produce less mRNA, less new protein. Possibly, the smaller this ratio, the greater are morphological differences, which can be why the effects were not seen until tail bud stage NF25 (Harris and Hartenstein, 1991). Alternatively, the lower cell number of older embryos may not match the increasing morphological demands associated with organogenesis. At the later stages, staging was done based on the developmental time table (Nieuwkoop and Faber, 1994) and Mock treated siblings' morphology. In summary, about half of the embryos still survived when the treatment started from stage NF10.5.

Hydroxyurea and Aphidicolin block cell division

Impact on the cell cycle

The block of cell division was tested by performing immunocytochemical staining against H3S10Ph histone modification (Fig. 5A), which accumulates in M-phase cells (Wang and Higgins, 2013). We determined the number of H3S10Ph positive cells from the entire surface of the embryo employing an Image J software (Fig. 5B). We observed a significant drop in mitotic activity in HUA-embryos, compared to Mock condition, right from the first analysed timepoint on. At NF13, HUA embryos contained at least 8-fold less mitotic cells than mock embryos, a difference that increases to 17-fold by NF32.

Unexpectedly, we detected a small, but reproducible increase in H3S10Ph positive cells in HUA treated neurula (NF18), compared to the other analysed stages (Fig. 5B). This finding might be related to i) cells being already in S-phase, when the treatment starts. Such cells may finish their cell cycle and enter mitosis one last time; ii) cells located in the interior of the embryo, which could get in touch with the inhibitors later than superficial cells. Indeed, the epidermal cell layer of the embryo is known to accumulate cells from deep positions by intercalation (Stubbs *et al.,* 2006), which could contribute to H3S10P positive cell counts; and iii) some cells might be resistant to the drug effect, as it was shown for yeast and mammalian cell lines (Matmati *et al.,* 2013, Liu *et al.,* 1984). Lastly, a recent study demonstrated that a substantial portion of previously considered postmitotic cells in Drosophila embryos are actually arrested in the G2-phase (Otsuki and Brand, 2018). If this was true also for *Xenopus*, such cells may enter mitosis any time, depending on extrinsic signals.

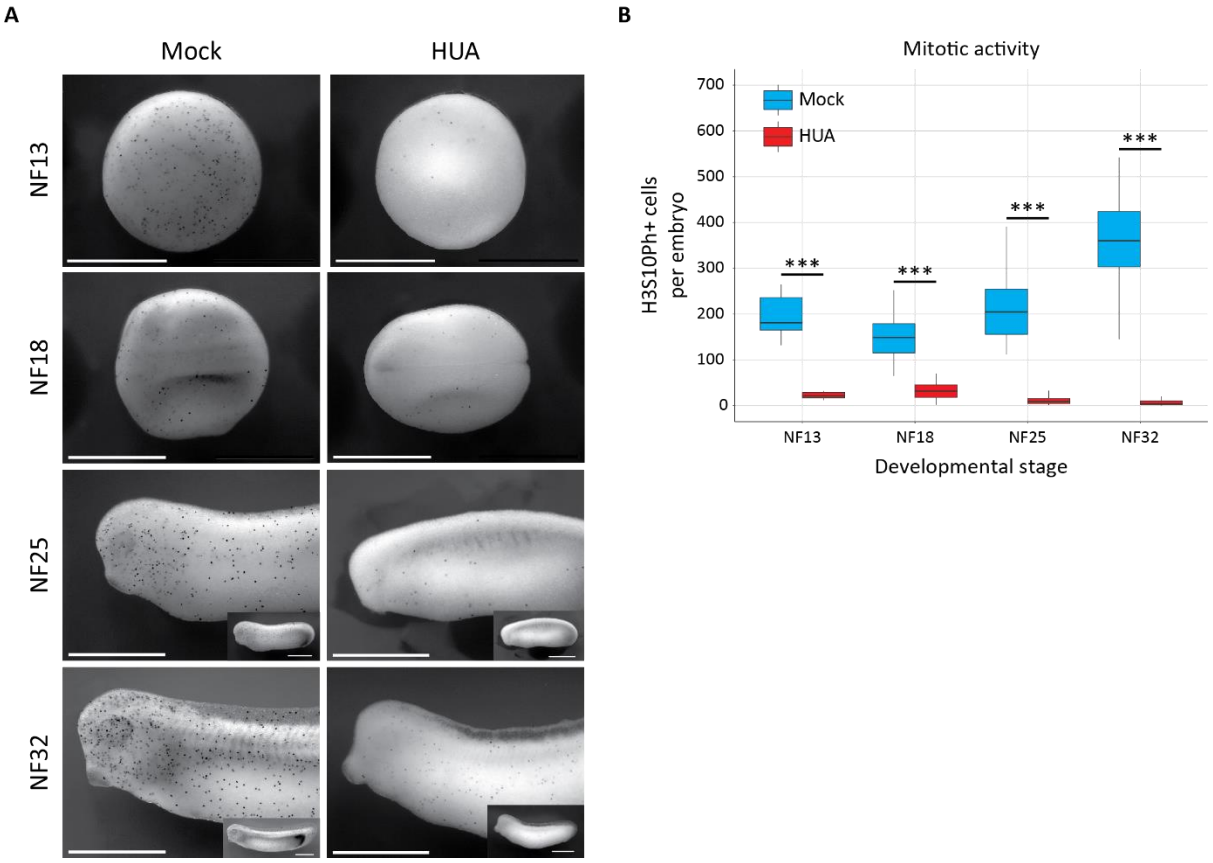

Figure 5. Continuous HUA treatment inhibits mitotic activity from gastrula to tadpole stages. A) Immunocytochemical staining (ICC) for the mitotic histone H3S10Ph mark. Mitotic cells are marked by black dots. Elongated, older embryos are recorded as anterior halves, i.e. at same magnification as younger stages, and in whole mount views as inserts. Scale bars: 1mm. B) Abundance of mitotic cells in Mock and HUA treated embryos. Box plots based on H3S10Ph-positive cells present on the recorded surface of embryos (n=3 biological replicates/condition; mean ± s.e.m.; Student's t-test [unpaired, two-tailed]; *** p<0.001).

Morphological changes upon the HUA

Overall body shape and gastrulation

Embryos, treated with HUA from the stage NF10.5 onwards, demonstrated normal gastrulation and survival without any visible defects until NF13 (Fig. 6). However later, at the stage NF18 we detected a delay in neural tube closure, with more major abnormalities in development upon the continuous treatment. At even later stages, HUA treated embryos lacked the tail structure and had undeveloped eye cup in addition to an absence of melanocytes.

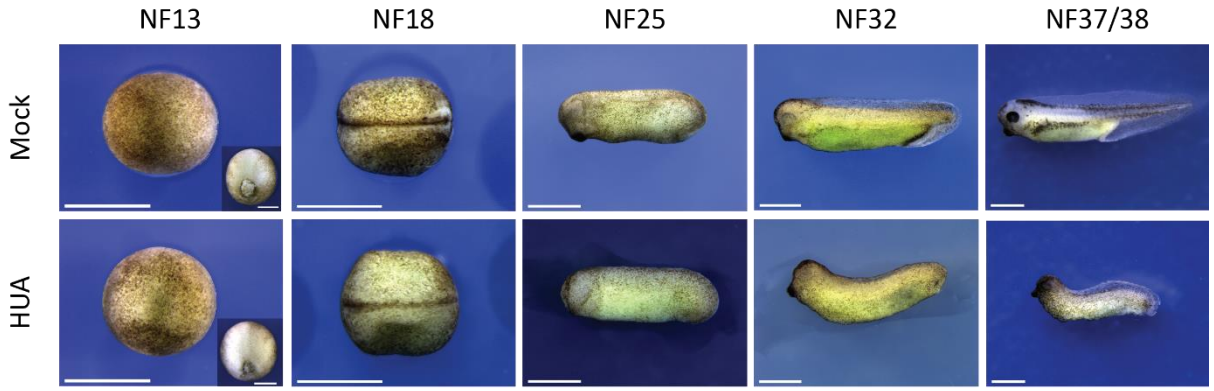

Figure 6. Morphological development of HUA-arrested embryos. During gastrulation, Mock and HUA embryos are indistinguishable. At NF18, the latter shows a delay in neural tube closure. More severe malformations are detectable at stages NF25 and NF32, most notably reduced eye formation and absence of tail bud. Scale bars: 1mm.

Strikingly, the size of arrested and Mock treated embryos was almost the same until stage NF25 (Fig. 6, scale bar 1mm). Unlike mammals, the *Xenopus* embryo starts out from a zygote, gigantic in size, which is subdivided by cell division into smaller and smaller cells. In fact, feeding starts after embryogenesis is completed. Embryos, in which cell division is blocked, could therefore consist of fewer, but larger cells.

To test this assumption, we took a closer look at the surface of HUA treated embryos. Compared to control siblings, G1/S-arrested embryos consisted of bigger cells at the neurula stage (Fig. 7A). To verify the finding we performed an immunofluorescent staining and acquired pictures under the confocal microscope (Fig. 7B). Cell borders are indicated in red and H3S10Ph positive cells in green. The HUA treated embryos had larger cells on their surface. Additionally, no signal from H3S10Ph was detected upon treatment. Embryonic skin consists of 4 cell types: approximately 60% of cells in this tissue are goblet cells, 18% are ciliated cells and approximately 22% represent small secretory cells and ionocytes (Dubaissi and Papalopulu, 2011). Based on this two-dimensional information, HUA treated embryos appear to maintain cell size in a proportionate manner across the 4 cell types.

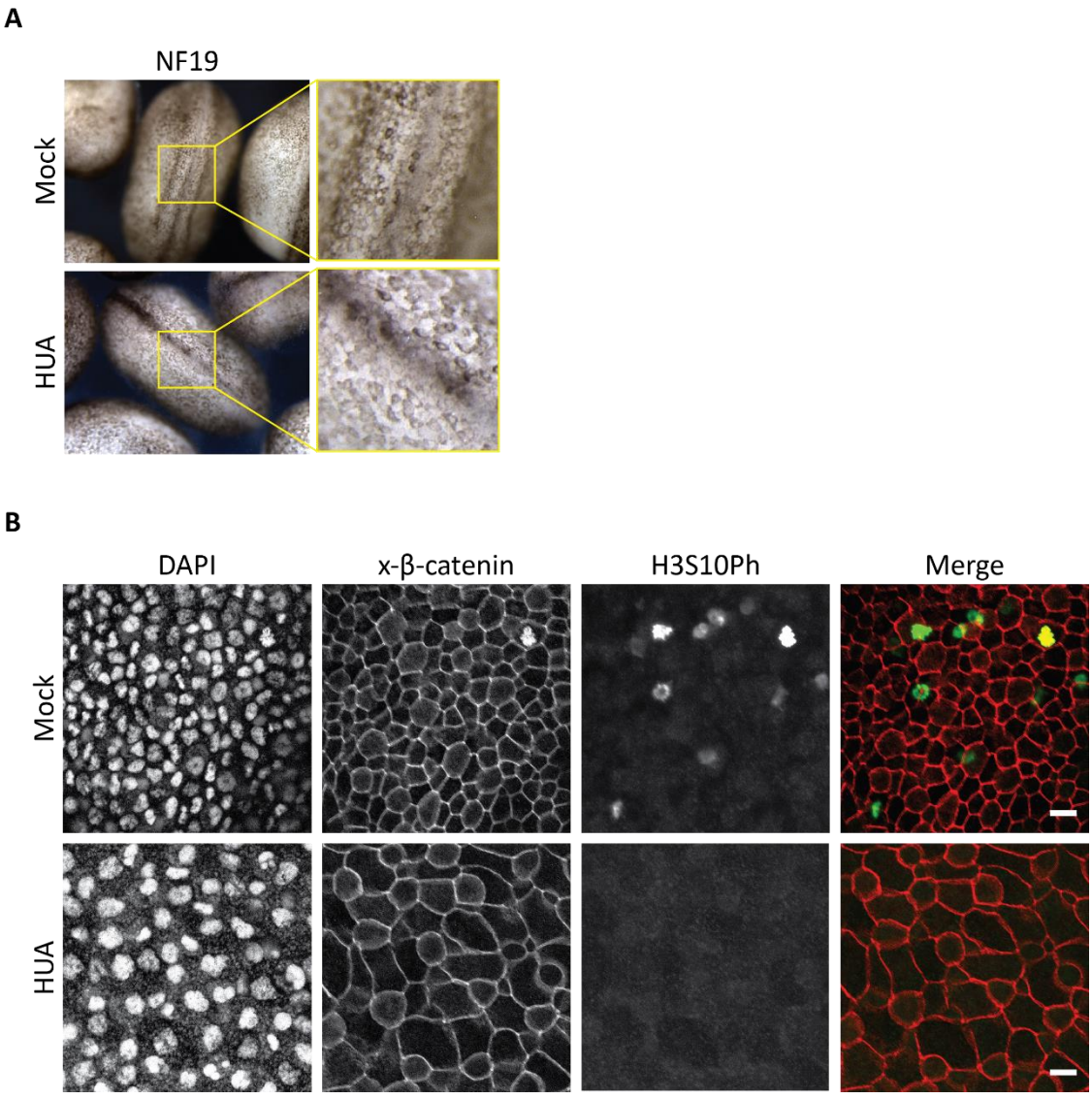

Figure 7. HUA cell cycle arrested embryos have larger cells. A) The first morphological effect of HUA treatment is apparent at stage NF19 as a delay in neural tube closure. Under higher magnification, HUA embryos contain larger cells. B) Cell size at tail bud stage. Flattened Z-stack images show fields from embryonic skin at constant magnification (scale bars: 20µm). Immunofluorescence detects cell borders (x-β-catenin), nuclei (DAPI), mitotic cells (H3S10Ph).

Embryo differentiation upon continuous HUA treatment

Cell proliferation and differentiation are in most cases mutually exclusive processes. With the first active, the second can not occur (Weintraub *et al.,* 1991). To investigate the developmental relationship of Mock and HUA-treated embryos, we compared the expression of 25 organ-specific gene markers. For the sake of simplicity, we decided to group the genes based on their germ-layer specific expression. The stages for this analysis were chosen based on temporal expression profiles of the markers and/or their first appearance in development. Therefore, some genes were tested outside the usual stages of the HUA experiment.

Ectoderm specific markers

To examine ectodermal organs and tissues we performed RNA *in situ* hybridization analysis for three markers: *xcg1* (expressed in the cement gland), *alpha-tubulin* (can be found in epidermal multiciliated cells, brain and in pronephros) and crystallin alpha A (*cryaa*; expressed in the lens) (Fig. 8). Whereas the staining from the first two markers was always detected in the Mock and HUA treated embryos, the *cryaa* mRNA was always absent from the HUA treated embryos.

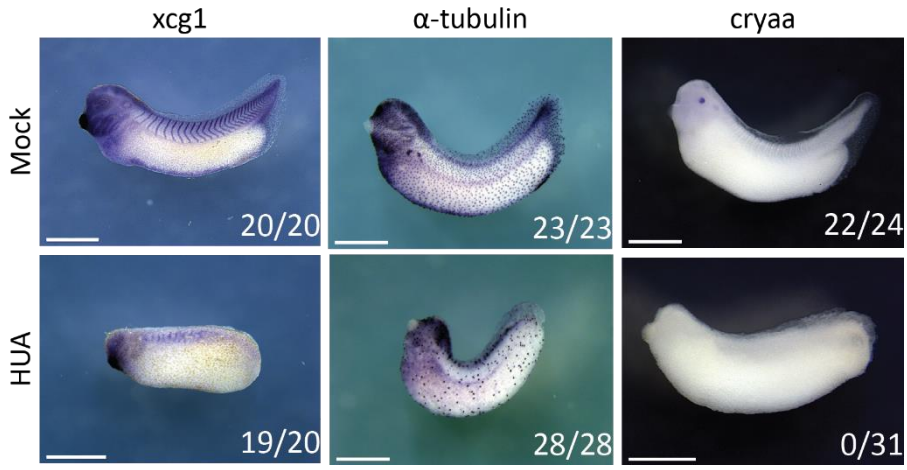

Figure 8. Whole mount RNA *in situ* hybridization for marker genes specific for tissues and organs derived from ectoderm. *Xcg1* is expressed in the cement gland, *alpha-tubulin* can be found in epidermal multiciliated cells, brain and in pronephros, crystallin alpha A (*cryaa*) is expressed in the lens. Images are representative for the majority of Mock and HUA treated embryos. Numbers indicate embryos positive for the marker over the total number of analysed embryos. Scale bars: 1mm.

Neuro-ectoderm specific markers

Major tissues and cell types of the neuro-ectoderm are represented by the eye, brain, spinal cord and cranial neural crest. We tested 6 tissue-specific markers for these structures (Fig. 9).

First, we decided to check the early expressed markers *zic1* and *zic2* (Fig. 9A), which are transcriptional regulators involved in neural ground state formation. At early (NF13) and later (NF25) stages, these genes were expressed properly under both experimental conditions. *Zic1* has multiple key roles in the regulation of neural induction and neurogenesis, promoting both pre-placodal and neural crest cell fates. At the stage NF13, *zic1* mRNA was detected with slightly lower intensity in the HUA embryos. Additionally, the expression domain border of the *zic1* staining in the HUA embryos was not as sharply defined as in control embryos. In contrast to *zic1*, *zic2* is a transcriptional repressor, which inhibits neurogenesis and induces neural and neural crest differentiation. At the stage NF25 it was detected in the eyes and neural tube without any visible differences between Mock and HUA embryos. Altogether, this

result indicates normal regulation of the *zic1* and *zic2* dependent developmental programs upon the cell cycle block.

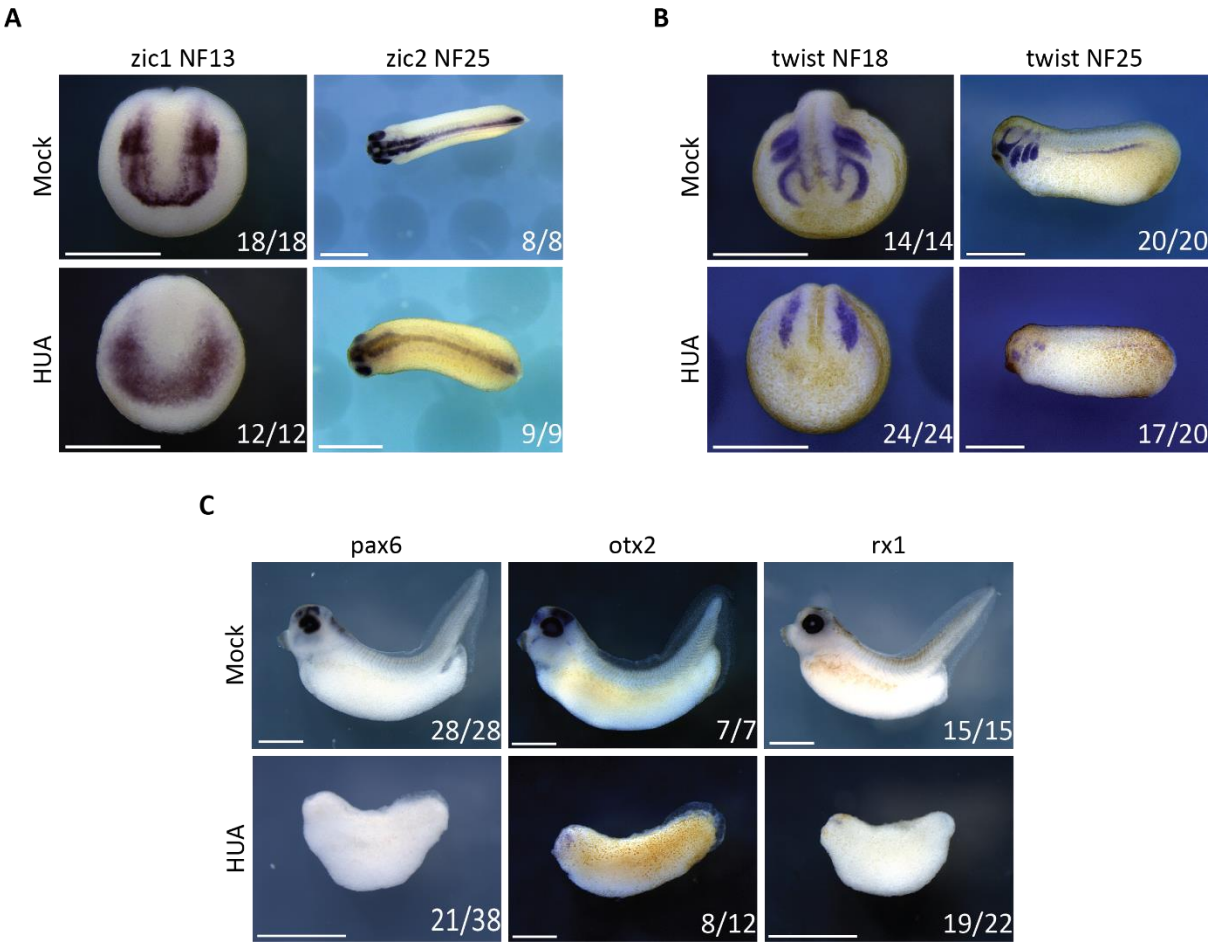

Figure 9. Whole mount RNA *in situ* hybridization for marker genes specific for tissues and organs derived from neuro-ectoderm. Images are representative for the majority of Mock or HUA treated embryos. A) Early expressed genes *zic1* and *zic2*, transcriptional regulators involved in neural ground state formation. B) Expression pattern of neural crest specific marker *twist*. C) Markers of late differentiating organs: *pax6* marks eye, forebrain and midbrain; *otx2* marks eye and brain structures; *rx1* marks eye. Numbers indicate embryos positive for the marker over the total number of analyzed embryos. Scale bars: 1mm.

Next, we investigated the neural crest specific marker *twist* (Fig. 9B). At stage NF18 in the Mock embryos we detected a prominent expression of *twist* marking cranial neural crest cells. In the HUA embryos the expression was detected as well, however, the expression domain was less defined. Nevertheless, later at NF25 we observed *twist* expression in the HUA embryos around the forming eye cup, comparable to Mock embryos, however, covering smaller territory. Altogether, we showed that the HUA treatment perturbed a normal expression of the neural crest marker, however, embryos managed to proceed with their development despite the continuous cell cycle block.

Finally, we focused on late differentiating organs such as the brain and eye (Fig. 9C). *Pax6* at the stage NF32 was detected in the proper domains, namely the eye, forebrain and midbrain in the Mock embryos. However, in about half of the investigated HUA embryos staining was present at the right place, although in a smaller domain. In the other half, the gene expression was not detected at all. Contrary, *otx2* and *rx1* markers, which are normally expressed in the eye and brain as well, were detected in the HUA embryos regularly, although only in much smaller domains.

Overall, the analysis of the neuro-ectodermal markers revealed a robust expression of early regulatory genes. A moderate influence of the cell cycle arrest on the unfolding neuro-ectoderm specific differentiation programs was detected in the late expressed gene markers, which can be explained by the decrease in cell numbers in HUA treated embryos, which limits organ growth.

Mesoderm specific markers

Next, we focused on the mesoderm specific gene marker expression (Fig. 10). Derivatives of this germ layer include muscle (smooth, cardiac and skeletal), blood cells of the hematopoietic system, blood vessels, and pronephros, the embryonic kidneys. In total, we tested 11 marker genes, which are grouped based on the specific area of their expression.

Blood system and heart specific markers

Blood development is known to be highly conserved during evolution, although superficially hematopoietic cells emerge from different locations in amphibian, fish and mammalian embryos (Ciau-Uitz and Patient, 2016). The first blood cells to arise in *Xenopus* embryos are erythrocytes, and they appear in the so-called ventral blood island (VBI) on the belly of the embryo (Ciau-Uitz *et al.,* 2010).

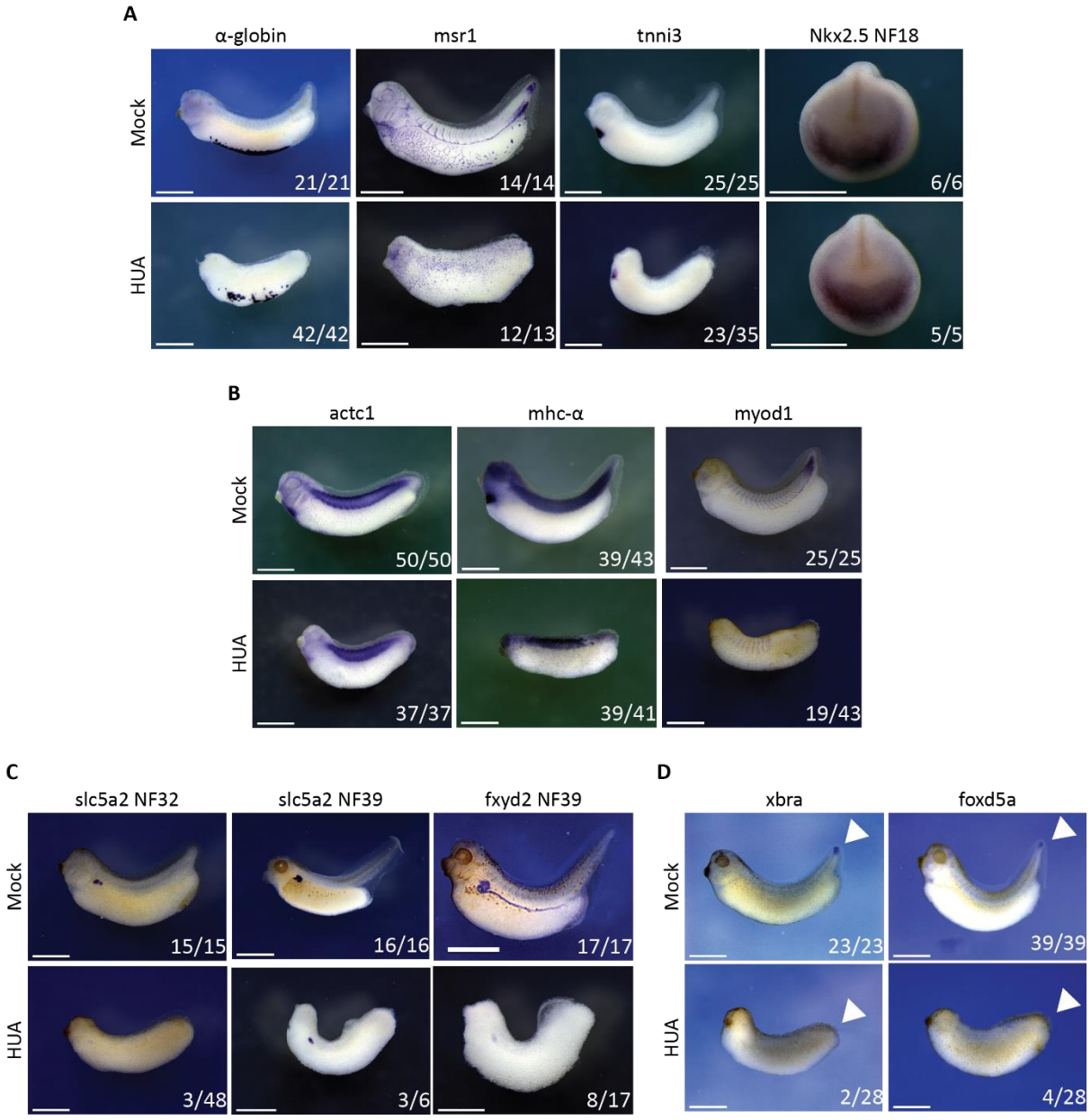

Figure 10. Whole mount RNA *in situ* hybridization for marker genes specific for tissues and organs derived from mesoderm. Images are representative for the majority of Mock or HUA treated embryos. A) Blood system and heart specific markers: *α-globin* marks blood precursor cells; *msr1* marks forming blood vessel tubes; *tnni3* is expressed in late heart; *Nkx2.5* marks early heart Anlage. B) Muscle and somite specific markers: *actc1* is expressed in epaxial muscles, heart and somites; *mhc-α* is specific for cardiac, skeletal muscles and somites; *myod1* marks somites. C) Kidney specific markers: *slc5a2* marks early and late proximal tubules; *fxyd2* is expressed in entire embryonic kidney. D) Tail bud markers: *xbra* and *foxd5a* mark tail tip. Numbers indicate embryos positive for the marker over the total number of analyzed embryos. Scale bars: 1mm.

To address development of the blood system in the HUA embryos we tested 2 markers: *alpha-globin* and *msr1* (Fig. 10A). Upon the HUA treatment *alpha-globin* was detected at the proper area marking the blood islands on the ventral side of the embryo. We detected the gene marker expression in 100% of the analysed Mock and HUA embryos. HUA treated embryos at the stage NF32 are smaller than Mock (Fig. 10A, scale bar 1mm), however, the

size of the *alpha-globin* expression domain appeared proportional. In this region blood precursors differentiate. Later during development, the blood vessels form, which can be visualized by *msr1* staining. In contrast to the well-defined *alpha-globin* staining, *msr1* demonstrated a diffused staining on the sides of the HUA embryos, while in the Mock it was detected in the forming blood vessel tubes. This discrepancy can be explained by the fact that the HUA embryos consist of fewer cells, and therefore might not be able to form a proper vascular system at these later stages. Nonetheless, an appearance of the *msr1* staining itself indicated that vascular precursors are present in cell cycle arrested embryos.

In parallel to the blood system development, the heart is forming in the anterior-dorsal region of the embryo. To visualize the heart region at the early stage we tested *Nkx2.5* gene marker, while to analyse its further differentiation we used the *tnni3* marker (Fig. 10A). At the earlier stage NF18, *Nkx2.5* expression identified the heart-forming region. In HUA embryos at stage NF18, the area marked with *Nkx2.5* was indistinguishable from the control embryos. Later, however, only about 66% of the HUA embryos showed *tnni3* expression in the heart. Altogether, it indicates that the induction of the heart formation at the earlier stage was not affected by the block of the cell cycle, however, subsequent growth and differentiation of the heart Anlage was compromised in arrested embryos.

Skeletal muscle markers

The three markers to check muscle differentiation and formation of somites were *myod1*, *actc1* and *mhc-alpha* (Fig. 10B). During early embryogenesis muscle differentiation is driven by *myoD* (Rudnicki *et al.,* 1993, Chal and Pourquie, 2017), which at the later stages maintains muscle-specific gene expression and can be found in the tail bud and somites. In Mock embryos, we detected a prominent and specific myod1 staining in the somites and in the tail bud in all analysed embryos. Upon cell cycle arrest some 44% maintained myod1 expression. Additionally, even if the HUA embryo had a staining in the somites, it was missing in the tail bud region. The missing signal in the tail bud region can be explained by the previous observation: HUA treated embryos fail to develop the tail structure (Fig. 6).

In contrast to *myod1*, *actc1* and *mhc-alpha* are expressed in already differentiated muscles: *actc1* — in epaxial muscles, heart and somites; *mhc-alpha* — in cardiac, skeletal muscles and somites as well. *Actc1* expression was observed in 100% of the HUA treated embryos at the proper places. *Mhc-alpha* staining was detected in 95% of the HUA embryos.

A notable difference was observed in the *mhc-alpha* staining: treated embryos did not have a well defined somite structure compared to controls. This might indicate a differentiation problem, although *myod1* and *actc1* staining in HUA embryos verify the presence of myotomes in these embryos. Additionally, *mhc-alpha* staining was missing in the cardiac muscle of arrested embryos.

Pronephros

As one of the lateral plate mesoderm derived organs we decided to examine differentiation of the pronephros. In *Xenopus* embryos pronephros can be subdivided into three distinct domains: the glomus, the tubules and the duct. The glomus is responsible for the blood filtration; the proximal tubules are responsible for reabsorption of ions, amino acids, glucose and water. The pronephric duct connects the tubules to the cloaca to excrete urine (Reggiani *et al.,* 2007).

We tested expression of the two pronephros specific genes: *slc5a2* and *fxyd2* (Fig. 10C). The first gene is expressed in proximal tubules only, while the second marker is uniformly expressed in the whole organ, covering pronephric nephron, pronephric tubule, proximal tubule, distal tubule and pronephric duct.

Slc5a2 staining was tested at the two developmental stages NF32 and NF39. In the Mock condition, its mRNA was found in all embryos. In HUA arrested embryos, *slc5a2* expression was strongly diminished or absent. Only 6% of embryos at stage NF32 and 50% at stage NF39 were positive for this marker gene. *Fxyd2* marker expression was tested at the stage NF39 of the Mock and HUA embryos. In the Mock condition it was found in all analysed embryo, while in the HUA it was detected in about half of the embryos (47%). One should also note, that even when the *fxyd2* expression was observed in the HUA embryo, it clearly did not resemble a normally formed organ. Altogether, we at the first time detected an entire organ, that was severely affected by the cell cycle arrest. This may be correlated with the timing of kidney formation. While it is induced early around stage NF14, its actual differentiation commences after NF28. At that time, HUA treatment may have impacted the differentiation capacity of the kidney precursor cells.

Tail bud markers

The postanal tail is a transient structure in premetamorphic *Xenopus* tadpoles, which is needed to support swimming. It is resorbed and disappears during thyroid hormone induced

metamorphosis. From the morphological analysis it became clear that the tail structure did not form upon the HUA treatment (Fig. 6). It was unclear, whether this was due to a failure in activating the tail-forming genetic program or to the absence of cell division? To test this, we used *xbra* and *foxd5a* markers (Fig. 10D). At the stage NF32, *xbra* is expressed in the chordoneural hinge and notochord at the tail tip area; *foxd5a* is expressed in tail bud structure. Neither of the two markers were found in the tail of the HUA embryos.

Together with the missing pronephros, this is another interesting observation of a missing tissue. The tail formation of the *Xenopus* embryo is multistep complex process. In short, there are seven distinct regions of the tail bud as outgrowth commences defined as early as at the end of gastrulation NF13 (Beck and Slack, 1998). In our experimental set up, we reach the cell cycle block at the stage NF13 already. Apparently, this block does not influence an induction of the tail formation, as we observed one of the tail bud markers at the stages NF18 and 25. However, at the later stage NF32 the tail bud structure and tissue-specific genes were missing. Given this, we assume, that the cell cycle block had a negative influence on the tail bud formation somewhere in between NF25 and NF32 stages.

Endoderm specific markers

The endoderm germ layer gives rise to organs such as liver, pancreas and gut. In *Xenopus*, these organs develop rather late, close to the end of embryogenesis. Hence, in the frame of this work it was difficult to assess these organs in detail. However, it is still possible to investigate endoderm derived organ precursors, such as the pancreatic Anlage.

The first endocrine marker to be expressed in the pancreas at NF32 is *insulin* (Fig. 11) (Pearl *et al.,* 2009). Expression of most exocrine markers, including amylase, trypsinogen and elastase, is first detected at NF41 (Horb and Slack, 2002). When we tested *ins* expression in the Mock and HUA embryos, we found that upon HUA there was no signal in all tested embryos. Together with pronephros and tail bud, this is the third example of an organ, which is missing from cell cycle arrested embryos

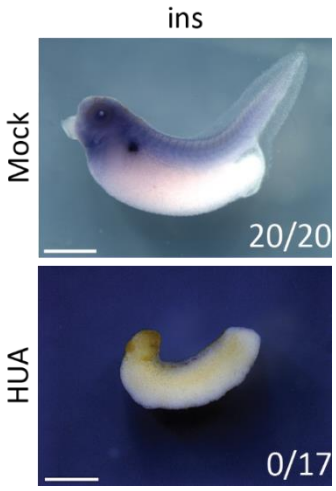

Figure 11. Whole mount RNA *in situ* hybridization for marker gene *ins* specific for embryonic pancreas, which is derived from endoderm. Images are representative for the majority of Mock or HUA treated embryos. Numbers indicate embryos positive for the marker over the total number of analyzed embryos. Scale bars: 1mm.

Later in the course of this work, we examined two additional pancreatic transcription factors: *pdx1* and *ptf1a*. Both genes are expressed in pancreatic progenitors, and are necessary and sufficient for pancreas development (Horb *et al.,* 2003, Afelik *et al.,* 2006, Jarikji *et al.,* 2007). We assessed them in the Experiment type B.

Other markers

Undifferentiated cell state marker

Expression of some markers is needed to maintain the undifferentiated state of the cells and to promote their active proliferation. It is especially important during the early embryo development. To test if the HUA treatment could influence these genes, we tested *oct25* at the stage NF18 (Fig. 12).

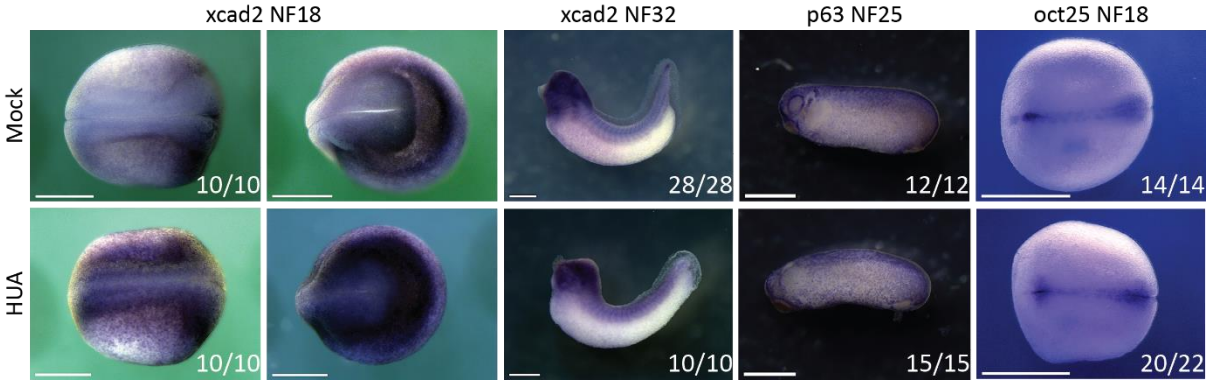

Figure 12. Whole mount RNA *in situ* hybridization for marker gene specific for undifferentiated cell states — *oct25*; axis induction competence marker — *xcad2* (first panel: dorsal view, second panel: anterior view); tumor suppressor marker — *p63*. Images are representative for the majority of Mock or HUA treated embryos. Numbers indicate embryos positive for the marker over the total number of analyzed embryos. Scale bars: 1mm.

Oct25 is a member of POU class V (POU-V) homeodomain transcription factors which play an important role in maintenance of pluripotency and cell differentiation. The *oct25* gene is mainly transcribed during blastula and gastrula stages in the newly forming ectodermal and

mesodermal germ layers (Nishitani *et al.,* 2015, Cao *et al.,* 2004). We detected a wild type like expression of the marker in the HUA embryos in 91% of the embryos. The area of *oct25* expression was not different between HUA and Mock embryos. This Indicated that despite the block of the cell cycle, the undifferentiated cell state was not perturbed.

Regulatory genes involved in axial induction

The competence of marginal zone cells to respond to organizer-inducing signals is under the temporal control of the homeobox transcription factor Xcad2 (Levy *et al.,* 2002). In other words, Xcad2 has a developmental role in elongation of the body axis and positional specification, which is mediated through mild repression of anterior *Hox* genes (*Hox1* and *Hox2*) and strong activation of posterior *Hox* genes (Brooke *et al.,* 1998, van den Akker *et al.,* 2002, Isaacs *et al.,* 1998).

Here we tested *xcad2* expression at the stages NF18 and NF32 (Fig. 12). Consistent with HUA embryos displaying no problems in axis formation aside from the postanal tail, the *xcad2* was expressed comparably under both conditions and stages. At the early stage NF18 it was detected in the ectoderm and neural plate, and at the later stage NF32, it stained the brain and somites.

Tumor suppressor marker

P63 – tumor protein p63 is a tumor suppressor, which induces growth arrest or apoptosis depending on the physiological circumstances and cell type (Bergholz and Xiao, 2012). We tested the expression of this marker at the stage NF25 (Fig. 12). In 100% of the Mock as well as HUA embryos *p63* was detected in the neural crest and epidermis. We did not observe differences between the Mock and HUA embryos in the marker expression profile. The ΔNp63 variant, exclusively present in early *Xenopus* embryos, protects the epidermis from apoptosis (Canella *et al.,* 2012, Tribulo *et al.,* 2012). Although we have not assessed this issue directly, its normal expression suggests no increase in cell death in HUA-treated embryos.

The “molecular age” of HUA arrested embryos

We have demonstrated that embryos under continuous HUA treatment develop largely normal — with some notable exceptions — until mid-neurula stage. Later on, however, their morphology becomes more and more compromised, most clearly visible at the NF32 time

point (see Fig. 6). It was unclear, whether cell cycle-arrested embryos are only retarded in development, or whether they are blocked in differentiation?

To address the issue of delay, we compared by qRT/PCR the timing and relative levels of gene transcription between mock and HUA treated embryos (Fig. 13). We examined eight genes, grouped in pairs based on shared activation timepoints: *pax6* and *actc1; twist* and *myt1; tnni3* and *pdx1; fabp2* and *ins*. In each experiment the mRNA levels were normalized to the housekeeping gene *odc*. A significant difference between Mock and HUA gene expression was found only in the case of *pax6* at stage NF32. The mRNA levels of the other seven genes were proportionate between the two conditions. Most notably, this applies even for the late-induced *fabp2* gene.

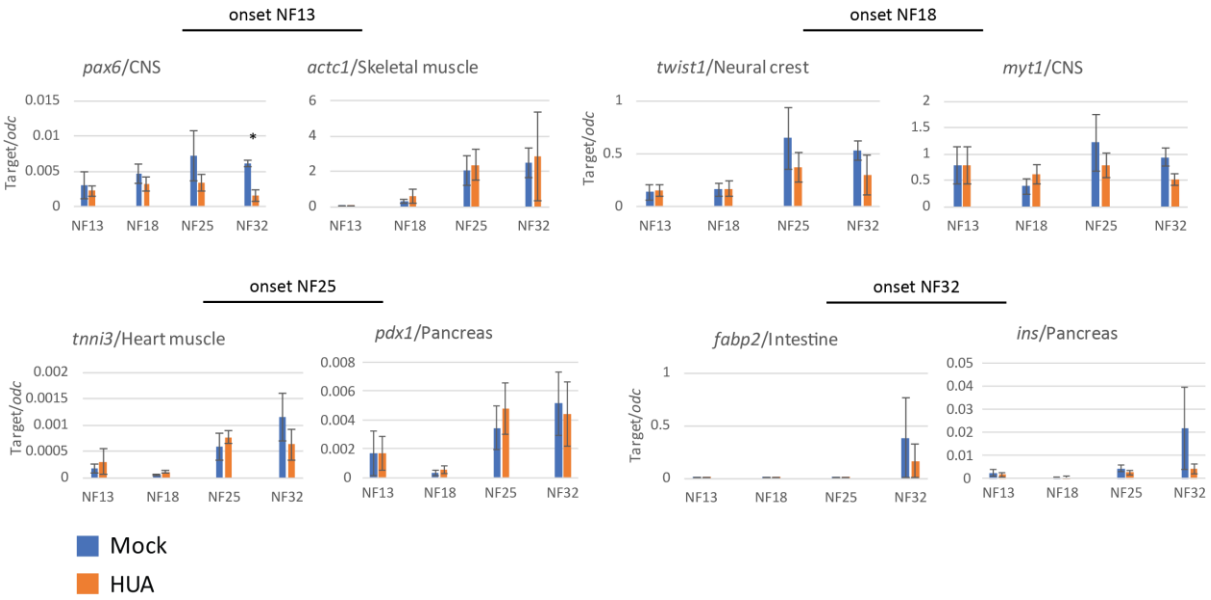

Figure 13. "Molecular age" of embryos is not compromised upon the treatment. Comparison of temporal expression profiles for selected marker genes in Mock and HUA conditions by qRT/PCR, normalized to *odc* mRNA. Genes are grouped according to their activation time point. N=3 biological replicates/condition; mean ± s.e.m. Significant difference was detected only in case of *pax6* expression level at NF32 stage (Student's t-test [two-tailed, paired]; * $p<0.05$). No other significant differences were detected between the two conditions, indicating a proportionate gene expression pattern, consistent with the increasing developmental age.

Altogether, the results suggest that the absence of certain marker gene mRNAs can not be explained by a general delay of embryonic development under the cell cycle arrest. Instead, we assume that the absence of expression of certain regulatory genes in the HUA embryos must be due to other mechanisms.

Late physiological observations

Although HUA-treated tadpoles are morphologically impaired, they are nevertheless responding to touch stimulation (see “HUA NF33 flight response” and “Mock NF33 flight response” videos). The burst of swimming activity involves a physiological connection between sensorial neurons, the CNS, and the body wall musculature (Roberts *et al.,* 1998). It is shown in the videos how the embryos react to a touch stimulus, trying to escape from it. In the absence of the muscular tail, which serves as major swimming force, HUA-embryos respond mostly by twitching and bending, although rudimentary swimming can be occasionally observed.

Additionally, we tested, if HUA treated embryos develop a heartbeat (see “HUA NF33 heartbeat” and “Mock NF33 heartbeat”). Normally, the heart starts to beat at the stage NF33/34. The HUA treated embryos had a hardly detectable heartbeat compared to their control siblings. Surprisingly, we demonstrated a recovery of the heartbeat in the HUAwo chapter.

Conclusions from the developmental analysis of HUA embryos

Overall, the whole mount RNA *in situ* hybridization analysis covered 25 differentially expressed gene markers from 17 tissues and organs derived from all three embryonic germ layers. Of this group, only four genes were either not found expressed at all in the HUA treated embryos, or were transcribed at very low level. These include i) pronephros-specific *slc5a2* and *fxyd2*; ii) tail bud-specific *xbra* and *foxd5a*; and iii) pancreas-specific *ins*.

On the other hand, this means that most investigated markers were expressed at the correct time and place. This suggests that embryonic patterning and organ precursor specification occurs largely normal in the absence of cell proliferation, although some notable cell types are absent.

Results derived from the RT-qPCR analyses of the stage-specific markers confirmed that with the arrested cell cycle embryos differentiate synchronously.

Execution of the flight response indicated a functionally established connection between the neural system and muscles at the later stages, despite the cell cycle block. Of note, the twitching of the HUA embryos could possibly be due to a spontaneous electric

stimulation of the underlying muscle cells as a result of applied compression (the touch stimulus). To address this in more detail, other physiological experiments are needed.

Altogether, we consider this a key result, since it allows to interpret any potential changes in histone modification patterns as consequence of cell cycle arrest, rather than as a consequence of grossly abnormal differentiation.

Analysis of the histone post-translational modifications (PTMs)

LC-MS/MS: critical steps and prerequisites

MS sample preparation (general notes)

To study histone post-translational modifications (PTMs) during *Xenopus* development, we extracted histones from HUA treated and control cohorts of embryos from the 4 developmental stages (Fig. 14A). The histone extraction was based on the previously developed protocol by Tobias Schneider, a former member of our laboratory. This protocol is based on cell nuclei preparations, purified from embryonic lysates by centrifugation through a sucrose cushion, acidic histone extraction and subsequent dialysis. In a second step, embryonic bulk histones were further purified by SDS-Page electrophoresis and visualized by Coomassie staining. The proper bands were excised as on block of four core histones from the gel and propionylated in preparation for subsequent Trypsin digest.

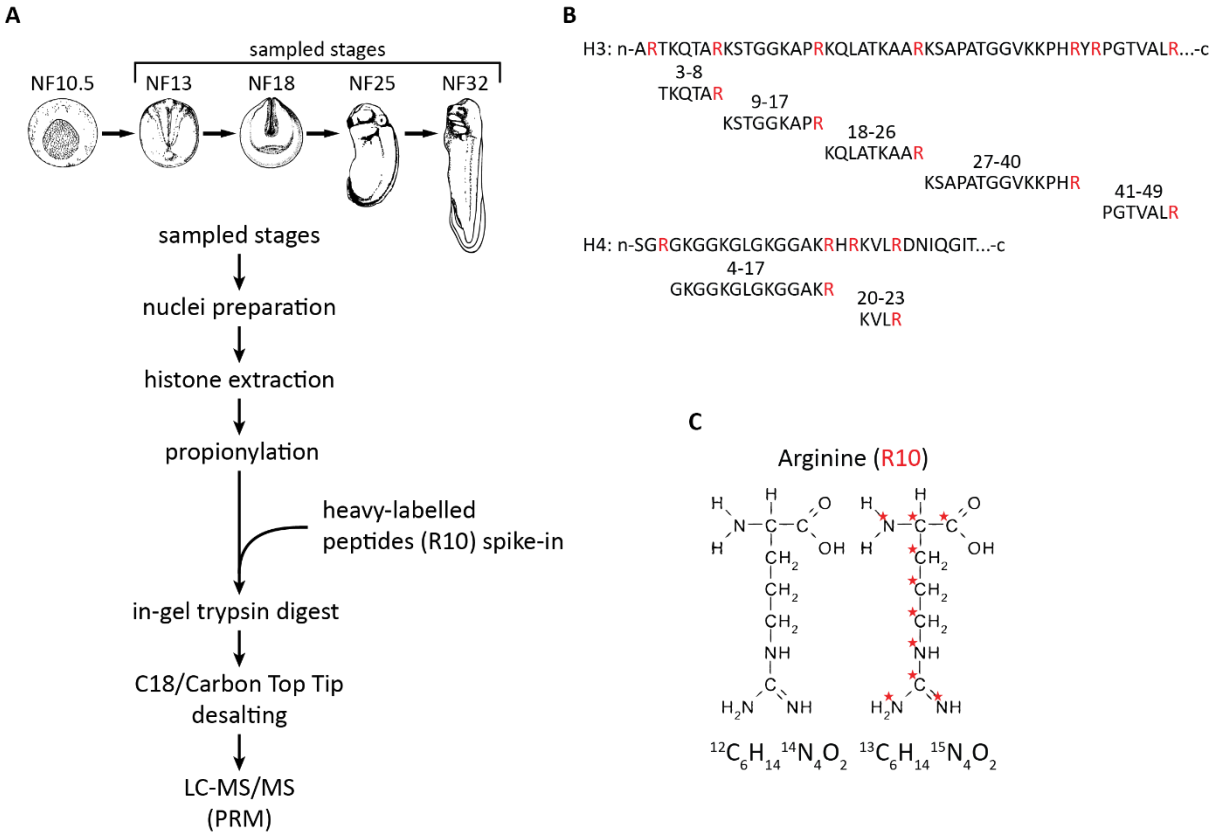

Figure 14. A pipeline of the sample preparation for the following quantification of histone post-translational modification states by scheduled PRM LC-MS/MS. A) Upper panel shows embryo stages taken for the following MS analysis. Lower panel illustrates a pipeline of mass spectrometry analysis of histone modifications from *Xenopus laevis*. Bulk histones are isolated from purified nuclei of embryos from the four sampled stages by acidic extraction and separated by SDS-PAGE. Propionylation blocks all endogenously unmodified and monomethylated Lysine residues from being cleaved in the subsequent trypsin digest, thereby creating an optimized peptide pool for mass spectrometry analysis. After propionylation, but before trypsin digest, we added to each sample a so-called R10 library, which consists of isotopically heavy-labelled Arginine peptides (R10). B) H3 and H4 histone N-tails and their tryptic peptides. C) Isotopically heavy-labelled Arginine with heavy Carbon13 and Nitrogen15 atoms.

In-gel propionylation results in propionyl groups covalently bound on the naturally unmodified and mono-methylated Lysine amino residues. Otherwise, the following trypsin digest would produce a subset of very small peptides that are inappropriate for the MS analysis. Due to the propionylation step, in the following text and graphs naturally unmodified Lysine residues are named as propionylated (p), for example, H3K4p — unmodified Lysine in position 4 on the histone H3.

The following step after propionylation, is in-gel trypsin digest. In principle, trypsin cleaves peptide bonds after unmodified Lysine and Arginine amino acid residues. Exceptions are modified Lysine residues or Arginine-Proline sequence, which are not cut by trypsin. In this work, we blocked naturally unmodified Lysine residues, therefore, trypsin cut only after

Arginine. Histone H3 and H4 tails represent entire proteins, after the Trypsin activity they are digested into so-called tryptic peptide (Fig. 14B). Almost every tryptic peptide carries one or several amino acid residues which can be found with different modifications on them. A certain combination of these modifications on a tryptic peptide forms a so-called modification state.

Isotopically heavy-labelled peptides (R10)

Our original protocol (Schneider *et al.,* 2011) suffered from the problem that histone modifications could only be quantitated in relative, but not absolute terms. Specifically, this may lead to an overestimation of changes for modifications, present at low abundance. To overcome this problem, we ordered a collection of tryptic peptides with the modification states of interest, in sequence of which the Arginine was labelled with stable heavy isotopes of Carbon (13) and Nitrogen (15) atoms (Fig. 14C). In the molecule of Arginine there are 6 Carbons and 4 Nitrogens that makes a shift in 10kDa compared to the light peptides. From this combination: heavy-labelled Arginine (R) with +10kDa in its mass, comes the abbreviation "R10".

R10 based control

There are three main criteria (dimensions), which are recorded during tandem mass spectrometry analysis: mass to charge ratio (m/z), intensity and retention time (Fig. 15A). Since the R10 peptides are synthetic analogues of their light endogenous forms, both forms elute from the chromatography column simultaneously (i.e. at the same retention time). Due to the shift in mass of 10kDa, they can be separated from corresponding endogenous peptides based on the m/z ratio. Application of the R10 peptides offers many advantages — it can be used for peak identification based on the retention time; it normalizes for ionization differences between peptides during the MS machine run; most importantly, one can calculate and compare the absolute fold-changes between histone modifications under different experimental conditions.

A

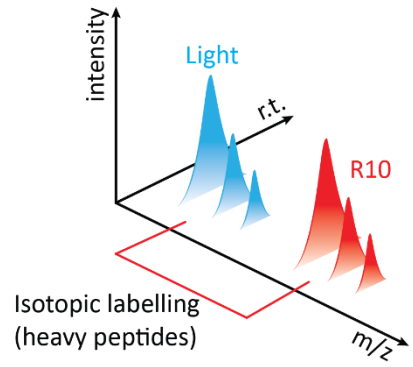

B

R10 library	H3	H4
Known mod. states	≈ 77	≈ 12
# peptides	59	6
Coverage	76%	50%

Figure 15. Application of the isotopically heavy-labelled R10 peptides. The individual R10 peptides are mixed in equimolar concentration and mimic 65 histone H3/H4 modification states. These isotopically heavy-labelled peptides serve as an internal and inter-sample control, allowing to minimize technical variations and to quantitate abundances of histone modification states on the absolute scale. A) Representation of the R10 spike-in peptide control. Each of the analyzed endogenous histone modification states has a synthetized R10 peptide analogue. Due to the same chemical properties, endogenous tryptic peptides and their R10 spiketide analogues elute at the same retention time (r.t.); however, they can be distinguished based on the mass to charge (m/z) ratio. Additionally, R10 spiketides help with peak identification based on retention time and detail fragmentation spectra for isobaric peptides. B) A table shows a rough estimate of amount of known histone PTMs on histone H3 and H4 tails if taking into account methylation, acetylation and phosphorylation; amount of R10 peptides in the library and an approximate coverage of the endogenous PTMs.

R10 library

The different R10 peptides were mixed at equimolar concentration and the resulting library was added to each analyzed histone sample, prior to the trypsin digest. The R10 library consists of 65 peptides, 59 of them representing different histone H3 modification states, and the remaining six reporting histone H4 modification states (Fig. 15B). Considering only confirmed methylation, acetylation and phosphorylation events on the amino terminal tails, the library covers of 76% of the histone H3 and 50% of the histone H4 modification states.

Overall, mixing this R10 library, which consists of 65 heavy peptides at equimolar concentration, with purified bulk histones from *Xenopus* embryos prior to propionylation and trypsin digest, provides us with an inter- and intra-sample control, which allows me to quantify the Intensity of the histone modifications on the absolute scale.

MS analysis method and the machine run

In order to identify and measure the abundance of the histone PTMs we used the method of scheduled parallel reaction monitoring (scheduled PRM) (Liebler and Zimmerman, 2013) on a QExactiveHF LC-MS/MS machine. This approach allows to isolate a target peptide ion based of the mass and retention time window, fragment it and analyze the masses of all fragment ions simultaneously (Fig. 16A). Therefore, we can distinguish and identify peaks

from isobaric peptides (tryptic peptides with different modification states but the same m/z ratio).

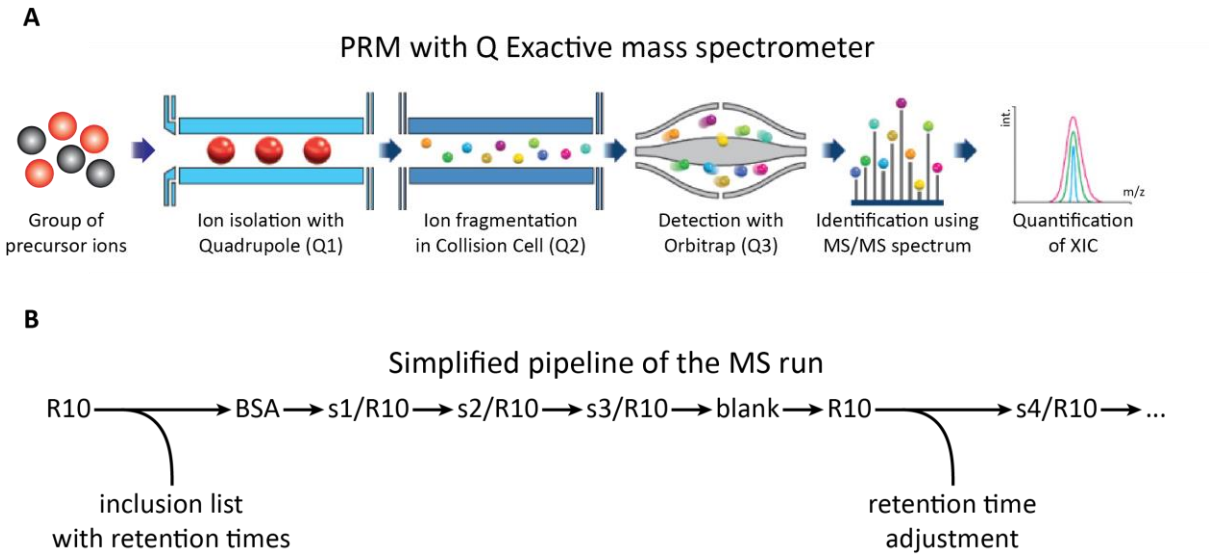

Figure 16. Upper panel A) depicts Parallel Reaction Monitoring (PRM), which is a targeted MS/MS analysis, in which full fragment ion spectrum of each precursor in a target list is recorded continuously throughout the entire LC separation. Q3 is substituted with a high-resolution mass analyzer (Orbitrap) to detect all target product ions. The scheme was adopted from Thermo Fisher web-page and modified, Q — quadrupole, int. — intensity, XIC — extracted ion chromatogram. Lower panel B) represents a simplified pipeline of the MS machine run.

To set the retention time windows for the scheduling, we first performed test runs with the R10 library only (Fig. 16B). During this procedure we repeatedly detected all 65 R10 peptides. Then the retention times of the peptides were estimated and introduced for the histone samples. The order of the samples was randomized and then they were grouped in triplicates with a quality control sample contacting BSA and another R10 only-sample in between.

Peak identification and quantification

During the mass spectrometer run tryptic peptides get charged (ionized), forming charged precursor ions; then they are fragmented into y- and b-ion precursor-specific fragments. During the MS run, data acquisition was performed on two levels: the MS1 level determines the intensity of the precursor ions, while the MS2 level detects the precursor-specific fragments.

In most cases, identification of the peaks corresponding to one or another modification state was performed based on the combination of the m/z ratio and retention time of the R10 sibling (Fig. 17A). A special case exists for so-called isobaric peptides, which share the same

m/z ratio but have different modification states. During the peak identification based the m/z ratio values, isobaric peptides appear as multiple peaks in the extracted ion chromatogram (Fig. 17B, C). Their identification is based on the distribution of the y- and b-fragments of the ion precursor peptides. In most cases, it is still possible to distinguish one isobaric peptide from another and quantify them based on the MS1 level, because at the chromatography step they elute at the different time. However, sometimes isobaric peptides co-elute, which makes it impossible to quantitate them individually without interference. In those cases, both their identification and quantification were done on the MS2 level by quantifying the abundance of the y- and b-precursor-specific fragments.

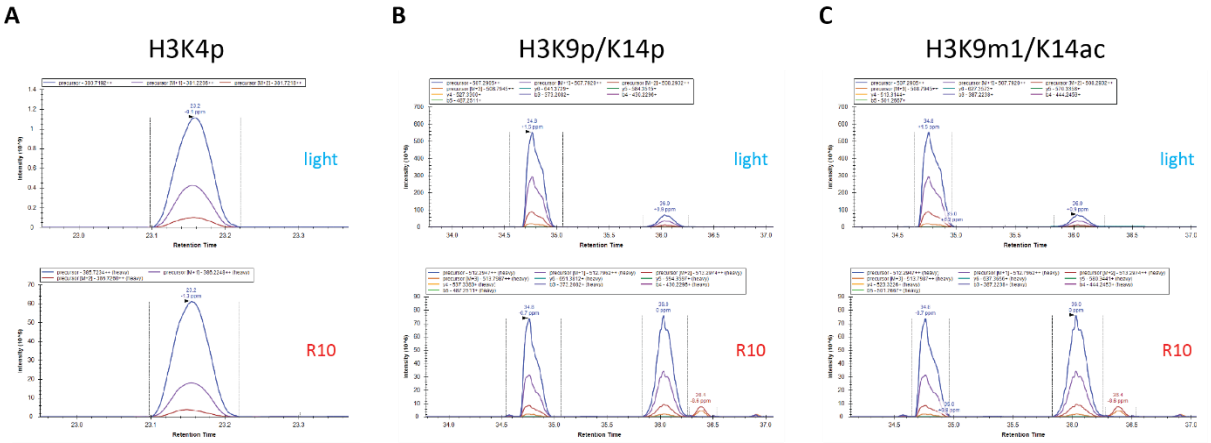

Figure 17. Examples of R10 spiketide-based peak identification in Skyline. A) Identification of a histone modification peak based on the retention time of the corresponding R10 spiketide. Upper panel: unmodified endogenous peptide aa 3-8 from histone H3 (light) in, lower panel: the corresponding H3K4p R10 spiketide (R10). Panels B and C: Distinction of isobaric peptides H3K9p/K14p and H3K9m1/K14ac with the same molecular weight 507,2905 Da by matching fragmentation spectra of the corresponding R10 spiketides. In B) light and R10 automatically selected left peaks for H3K9p/K14p; in C) light and R10 automatically selected right peaks for H3K9m1/K14ac.

Overall differences in the Mock and HUA epigenomes (PCA)

In the Experiment type A (continuous HUA treatment, Fig. 3), histone modifications were analysed from 4 developmental stages under 2 experimental conditions in 3 biological replicates. In total this sums up to 24 individual data sets, with 65 histone PTM intensities measured in each data set. Of note, hereafter, the K9m2/K14ac modification state on histone H3 was excluded from the following analyses, because its R10 sister peptide could not be quantitated consistently. We detected high fluctuations in the R10 peptide abundance and shifting retention time windows among the biological replicates. We suspect the irreproducible behaviour of this particular R10 peptide to be due to chemical instability.

PCA separates the data points

Before going deep into details of the behavior of individual modifications, we decided first to test, how the two experimental conditions were different from each other by principle component analysis (PCA) (Fig. 18). By definition PCA analyses a data table, in which observations are described by several inter-correlated quantitative dependent variables. Its goal is to extract the important information from the table, to represent it as a set of new orthogonal variables called principal components, and to display the pattern of similarity of the observations and of the variables as points in maps (Abdi and Williams, 2010). In our case the principle components could indicate changes in the absolute histone PTM intensities, obtained by normalization to their R10 analogues.

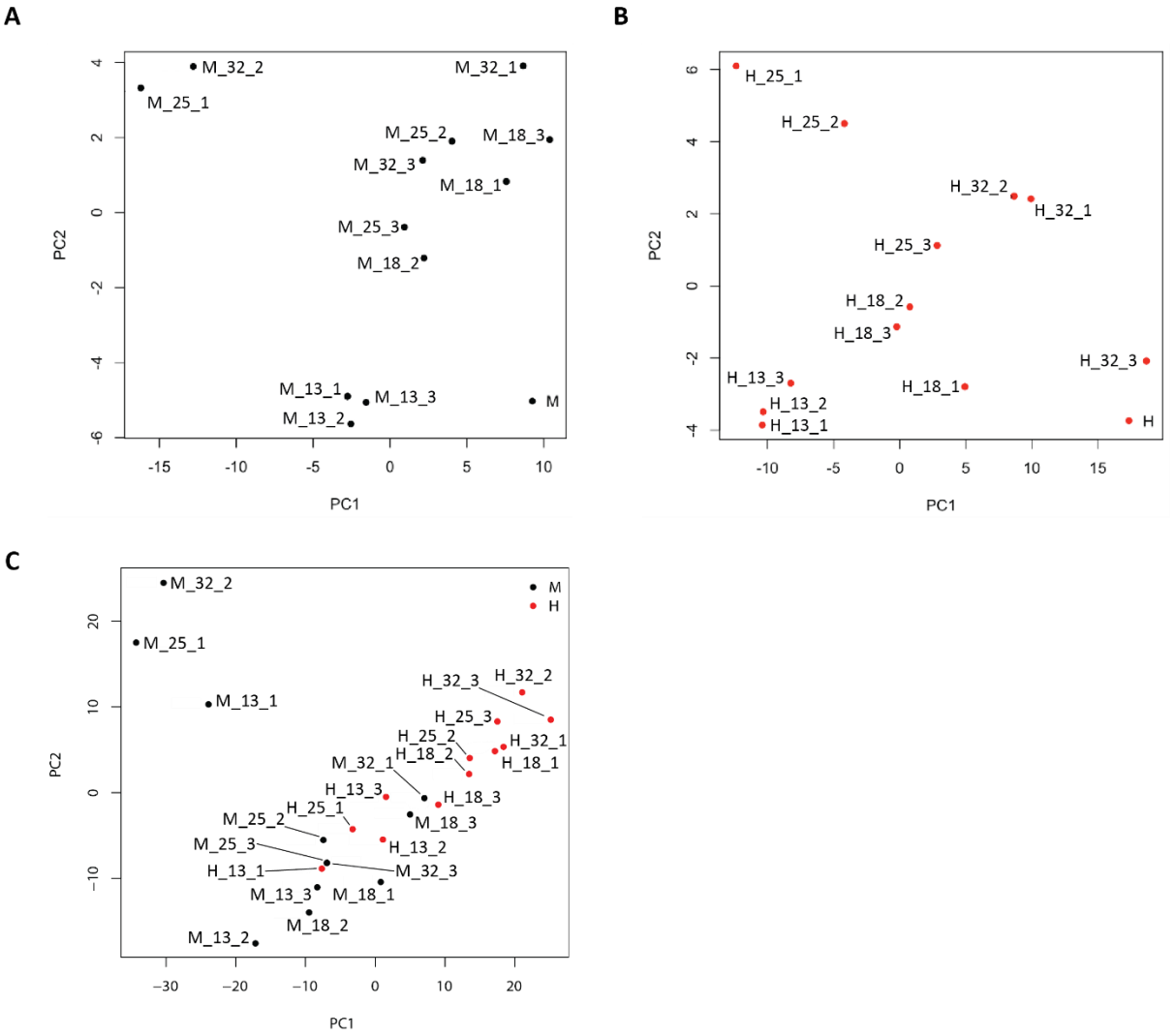

Figure 18. Principle component analysis (PCA) for Mock and HUA-treated HPMs. A) PCA on Mock treated samples only. B) PCA on HUA treated samples only. C) PCA on the Mock and HUA treated samples together. Each data point represents 65 modification states, measured by LC-MS/MS in PRM mode, with absolute abundancies calculated with R10 spiketide normalization. Mock and HUA data sets are partially separated, with younger HUA samples intermingling with older Mock samples.

We performed PCA on Mock samples and HUA samples both and separately, in order to see the distribution of the data points inside the experimental conditions, and together, to visualize a possible influence of the HUA treatment on the Mock condition (Fig. 18).

For the Mock samples, the data points were separated into three groups: outliers (top left corner), samples from the stage NF13 (bottom middle part), and the rest (top right area) (Fig. 18A). We did consider the first group as outliers because it consisted of two samples from two different stages NF32 and NF25, derived from two different biological replicates. Possibly, these samples contained the least material from all sample preparations. The PCA analysis was performed on the absolute intensities of the endogenous histone PTMs normalized to their R10 analogues, thus if the overall injected material in the mass spectrometer was considerably different from the other samples, on the absolute level it could lead to bigger differences plotted in the PCA. However, this did not influence the distribution of the relative histone modifications within individual tryptic peptides. The second group consisted solely of the three biological replicates of the NF13 stage. The third cluster grouped all other samples from stages NF18, NF25 and NF32. A relation between the second and the third groups might indicate that the epigenome matures in one major step between late gastrula (NF13) and mid-neurula, i.e. during the gastrula-neurula transition. The Individual PCA analysis on the HUA samples showed a less structured picture (Fig. 18B). We also found outliers (NF25 first biological replicate; NF32 second biological replicate), but in this case, they were not that distinctly apart from the others. Furthermore, the early NF13 samples grouped together in the bottom left corner, suggesting that even under systemic G1 arrest, the epigenome of the early stage remains different from later stages.

The comparison between Mock and HUA-treated samples by PCA gave an interesting result (Fig. 18C). As in the individual tests, we found three outliers from Mock treated samples NF13, NF25 and NF 32, from different biological replicates (top left corner). Mock and HUA samples clustered into two groups (middle right for mainly HUA and bottom middle for mainly Mock). Despite a decent separation of the Mock and HUA samples, there was an overlap detected. Older samples of Mock and younger samples from HUA were found in the overlapping territory. This might indicate that the epigenomes of younger HUA treated embryos was related to the epigenomes of older control embryos.

Stage-specific histone modification profiles

By performing mass spectrometry analysis as described above, we have detected quantitative changes in 64 histone modification states across 4 developmental stages under 2 biological conditions. The combination of all modification states at a certain developmental timepoint constitute a so-called stage-specific histone modification profile (HMP) (Schneider *et al.,* 2011). Given the differences in bulk histone modifications detected by PCA, we sought to investigate the impact of cell cycle arrest on embryonic chromatin on the level of HMPs.

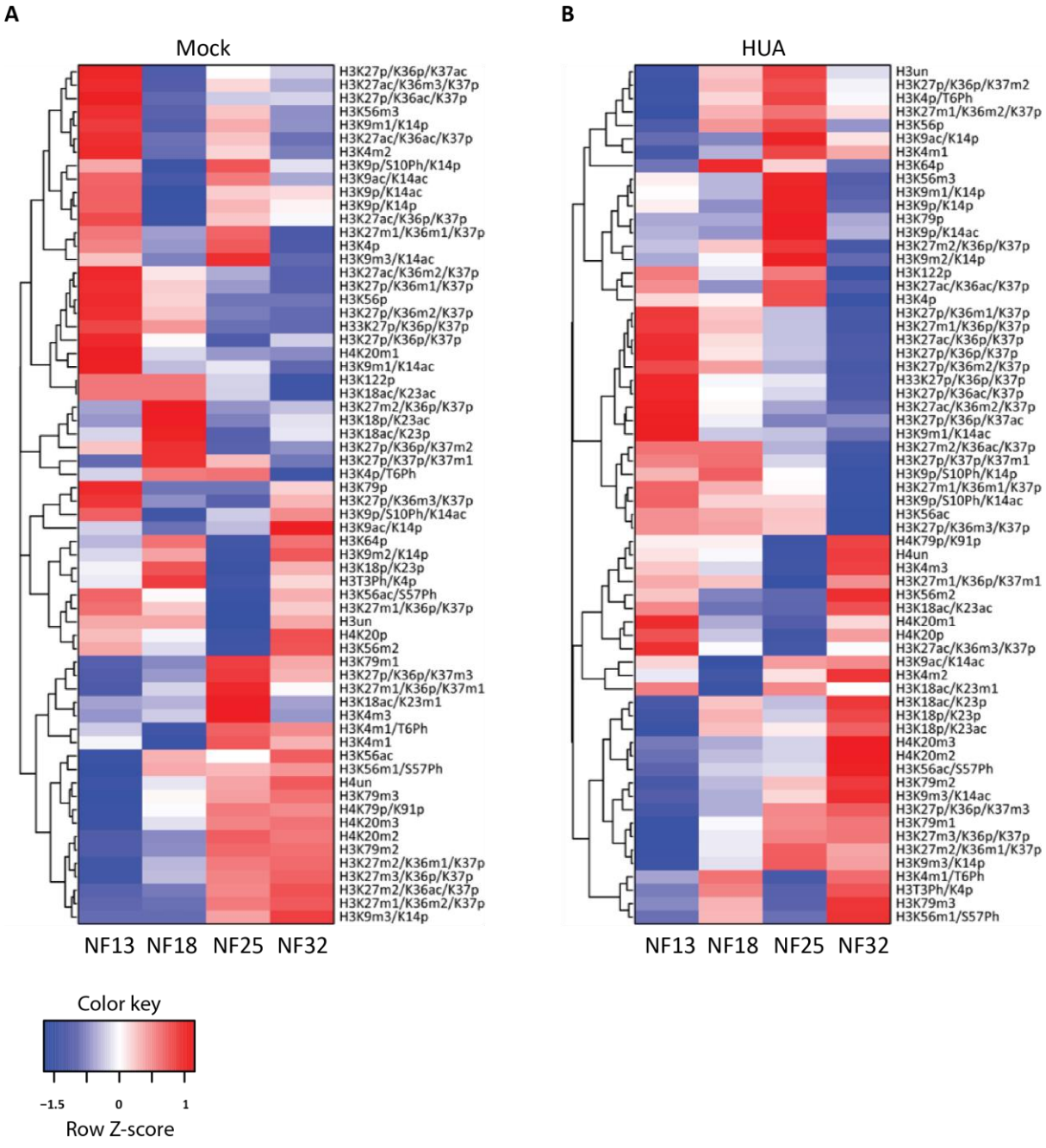

Figure 19. Two global absolute heatmapts representing HMPs derived from A) Mock and B) HUA embryos. Heatmaps of the absolute abundancies of individual histone modification states, normalized to the

corresponding R10 spiketides. Data in columns represent an average from 3 biological replicates/condition. Color key: row Z-score.

To visualize the changes in the HMPs, we performed a hierarchical clustering analysis (Fig. 19) and built stage-specific heatmaps for Mock and HUA samples either separately or together heatmaps. Importantly, the clustering was based on the absolute intensity values of endogenous peptides, normalized to the R10 spiketides.

Individual HMPs of Mock and HUA samples

Stage-specific histone modification profiles were initially described by our lab in 2011 (Schneider *et al.,* 2011). However, the MS detection method used here is different from the one used in 2011. Most importantly, we applied R10 peptides as standards, which allowed me to quantify absolute changes in modification abundance, rather than only relative changes measured in the earlier study. Additionally, due to the constraints of the HUA treatment, the analysed embryo stages differed between the two studies. Therefore, we should bear in mind, that a direct comparison between the two data sets is not possible. Despite these differences, the results derived from the Mock condition in our study resemble both structure and developmental trends of the stage-specific HMPs as described in 2011.

Similar to the previous results, HMPs were stage-specific in Mock as well as in HUA and they changed throughout development of the embryo (Fig. 19). These results, in particular for the Mock condition, resembling unperturbed, wild type-like embryos, corroborate the hypothesis of a developmental chromatin maturation. To emphasize the major differences between stage-matched embryonic chromatin in the two conditions, we have performed a hierarchical clustering analysis for Mock and HUA samples simultaneously and visualized the results in one “global” heatmap (Fig. 20).

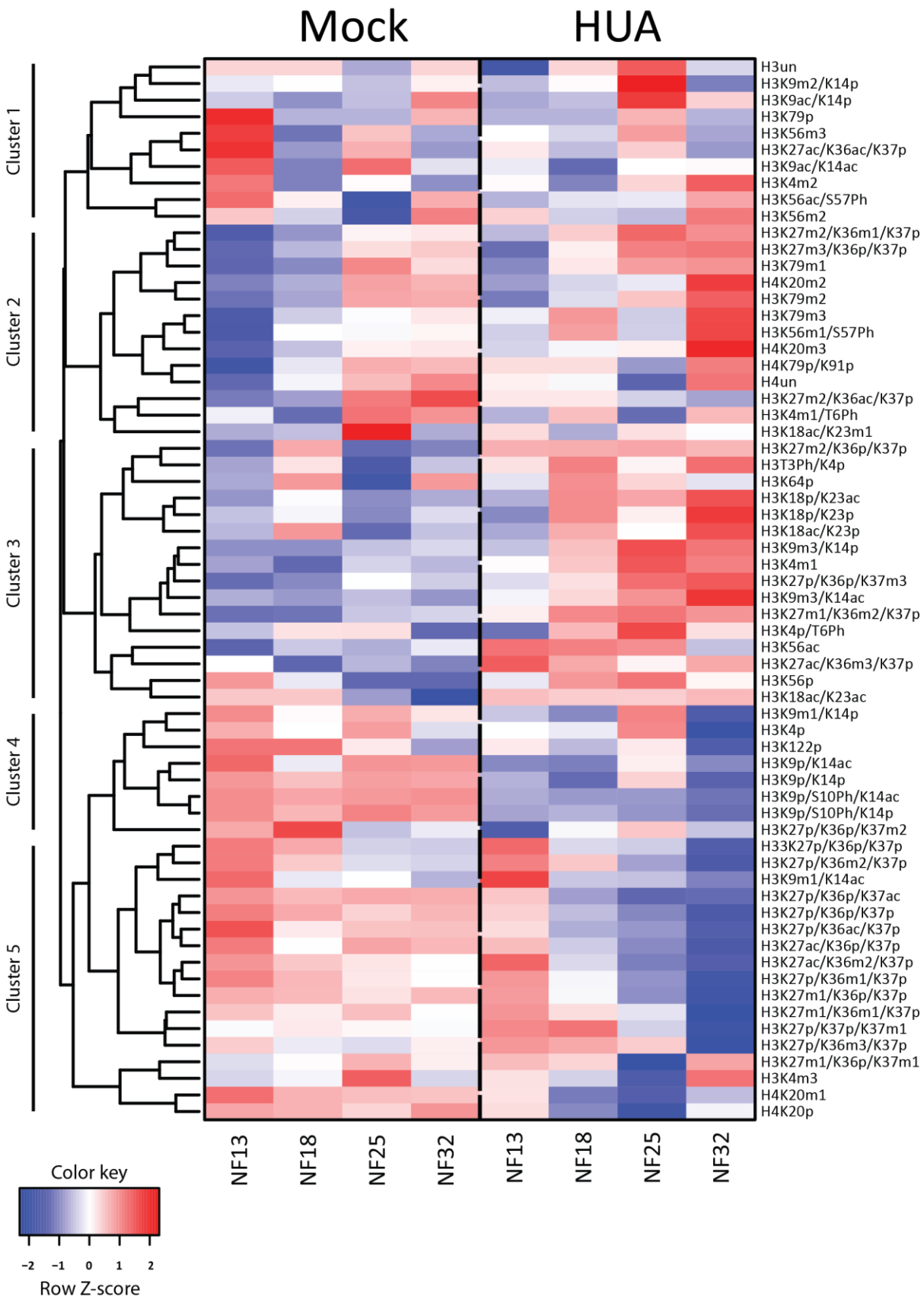

Figure 20. Mitotic activity shapes stage-specific histone modification profiles. Heatmap of the absolute abundancies of individual histone modification states, normalized to the corresponding R10 spiketides. Data in columns represent an average from 3 biological replicates/condition. Color key: row Z-score.

Global combined HUA and Mock heatmap

The first three levels of the dendrogram on the left axis of the heatmap reveal five clusters across the analysed development stages between the two experimental conditions (Fig. 20). The major features of these clusters could be described as follows:

Cluster 1, in the upper part of the heatmap, groups histone PTMs, whose abundance changes in control embryos from being enriched at either NF13 or NF25 to lower values at NF18 and NF32, respectively. In arrested embryos, several modifications enriched at NF25 while being low abundant at NF13, NF18 and NF32 in HUA.

Cluster 2 included modification states, which gradually increased their abundance in both conditions.

Cluster 3 included PTMs, which were overall at low level in Mock, however increased their abundance in HUA.

Cluster 4 and 5 represented highly abundant modification states in Mock, which became decreased upon HUA treatment.

In summary, these heatmaps visualize a global, stepwise maturation of the embryonic epigenome, particularly strong between the first and the later stages. As reported previously (Schneider *et al.,* 2011), the observed quantitative flux constitutes stage-specific histone modification profiles, where each profile is a list of histone modifications at their individual maximal abundance, which describe the four developmental stages that we analysed. Second, the differences observed in HUA and control embryos indicate that the cell cycle state — probably cell proliferation in general — is one parameter, which coordinates the developmental decoration of chromatin with covalent modifications.

Individual effects on selected histone marks

Absolute measurements gave us an overall picture of these chromatin dynamics. From the combined global heatmap it became clear that the HUA block perturbed the histone PTM profiles. However, it was still unclear how the histone modification states differed relatively to each other. To focus on this issue, we converted the absolute changes of individual histone modification states into changes in relative abundances in the context of individual tryptic peptides.

Each tryptic peptide came with a different combination of modification states on it. To estimate a relative abundance of one or another modification state, we summed all modification states which were specific to one tryptic peptide, and then calculated the percentages (Fig. 21, Fig. 22, Fig. 23). Having explained this, there were some exceptions. Four tryptic peptides (i.e. H3 aa 41-49, H3 aa 64-69, H3 aa 117-128, H4 aa 46-55) come only with one modification state, therefore, it was not possible to represent them relatively.

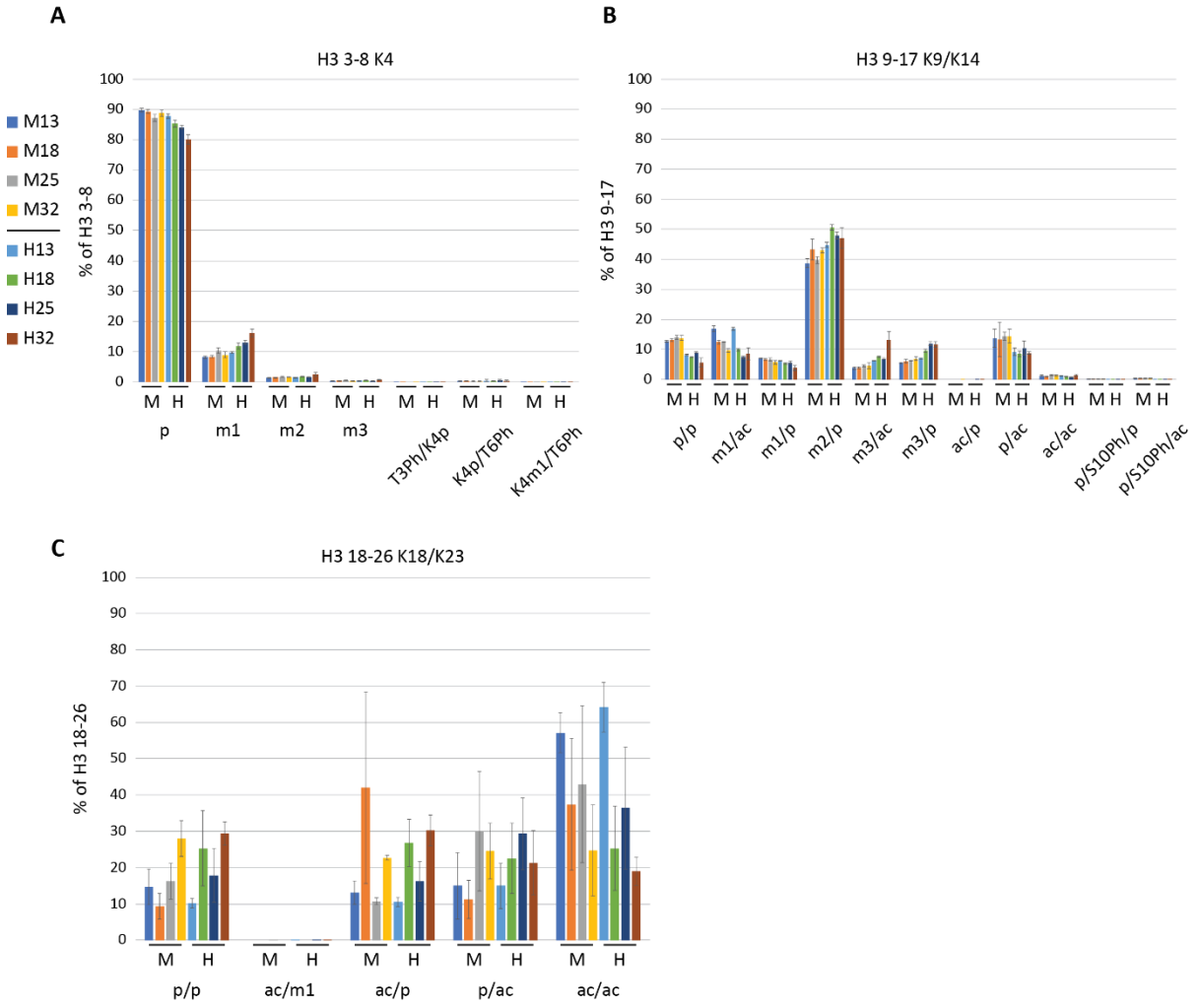

Figure 21. Relative histone PTM abundances in HUA and Mock treated embryos. Individual relative histone PTM distribution for histone H3 tail: A) aa 3-8 K4, B) aa 9-17 K9/K14, C) aa 18-26 K18/K23. Data are first normalized to R10 spiketide signals, then added up to 100% for all modification states measured for each specific tryptic peptide, from which the relative contribution of each state is then calculated. N=3 biological replicates/condition; mean ± s.e.m.

The following figures display the relative distribution of individual modification states on single tryptic peptides. The plots are arranged not in a function-dependent manner, but based on the sequence after trypsin digestion. The following example, dealing with the lysine in position 4 of the histone H3 tail, is used to illustrate, how these plots can be read (Fig. 21A).

This residue is part of the tryptic peptide aa 3-8, i.e. in short H3 3-8 K4. Different post-translational modifications are named as follows: propionylated (naturally unmodified) – p, monomethylated – m1, dimethylated – m2, trimethylated – m3, acetylated – ac, phosphorylated - Ph. In the vast majority of the tryptic peptides it is Lysine residues which are modified, if any other modified amino acid residue was detected on the same tryptic peptide, it is labelled individually under the corresponding bars in the plots as, for example, Threonine in position 3 – T3Ph/K4p.

Histone H3 K4

Both methylated and acetylated states of K4 on the histone H3 tail correspond to transcriptionally active chromatin. Di- and tri-methylation of K4 are tightly associated with the promoters of active genes (Barski *et al.,* 2007). A notable exception is K4m1, which is found on poised enhancers (Voigt *et al.,* 2013, Lauberth *et al.,* 2013).

The overall amount of the unmodified K4 in Mock embryos did not show a big fluctuation throughout development: it stayed rather constant in a range of 90-87% (Fig. 21A, Table "MS table Exp type A"). In contrast, HUA embryos demonstrated a gradual decrease in K4p abundance from the stage NF13 to NF32 from 88% to 80% respectively. Interestingly, the K4p decrease in the HUA condition was accompanied by an increase in the monomethylated state of K4 (K4m1) state from 10% to 16%. Mock embryos did not show a big amplitude in the K4m1 abundance, increasing only from 8% to 10%. The other two methyl states of Lysine 4 showed rather moderate changes of less than 2.5% (K4m2) or below 1% (K4m3). Finally, the abundances of several phosphorylation states associated with the H3 aa 3-8 peptide (i.e. T3Ph/K4p, K4p/T6Ph and K4m1/T6Ph) fluctuated together by less than 1%.

Overall, our results on the H3K4 modification states demonstrated that the cell cycle arrest allowed a maintenance of the active histone marks. The notable increase in K4m1, a mark found on the poised enhancers, can hint towards an increase of the poised enhancers.

Histone H3 K9/K14

Lysines 9 and 14 are both present on the tryptic peptide H3 aa 9-17. Additionally, on this peptide there is a Serine in position 10 which can be phosphorylated (S10Ph). Positions K9 and K14 can be methylated and acetylated. Depending on the modification state, different combinations can be a positive as well as a negative chromatin mark. H3K9 can turn genes on by getting acetylated (K9ac). H3K9ac also has a high co-occurrence with H3K14ac, together

they are the hallmarks of active gene promoters (Karmodiya *et al.,* 2012). Monomethylation of K9 (K9m1) is enriched at the transcriptional start site of active genes (Barski *et al.,* 2007). In contrast to the monomethylated state, di and tri- methylation of K9 (K9m2, K9m3) are often found at silenced genes and K9m3 is a prominent mark of constitutive heterochromatin (Lehnertz *et al.,* 2003). Acetylation of histone H3K14 (K14ac) regulates replication-depended nucleosome assembly and replicative aging and facilitates efficient activation of nearby replication origins (Feng *et al.,* 2016).

In our study, the most abundant modification state on histone H3 was K9m2/K14p (up to 51%) (Fig. 21B, Table "MS table Exp type A"). It gradually increased throughout development both in controls (from 39% to 43%) and HUA embryos, where K9m2/K14p was slightly more abundant (from 45% to 51%). An interesting behavior was detected for K9p/K14p (unmodified) and K9m3/K14p states. At all stages, the overall abundance of the unmodified state was lower in HUA samples (from 6% to 9%) compared to controls (around 13%), paired with a simultaneous increase in the heterochromatic modification K9m3/K14p. This mark was about twice as high in HUA samples (from 7% to 12%) compared to Mock chromatin (around 6%).

In contrast to observations in mammalian cell lines and Drosophila embryos, the PTM H3K9ac was never found alone on this peptide, but came always in combination with H3K14ac (i.e. K9ac/K14ac state) at nearly constant levels of about 1% in both conditions. Additionally, the H3K9p/K14ac state was somewhat more abundant in controls (around 14%) compared to HUA samples (around 9%). Another modification state of active chromatin, K9m1/K14p was detected at the level of around 7% in Mock with a very modest decrease in HUA up to 5%.

Finally, we detected two combinatorial modifications at abundant to moderate levels: continuously H3K9m1/K14ac, gradually decreasing from 17% to 9% in both conditions; and H3K9m3/K14ac, which increased from 4-5% of in controls to about 13% in arrested embryos. These last two modifications do not have an exact biological function. K9m1/K14ac might play an active role in transcription regulation, because monomethylation of K9 and acetylation of K14 individually are found on active loci. In contrast, the H3K9m3/K14ac modification state (approx. 4% abundance) was unexpected and in functional terms contradictory — K9m3 is a repressive, heterochromatic mark, while K14ac is correlated with gene transcription.

In short summary, the detected increase in K9m3 together indicated an over-accumulation of the repressive chromatin mark. However, the active transcription mark K9ac/K14ac remained stable, indicating of an ongoing, maintained transcription activity.

Histone H3 S10

Phosphorylation of S10 is known to be linked with the initiation of chromosome condensation in the late G2-phase and is also important for proper chromosome segregation at mitosis (Allison and Milner, 2003). Therefore, as in the ICC experiments described above, this modification reflects the mitotic cell population in the embryo.

In our study, H3S10 came in two flavors: as single modification on this peptide (i.e. K9p/S10Ph/K14p) and in combination with acetylated K14 (i.e. K9p/S10Ph/K14ac) (Fig. 21B, Table "MS table Exp type A"). Both of these modification states were low abundant, in comparison to the other modification states derived from the tryptic peptide aa 9-17. Nevertheless, in both modification states we detected a consistent and reproducible 10-fold decrease in HUA embryos, already at the first examined time point. This observation confirms that the cell cycle block is globally in place within 6 hours of inhibitor incubation.

Our finding here is consistent with the ICC staining on H3S10Ph mark of the HUA embryos (Fig. 5). Here we confirm by a different method that the embryos continuously incubated in the HUA solution from the stage NF10.5 had cell cycle arrested already at the first analysed stage NF13.

Histone H3 K18/K23

Along with Lysines 9 and 14, K18 and K23 are primary acetylation sites on histone H3. Acetylated K18 and K23 are involved in cell proliferation and correlate with transcription activation (Xue *et al.,* 2010).

Contrary to all other tryptic peptides, the aa 18-26 peptide showed a high variability among the biological replicates, resulting in large fluctuations throughout the analysed stages (Fig. 21C, Table "MS table Exp type A"). The maximal abundance reached 60% in case of the K18ac/K23ac double modification, the single modification states were detected between 10% to 30% on average. The K18ac/K23m1 modification state was absent from embryonic histones, although its R10 mimic could be measured with no problems. Interestingly, the

developmental fluctuations in acetylation of this peptide were observed in similar fashion for Mock and HUA condition.

Together with a stable level of K9ac/K14ac under the treatment, acetylation states of K18 and K23 indicated of an active transcription occurring in the cell cycle arrested embryos.

Histone H3 K27/K36/K37

There are three Lysines in the tryptic peptide H3 aa 27-40, corresponding to positions 27, 36 and 37. In theory, each of these residues can be mono-, di-, tri-methylated and acetylated. This gives a huge variety of different modification states with a lot of isobaric forms. However, not all theoretically possible modification states were ever detected *in vivo* or *in vitro*, e.g. acetylation of K37 or K27m3/K36m3 (Schneider *et al.,* 2011). Based on this knowledge, we decided to focus only on a subset of the possible states, which were discovered before (Fig. 22, Table "MS table Exp type A").

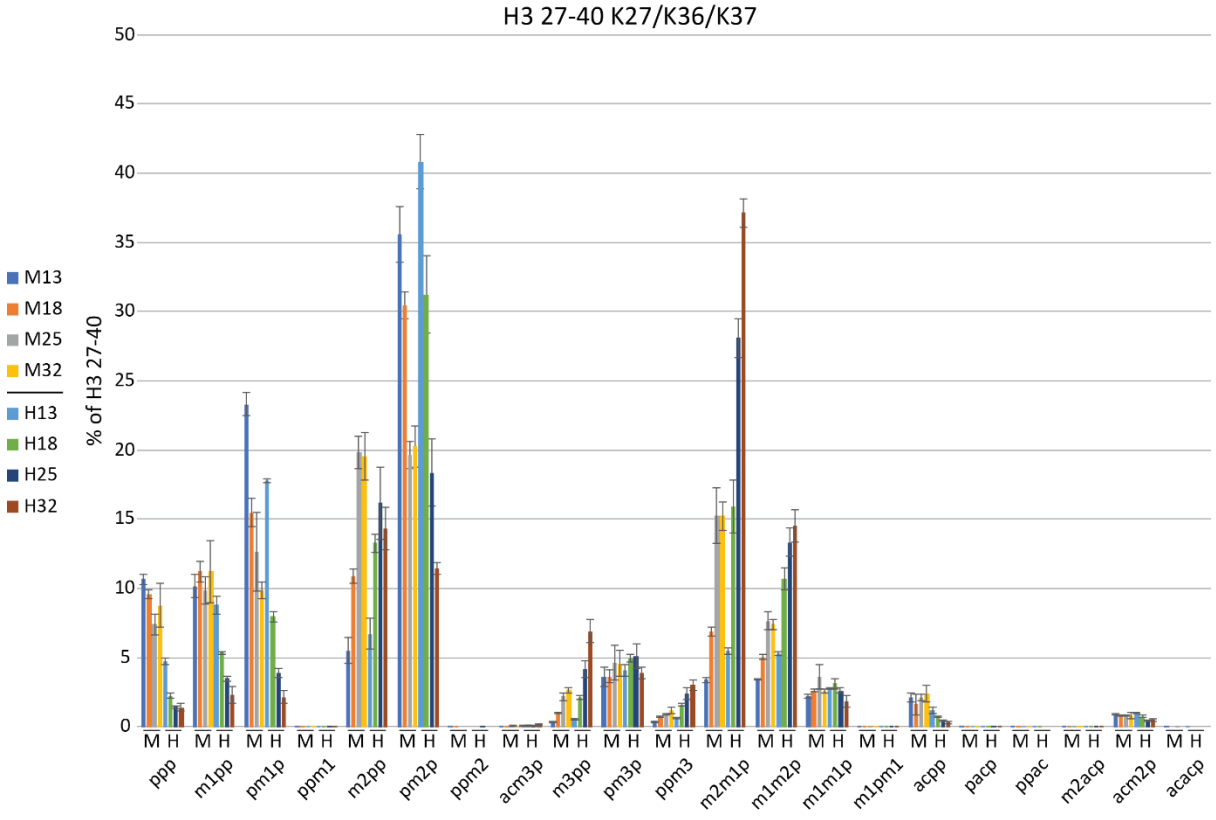

Figure 22. Relative histone PTM abundances in HUA and Mock treated embryos. Individual relative histone PTM distribution for histone H3 tail aa 27-40 K27/K36/K37. Data are first normalized to R10 spiketide signals, then added up to 100% for all modification states measured for each specific tryptic peptide, from which the relative contribution of each state is then calculated. N=3 biological replicates/condition; mean ± s.e.m.

The best studied and functionally annotated modifications occur on K27 of this peptide. The m1 state is associated with active promoters and positively affects transcription (Barski

et al., 2007). In contrast, dimethylated K27 is distributed broadly throughout the genome and is involved in silencing non-cell-type-specific enhancers (Ferrari *et al.,* 2014). Its abundance is only exceeded by the dimethylated H4 K20 modification (see below). Finally, trimethylated K27 is tightly associated with inactive genes, most notably developmental regulatory genes, via Polycomb Repressive Complex 2 (PRC2). Ezh2, an active subunit of PRC2, methylates Lysine 27 of histone H3 (H3K27m) (Boyer *et al.,* 2006, Bracken *et al.,* 2006, Cao *et al.,* 2002, Czermin *et al.,* 2002). Acetylation of K27 is antagonistic to the gene repression by H3K27m2/m3 and is associated with active transcription (Tie *et al.,* 2009).

We detected unmodified K27 state (K27p) with a mild fluctuation and a tendency to decrease during development (from 11% to 8%) in Mock embryos. In the HUA-treated samples, the overall abundance of K27p was reduced and the decrease was more prominent from 5% at the stage NF13 down to remarkable 1% at the stage NF32. The monomethylated state of K27 (K27m1) remained more or less constant around 10% in Mock embryos, but decreased rapidly in HUA from 9% at NF13 to 2% at NF32. In contrast, dimethylation of K27 (K27m2) showed a prominent increase in both conditions during development, namely from 6% to 20% in controls, and from 7% to 16% in HUA embryos respectively. Also, the trimethylated K27 state (K27m3) increased seven- to ten-fold during development in control (from 0.4% to 3%) and HUA embryos (from 0.6% to 7%). The acetylated form of K27 (K27ac) mildly fluctuated around 2% in Mock embryos and rapidly decreased in the HUA from 1% to 0.3%. Thus, the different modification states of H3K27 showed one of the largest fluctuations in development and differences between Mock and HUA conditions.

As many other Lysine residues, also the one in position 36 of H3 can become mono-, di, or tri-methylated and even acetylated. Dependent on the specific nature of modification, the underlying chromatin is endowed with different functional properties. Methylated K36 is found on transcribed gene bodies, a reflection of the fact that the responsible HMTs are loaded onto Serine 2-phosphorylated (i.e. elongating) RNA POL II (Sims *et al.,* 2004). There is a shift from mono-, to di-, to tri-methylation from the promoter to the 3' end of active genes (Barski *et al.,* 2007). Acetylation of K36 (K36ac), similarly to other common H3 acetylation, plays a role in transcriptional activation and is predominantly found at promoters of RNA POL II-transcribed genes (Morris *et al.,* 2007).

The monomethylated state of K36 (K36m1) decreased continuously from medium levels in Mock (from 23% to 10%) and, much more strongly, in HUA embryos (from 18% to 2%). Unexpectedly, dimethylated K36 (K36m2) was the most abundant modification found on this peptide in HUA-treated gastrula, but decreased during further development from 41% to 11%. In Mock embryos, the K36m2 state was also highly abundant initially, however, it decreased mainly between first and third stage, i.e. NF13 to NF25 (from 36% to 20%), while remaining constant until NF32. In contrast, trimethylated K36 (K36m3) was detected at much lower levels (around 4%) and displayed no prominent fluctuation over time and between conditions. Finally, the acetylated form of K36 (K36ac) was detected in every analysed sample, however, with an abundance below 0.02%.

Among the combinatorial modification states, which are present on the tryptic peptide aa 27-40, the profiles of K27m1/K36m2 and K27m2/K36m1 were the most dynamic. Both modification states gradually increased during embryonic development. Additionally, they showed an overall increase in abundance upon HUA. For instance, K27m2/K36m1 showed an increase from 3% to 15% in Mock, but from 6% to 37% in HUA embryos. Thus, the amplitude of the developmental increase was higher in both absolute value and fold-change under the HUA condition. Similarly, K27m1/K36m2 increased from 3% to 8% in controls, but from 5% to 15% in HUA embryos. In contrast, the double mono-methylated state (K27m1/K36m1), was present in about 3% of histone H3 proteins throughout development and was not altered by the cell cycle arrest.

The other modifications on this peptide, including mono-, di-methylation and acetylation of K37, as well as the combinatorial modifications K27m1/K36p/K37m1, K27m2/K36ac, K27ac/K36m3 and K27ac/K36ac were detected only at a very low levels (<0.2%) with two exceptions. These were K37m3 and K27ac/K36m2. With regard to K37, trimethylation was the only state found constantly in all samples and it showed a three- to four-fold developmental increase in both conditions (Mock: from 0.4% to 1.2%; HUA: from 0.7% to 3%). The other exception is K27ac/K36m2, which was detected with a developmentally constant abundance of about 1% abundance in both conditions.

A complex tryptic peptide aa 27-40 consisted of many modification states including methylation and acetylation of K27, K36 and K37 with different combinations. The most notable changes were detected in K27m1, a mark of active promoters; K27m3, a mark of

inactive promoters and repressed developmental genes; K27ac, a mark associated with active transcription; and two modification states marking actively transcribed genes, K27m1/K36m2 and K27m2/K36m1.

Altogether, a decrease in K27m1 and K27ac marks alone together with an increase of K27m1/K36m2 and K27m2/K36m1 might indicate of a lower amount of active promoters, which however still might be active and initiated transcription. A progressive increase in K27m3 modification state upon HUA might indicate of a quicker shut down of the developmental genes compared to Mock.

Histone H3 K56

The Lysine in position 56 of histone H3 is mainly known for its acetylated form. K56ac is found at the replicative induced DNA damage sites (Abshiru *et al.,* 2013).

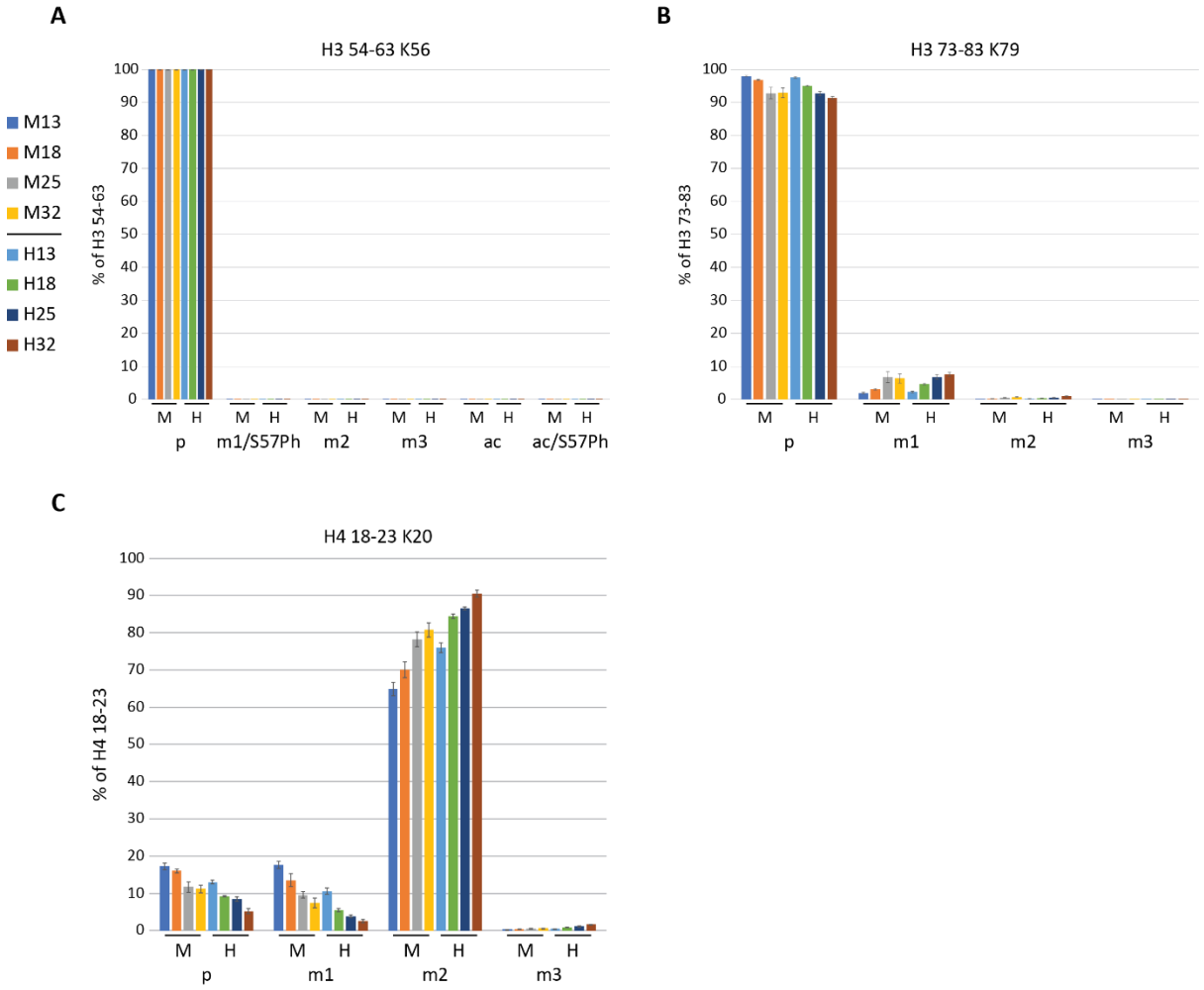

Figure 23. Relative histone PTM abundances in HUA and Mock treated embryos. Individual relative histone PTM distribution for histone H3 tail: A) aa 54-63 K56, B) aa 73-83 K79, and for histone H4 tail in C) aa 18-23 K20. Data are first normalized to R10 spiketide signals, then added up to 100% for all modification states measured for

each specific tryptic peptide, from which the relative contribution of each state is then calculated. N=3 biological replicates/condition; mean ± s.e.m.

We probed for 6 possible modification states on the tryptic peptide H3 aa 54-63, which includes K56 (Fig. 23A, Table "MS table Exp type A"). The Lysine residue was almost exclusively fond unmodified (K56p) up to 99.97% in both Mock and HUA. Mono-, di-, tri-methylation states together with acetylation was found at a very low levels, not higher than 0.03%.

We found very low, close to absence, levels of K65ac in both conditions, indicating no replication stress neither HUA nor in control embryos.

Histone H3 K79

The tryptic peptide aa 73-83 contains the Lysine residue in position 79 (K79). Monomethylated K79 marks enhancer regions and may facilitate interactions between enhancers and their target promoters. Di- and tri-methylation of K79 (K79m2 and K79m3) have been reported to be associated with transcriptional elongation and DNA repair. Furthermore, K79m2 may be enriched on mammalian origins of replication (Fu *et al.,* 2013).

Here, we found unmodified K79 (K79p) as the most abundant among the 4 possible states (Fig. 23B, Table "MS table Exp type A"). During development K79p decreased from 98% to 93% in Mock and had the similar tendency in HUA (from 98% to 91%). Only a small fraction of the H3 tails was monomethylated at K79, in contrast to the unmodified state. K79m1 increased during development from 2% to 7% in both experimental conditions. Dimethylated form of K79 (K79m2) showed similar to the K79m1 state increase throughout the analysed stages, however, with much lower abundance from 0.1% to 0.7% in Mock and from 0.2% to 1% upon HUA. Trimethylated state of K79 (K79m3) was found at all stages in both experimental conditions, however, with maximal 0.002% abundance.

A mirror-like behavior of K79m1 state could indicate of a relatively same amount of enhancer regions in both Mock and HUA embryos.

Histone H4 K20

Like all Lysine residues, H4K20 can be mono-, di-, or tri-methylated; some recent studies reported that K20 can be acetylated as well. The different H4K20 methylation states are found on specific locations in the genome. K20m1 is associated with transcriptional activation and has been reported at gene promoters activated by canonical Wnt signaling, while other

studies connotate it with gene repression (Asensio-Juan *et al.,* 2012, Wang *et al.,* 2014, Nishioka *et al.,* 2002, Oda *et al.,* 2009). It is strongly connected to the cell cycle, because the responsible HMT PR-Set7/SET8 protein is stabilized in S-/G2-phase (Wang *et al.,* 2008, Jorgensen *et al.,* 2013). Dimethylation of K20 (K20m2) is one of the most abundant marks on chromatin which plays role in silencing genes (MacAlpine and Almouzni, 2013), it is also believed to be important for marking points of origin for DNA replication (Kuo *et al.,* 2012). Trimethylated state of K20 (K20m3) is associated with repression of transcription, when present at promoters (Wang *et al.,* 2008), as well as in silencing of repetitive DNA elements, particularly retrotransposons (Schotta *et al.,* 2004, van Kruijsbergen *et al.,* 2017).

In this study, dimethylation of K20 was found as the most abundant modification state in the tryptic peptide aa 18-23 (Fig. 23C, Table "MS table Exp type A"). We detected a fluctuation of K20m2 abundance from 65% at stage NF13 up to 81% at stage NF32 in control embryos. In the G1-arrested embryos, K20m2 demonstrated a comparable developmental increase, however, at slightly elevated levels: from 76% at stage NF13 up to 91% at NF32.

In contrast, the unmodified and monomethylated states of K20 decreased throughout development under both experimental conditions. Specifically, K20p dropped from 17% at late gastrula to 11% in Mock tadpoles, while going from 13% to 5% abundance in HUA-treated embryos. K20m1 decreased from 18% to 7% in controls, respectively from 11% up to 3% under HUA.

The repressive K20m3 state was the least abundant modification of this peptide. We confirmed its increase over the developmental time course (Schneider *et al.,* 2011), which ranged from 0.3% to 1% in controls, and at slightly higher levels from 0.5% to over 2% in G1-arrested embryos.

Together with other repressive marks, K20m2 showed an increase upon HUA which might lead to a more closed chromatin state in general. The highest relative increase was detected in K20m3 (ratio heatmap) state, and together with an increase in the other negative mark K27m3 it might indicate of a faster maturation of the embryos under the experimental condition.

Epigenome maturation in embryos developing with an arrested cell cycle

The absolute quantification of histone modification states from different embryonic stages confirmed and extended our hypothesis of a developmental maturation of the chromatin interface (Schneider *et al.,* 2011). The global absolute heatmaps, generated from normalized raw data, give a directly comprehensible image of the global histone modification dynamics – each stage represents a unique pattern of individual modification abundancies, which most likely represent genome usage modes linked to phases of embryonic development. In addition, calculating the relative distributions of histone PTMs on individual tryptic peptides helped to scale these dynamics by telling the most (e.g. H3K27me2, H4K20me2) and least abundant (e.g. H3 K56 and K79 methyl states) modification states found overall. These tools and graphs, however, are complex and make it difficult to comprehend changes in chromatin dynamics, when comparing two experimental conditions.

In order to analyse, how much the cell cycle arrest in G1 has influenced these HMPs, we have generated a ratio heatmap of relative histone modification abundancies for selected histone marks. In a first step, the relative distributions of the selected modification states were calculated in percentages within each tryptic peptide. Then, the values from the HUA-treated chromatin were divided by the Mock values from mock treatment to produce the relative fold change between the two conditions. Then, the results of the division step were Log10 scaled and the color key was generated based on the Log10 scale. Numerical values in the cells indicate a fold-change between Mock and HUA conditions at a given stage. For example, values greater 1.0 indicate an increase of this modification under the HUA condition, whereas values smaller 1.0 indicate a lower abundance compared to Mock treatment. The results are shown in Figure 24, where we focus on modifications of amino acid residues with well-described biological functions.

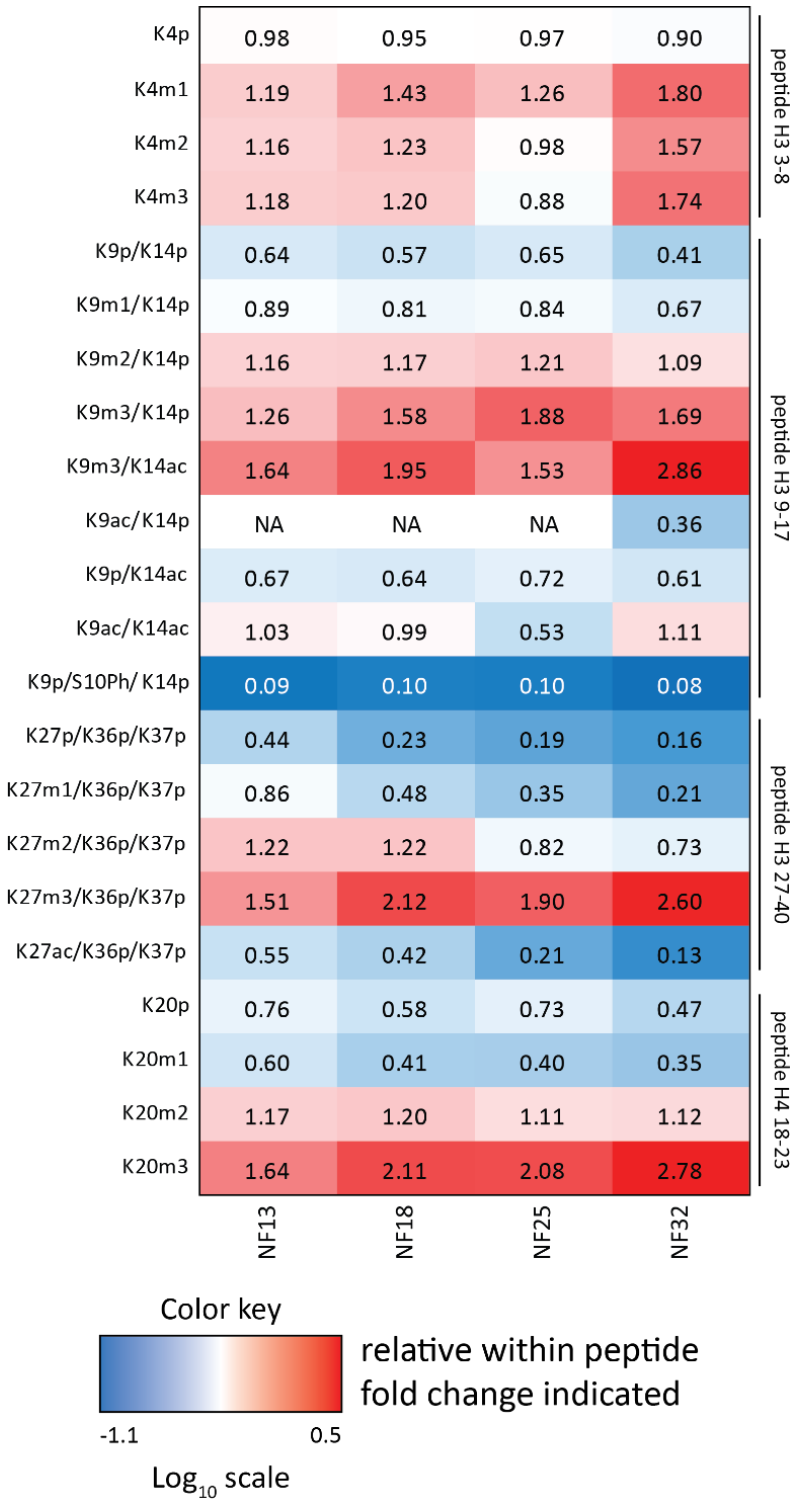

Figure 24. Ratio heatmap of relative histone modification abundancies for selected histone marks. In a first step, the relative distributions of the indicated modification states were calculated in percentages within each tryptic peptide. Then, HUA values were divided by Mock values to produce the relative change for each histone modification state between the two conditions. Color key is based on Log10 scale. Numerical values in the cells indicate the fold-change. Values greater 1.0 indicate an increase in HUA condition, values smaller 1.0 indicate a higher abundance in Mock condition.

The relative ratio heatmap confirms the permanent nature of the G1/S cell cycle arrest from the earliest to the latest assessed stage by revealing at least a 10-fold reduction of the mitotic chromatin mark H3S10phospho. Furthermore, it suggests that the absolute number of active promoters, marked by H3K4m2/m3, is not reduced, apparently even slightly

enhanced, which might be one of the reasons, whereby so many different tissues and cell types can be formed and maintained under the HUA-arrest.

Among the modifications, which are strongly reduced by HUA-treatment, are the acetylated states of K9 and K27 on histone H3. These modifications are thought to prevent the writing of repressive methylation marks on enhancer and promoter regions. Not surprisingly, the biggest winners in the HUA condition are indeed the trimethylated states of histones H3 K9, K 27 and H4 K20. They become globally elevated by more than 2,5-fold in the embryos, whose cells are arrested at the late G1-phase.

Overall, this study demonstrates that global manipulations of *Xenopus* embryos in the HUA solution is an efficient way to block the cell cycle of the embryos. Permanent block had consequences not only on the morphological aspects of the embryo development, but also was seen on the level of chromatin, by altering stage-specific histone modification profiles. The changes in the HMPs were visible in the overall picture as well as in the individual histone modification dynamics. Additionally, the current state of MS technology together with our experimental setup allowed us to assess the changes in the HMPs on the absolute level with very high reproductivity among the biological replicates.

Reversibility of HUA-dependent cell-cycle block

The key questions, arising from the embryological and chromatin analyses of HUA-arrested embryos, pertain to the issues of toxicity and causality. We decided to address these questions by asking, whether cell-cycle arrested embryos can return towards “normogenesis”, when the inhibitors are being removed again.

To this end we conducted the experiment, described as type B “HUA wash out” in Figure 3. In short, a cohort of embryos, treated with HUA from stage NF10.5 on, was split into two subpopulations at stage NF13. At this time point, the cell cycle arrest has been fully achieved (see Fig. 5 and Fig. 20). One half of the embryos remained further in HUA, while the other half was washed and returned to Mock treatment. In parallel, sibling embryos were constantly cultured in Mock condition (see Fig. 3).

Embryo survival and morphology in HUAwo condition

In a first step, we compared the survival rate of sibling embryos, cultured in parallel under Mock, continuous HUA and HUAwo condition (Fig. 25A). In each of four biological

replicates, washing out the inhibitors at NF13 significantly improved the survival rate. While this rate was compromised until stage NF25, comparable to continuous HUA siblings, it recovered and reached nearly the survival rate of Mock embryos at stage NF32.

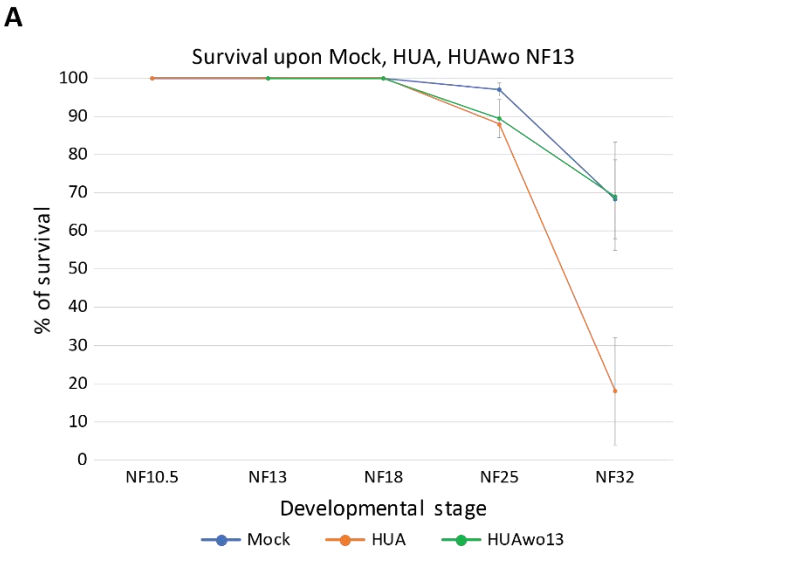

Figure 25. HUAwo embryos demonstrate better viability compared to continuous HUA. A) Embryonic survival curves under Mock, HUA and HUAwo condition. Data from N>3 biological replicates/condition; mean ± s.e.m. B) Recovery of the morphological hallmarks in the HUAwo experiment, reappearance of eye and postanal tail structures.

In addition, morphological hallmarks also recovered towards normal in HUAwo embryos (Fig. 25B). Unlike continuously HUA incubated embryos, the HUAwo group frequently developed postanal tails of nearly normal lengths, a clearly distinguishable fin surrounding trunk and tail, and, finally, eyes with well-developed retinal cups and lenses. These findings indicate that the major morphological defects of the HUA arrest are reversible.

The cell cycle block is reversible

The recovery in the HUAwo experiment differs markedly from the original report from Harris and Hartenstein, which had found that HUA removal at the tadpole stage did not ameliorate the morphological deficits of HUA-treated embryos. One explanation for these discrepant results could be that embryo are able to reinitiate cell proliferation at neurula, but not at the tadpole stage.

To test, if upon inhibitor removal cells can reinitiate the cell cycle, we stained siblings of the three experimental conditions for the H3S10P mark (Fig. 26A). The results confirmed an

increase of H3S10Ph positive cells on the HUAwo embryos. However, from the pictures it was not clear to what extend the recovery occurred. To address this, we calculated the number of mitotic cells and visualized it in the boxplots (Fig. 26B). Already at NF18, the first time point assessed after HUAwo, numbers of H3S10P positive cells were significantly increased compared to continuous HUA embryos. This means that mitotic activity has reappeared within 4 hours. At the endpoint of the experiments, mitotic cells were equally abundant in HUAwo and Mock conditions, indicating full recovery of the mitotic activity within 13 hours after inhibitor removal. Interestingly, we have not observed an overshoot in H3S10Ph positive cell numbers, suggesting that the embryos did not can not compensate for the absent cell proliferation under the initial HUA block (based on the normal cultivation conditions described in Nieuwkoop and Faber, 1994).

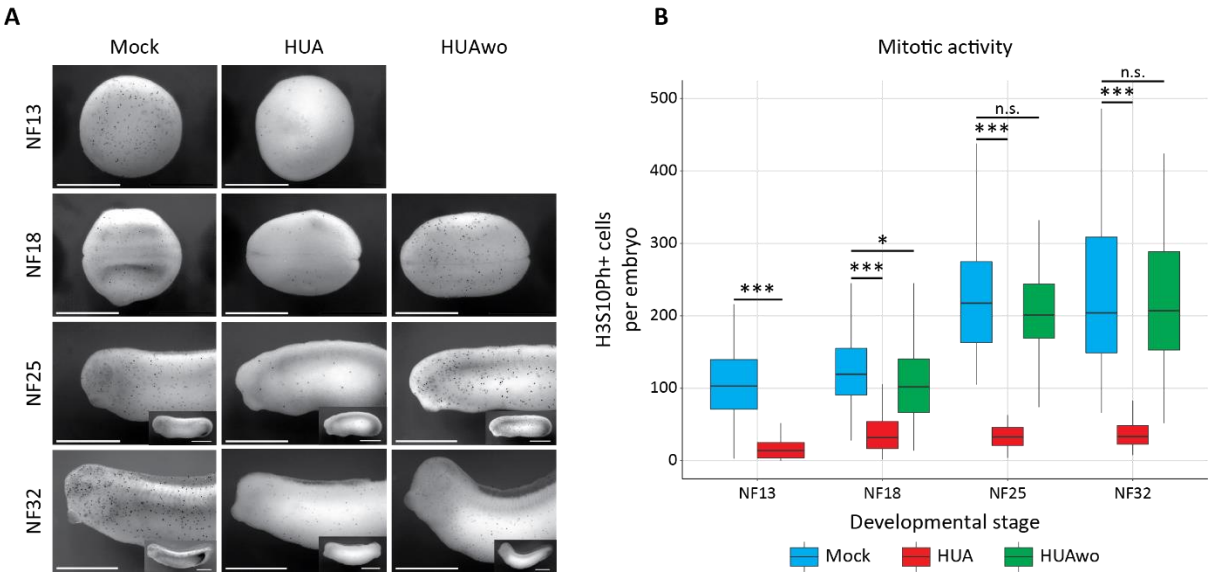

Figure 26. Recovery of mitotic activity in HUAwo embryos. Embryos, which have been transiently incubated in HUA solution and are mitotically arrested, were placed in Mock solution at NF13. A) Immunocytochemical staining (ICC) for the mitotic histone mark H3S10Ph at indicated stages. Mitotic cells are marked by black dots. Elongated, older embryos are recorded as anterior halves, i.e. at same magnification as younger stages, and in whole mount views as inserts. Scale bars: 1mm. N=3 biological replicates/condition. B) Abundance of mitotic cells in Mock, HUA treated, and HUA wash-out (HUAwo) embryos. Box plots based on H3S10Ph-positive cells present on the recorded surface of embryos (N=3 biological replicates/condition; mean ± s.e.m.; Student's t-test [unpaired, two-tailed]; *** p<0.001; * p<0.05; n.s. — not significant).

Differentiation recovery upon HUAwo

After these promising results, which indicate a morphological recovery of HUAwo embryos, we asked, whether also gene expression programs become normalized? This was again tested by whole mount RNA *in situ* hybridization. To this end, we have concentrated on those marker genes, which were missing under continuous HUA block (Fig. 27). The results

for the Mock and continuous HUA conditions in this new series of experiments were indistinguishable from the first series, shown in Figures 8-12, and are included again for comparison.

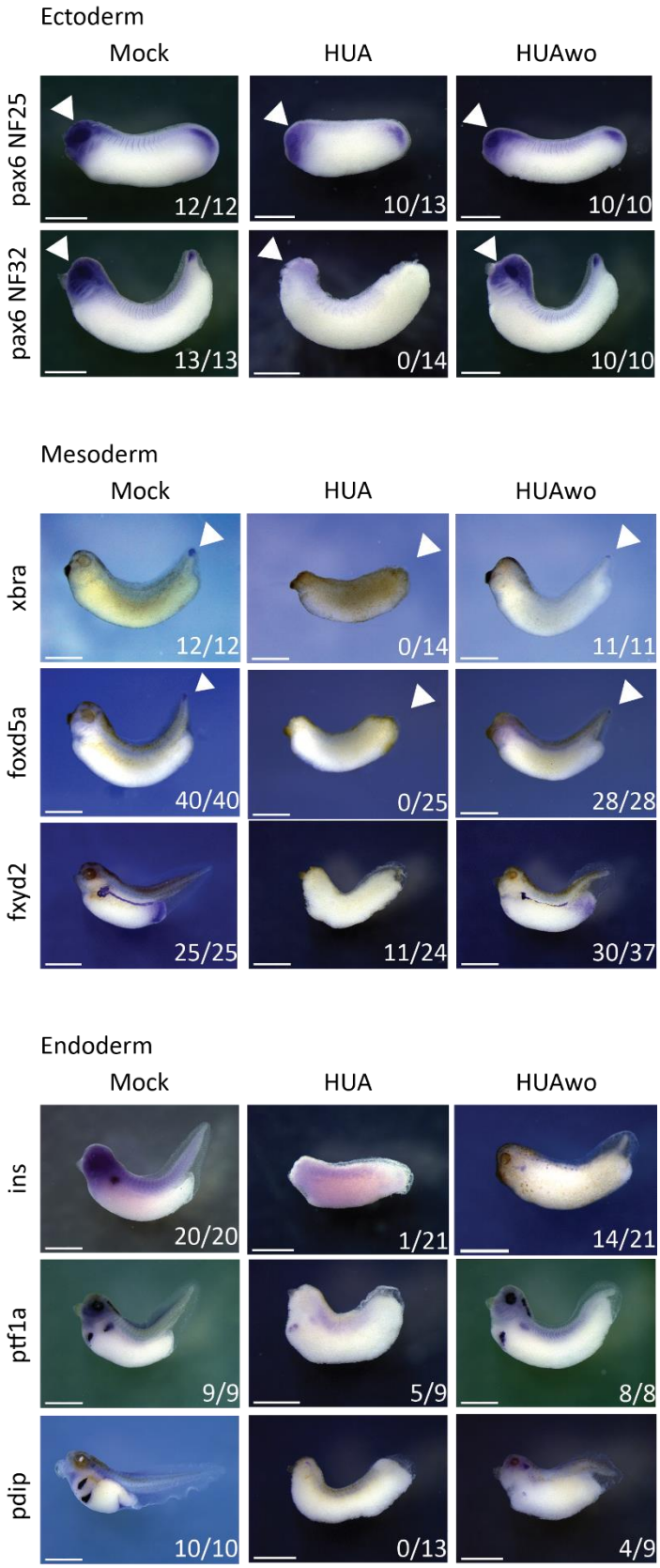

Figure 27. The HUA effects on embryogenesis are reversible. Morphological and molecular features of embryos at early tadpole stage. In contrast to continuous HUA treated embryos, HUAwo embryos regain eye cups, fin and tailbud structures. The upper panel represents ectoderm specific markers, the middle panel represents mesoderm specific markers, the lower panel represents endoderm specific markers. In all examples tissue-specific gene marker expression is recovered in the HUAwo embryos. Numbers indicate embryos positive for the marker over the total number of analyzed embryos (N=3 biological replicates/condition). Scale bars: 1mm.

Ectoderm specific markers

The ectoderm specific marker *pax6* was tested at two different stages, i.e. NF25 and NF32 (Fig. 27 Ectoderm). *Pax6* is mainly expressed in brain and eye regions in later *Xenopus* development. Like before (Fig. 9), the probes stained cells in the proper region at NF25, irrespective of the experimental condition. At stage NF32, however, pax6 mRNA was undetectable under continuous HUA treatment, while both gene expression domains were visible in HUAwo embryos.

Mesoderm specific markers

The marker genes *xbra*, *foxd5a* and *fxyd2* were used to assess the presence of mesodermal tissues and organs (Fig. 27 Mesoderm, arrowheads). At tadpole stage, *xbra* and *foxd5a* are expressed in the tail tip, while the *fxyd2* gene is active in the pronephros. Expression of all three genes was restored in HUAwo embryos, which also revealed a near wildtype like length for tail and trunk. Notably, the *fxyd2a* staining pattern was much improved over continuous HUA embryos, although it did not resemble the Mock state. This suggests a partial, but not full recovery of kidney differentiation.

Endoderm specific markers

In the case of endoderm, we examined the pancreatic marker genes *pdip*, *ptf1a* and *ins* (Fig. 27 Endoderm). Both *pdip* and *ptf1a* are expressed in the dorsal and ventral pancreatic buds. Later during development, these two pancreatic progenitors form an adult organ (Horb *et al.,* 2003, Afelik *et al.,* 2006, Jarikji *et al.,* 2007). Transcription of the first two markers was significantly recovered upon HUAwo, either with full (pdip: 100%) or somewhat lower penetrance (ptf1a: 44%). Strikingly, about two-thirds of the HUAwo embryos expressed insulin (67%), in contrast to 4% for continuous HUA treated embryos. Altogether, our results suggested that a transient cell cycle arrest from NF10.5 until NF13 had a minor influence on the developmental program of an endoderm derived organ such as pancreas.

Late physiological observations in the HUAwo condition

Continuously treated HUA embryos were touch-sensitive, but heart differentiation and heartbeat were severely reduced. Video-recordings of HUAwo embryos reveal a near normal heart contraction frequency, compared to Mock embryos (see “HUAwo heartbeat” video) as well as control-like flight response behavior (see “HUAwo flight response” video). Although we have not investigated this by gene expression, the large improvement in contractility must be accompanied by a significant restoration of cardiac muscle differentiation.

Stage-specific histone modification profile of the HUAwo embryos

Finally, we asked if also the histone PTMs restore their abundancies upon inhibitor removal? It has been shown before that some histone modification enzymes present in the cell during certain cell cycle phases. For instance, PR-Set7, which catalyzes H4K20me1 (Beck *et al.,* 2012), oscillates during the cell cycle, and regulates chromatin condensation and mitotic progression (Wang *et al.,* 2008). Since the HUA treatment blocks the cell cycle at the G1 to S phase transition, we assumed that different modifications would show different types of behavior. Theoretically, this could involve full or partial recovery of PTM abundancies; no response; or with an over- or undershoot increasing the HUA-induced perturbation even further.

To assess the reversibility of histone PTMs we performed mass spectrometry analysis on Mock, continuous HUA, and HUAwo embryos for the stage NF32. The results were visualized again in heatmap (Fig. 28), based on the normalized, relative values of histone PTM abundances. This allowed us to identify all three predicted behaviours: a group of PTMs, which reverts either fully or partially to their normal abundancies found in mock embryos; a second PTM group, which remains unaffected by the shift from HUA to HUAwo condition; and finally, a third group of PTMs, whose abundancies were altered in the same direction as they differ between HUA and mock conditions (“irreversible” changes). To estimate histone PTM dynamics in more detail, we decided to build bar plots with relative abundance of individual histone modifications within corresponding tryptic peptides (Fig. 29, Fig. 30, Fig. 31).

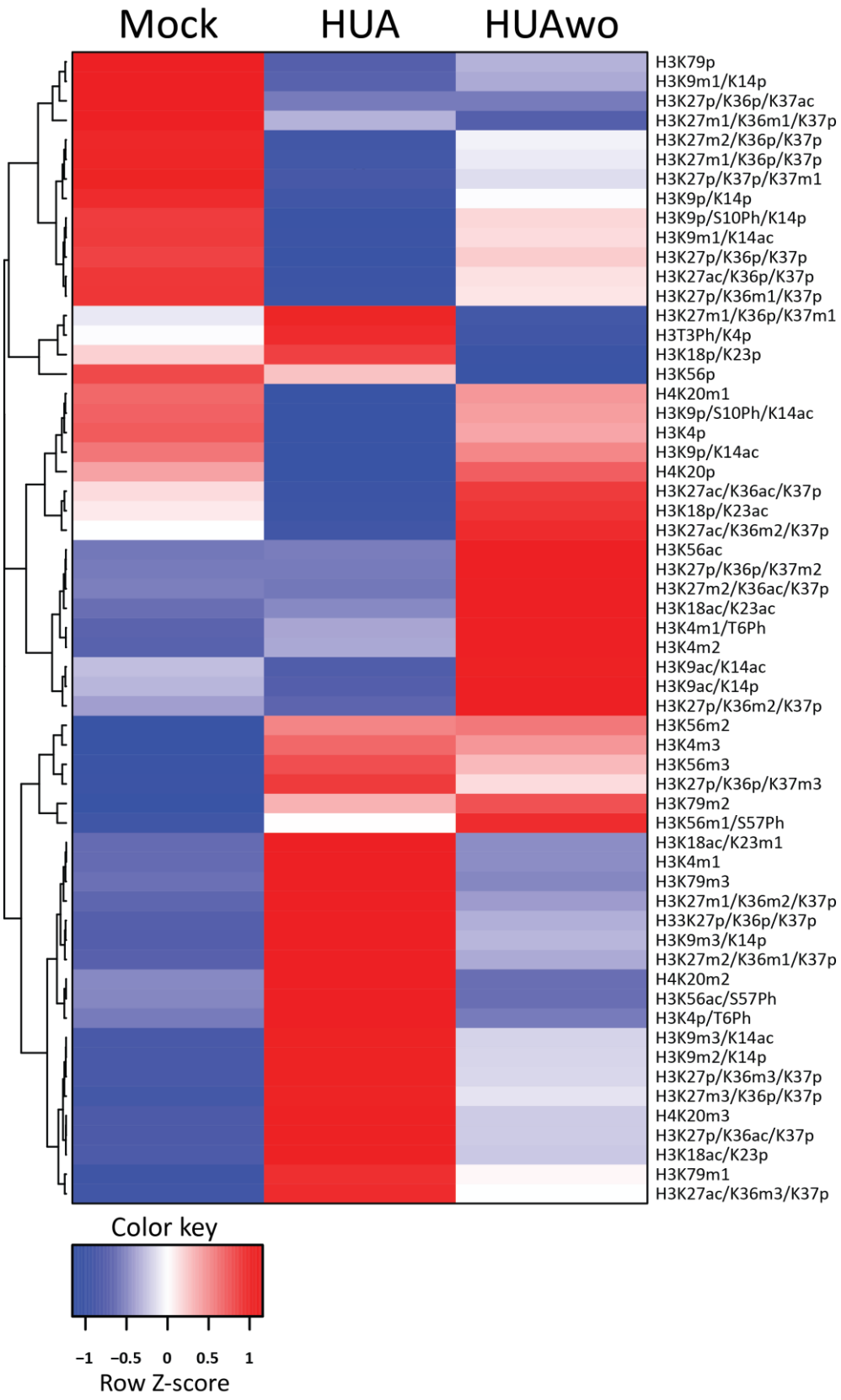

Figure 28. HMP changes are reversible. Heatmap of the relative abundancies of individual histone modification states under the indicated conditions. As before, the relative distributions of the indicated modification states are calculated in percentages within each tryptic peptide. Data in columns are collected from early tadpole stage embryos (N=1) independently from the data of Experiment type A. Note: relative differences between Mock and HUA samples of Experiment type B are highly similar to the results of Experiment type A. Color key, row Z-score.

Histone PTMs, which recover towards normal levels

The full or partial recovery group could be split into two distinct types of dynamics, based on the direction of the abundance fluctuation: positive and negative recovery. Positive recovery describes histone PTMs, whose abundance was decreased by HUA treatment, but reverted towards more normal abundancies, when the drugs were removed at stage NF13. Following the same logic, we defined a negative recovery group: histone modification, whose abundancies first increased upon HUA treatment, but decreased again in the HUAwo condition. Surprisingly, the majority of the analysed histone modification states fell into this group (41/64 PTMs, i.e. 64%). Notably, the modification states H3S10Ph, H3K27m1/m2/ac and H4K20 belonged to the positive recovery group (Fig. 29B, Fig. 30, Fig. 31C, Table "MS table Exp type B"); while H3K4m1, H3K9m3, H3K27m3 and H4K20m2/m3 to were among the negative recovery group (Fig. 29A, B, Fig. 30, Fig. 31C, Table "MS table Exp type B").

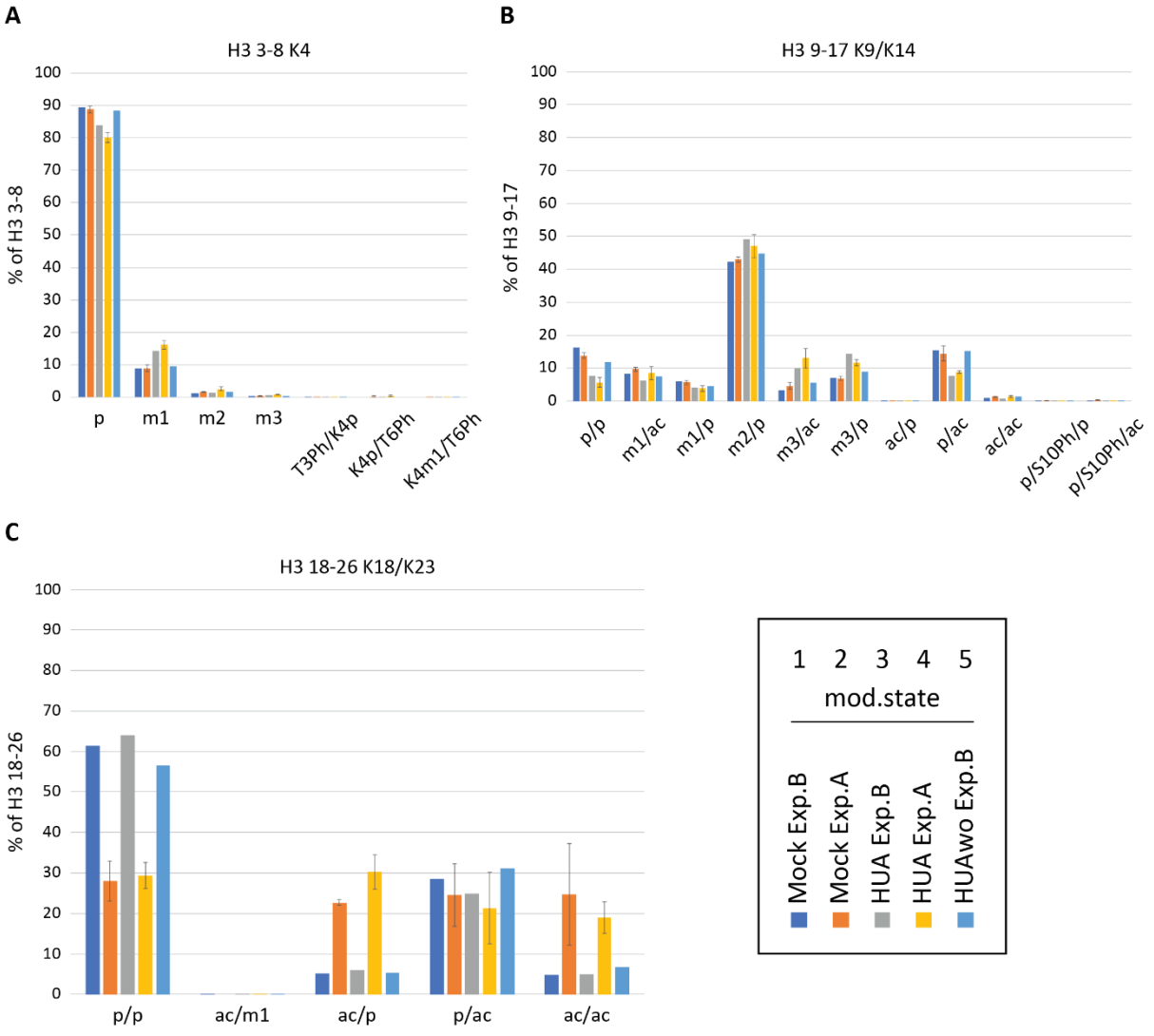

Figure 29. Comparison of relative histone PTM abundances from Experimental series type A and B. Relative PTM abundancies were calculated as described in Materials and Methods. A marked scheme illustrates the

arrangement and color coding of sample types for each modification state, simplifying the evaluation of similarities and differences between the three conditions from two experimental types. In the plots are results from histone H3 tail A) aa 3-8 K4, B) aa 9-17 K9/K14 and C) aa 18-28 K18/K23.

The “No recovery” group consisted of (3/64 modifications make up for only 4.6%) of the analysed modification states and comprised of H3K4m3, H3K27m1/K36m1 and H3K37m3/ac modification states (Fig. 29A, Fig. 30, Table “MS table Exp type B”).

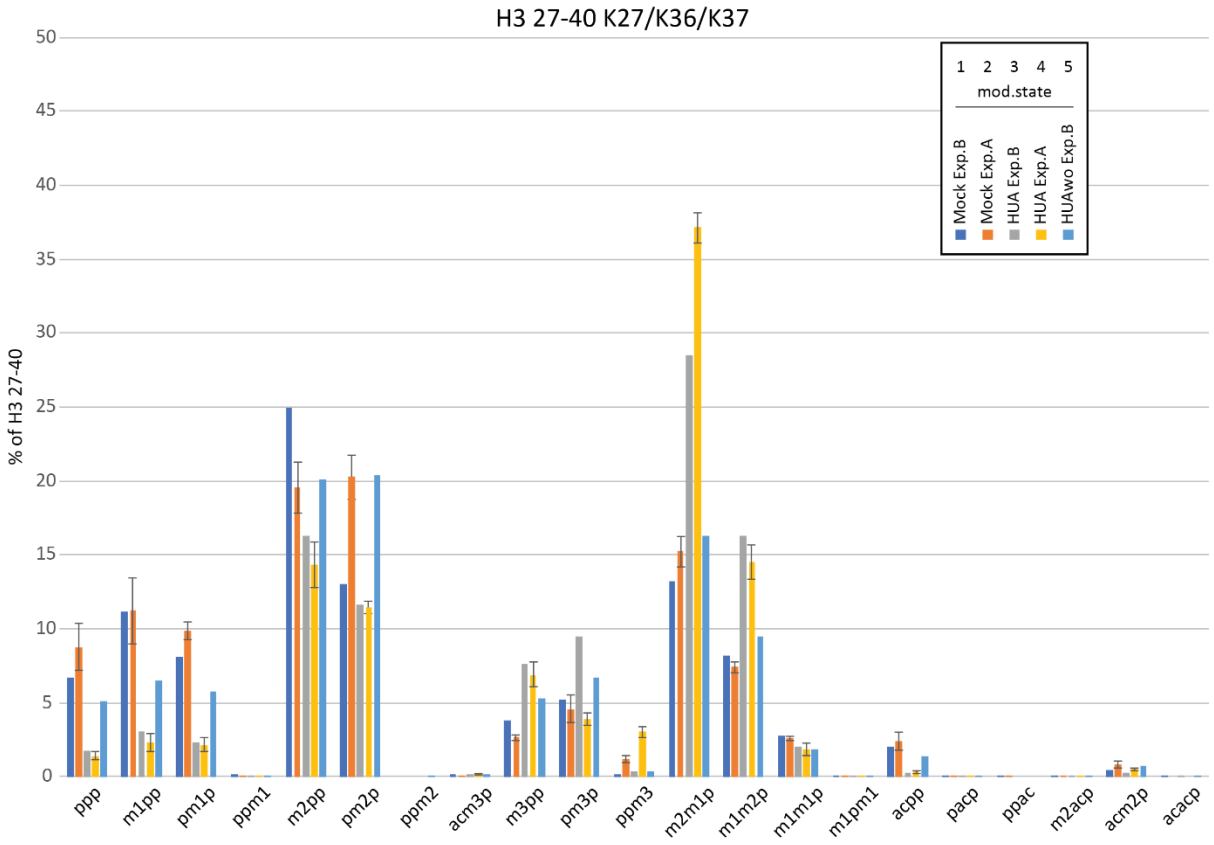

Figure 30. Comparison of relative histone PTM abundances from Experimental series type A and B. Relative PTM abundancies were calculated as described in Materials and Methods. A marked scheme illustrating the arrangement and color coding of sample types for each modification state, simplifying the evaluation of similarities and differences between the three conditions from two experimental types. In the plot are results from histone H3 tail aa 27-40 K26/K36/K37.

In contrast, we detected H3K4m2, H3K9ac and H3K14ac modification states to be in the group with irreversible changes of their abundance. This category made up for 26% of all analysed histone modifications (Fig. 29A, B, Table “MS table Exp type B”).

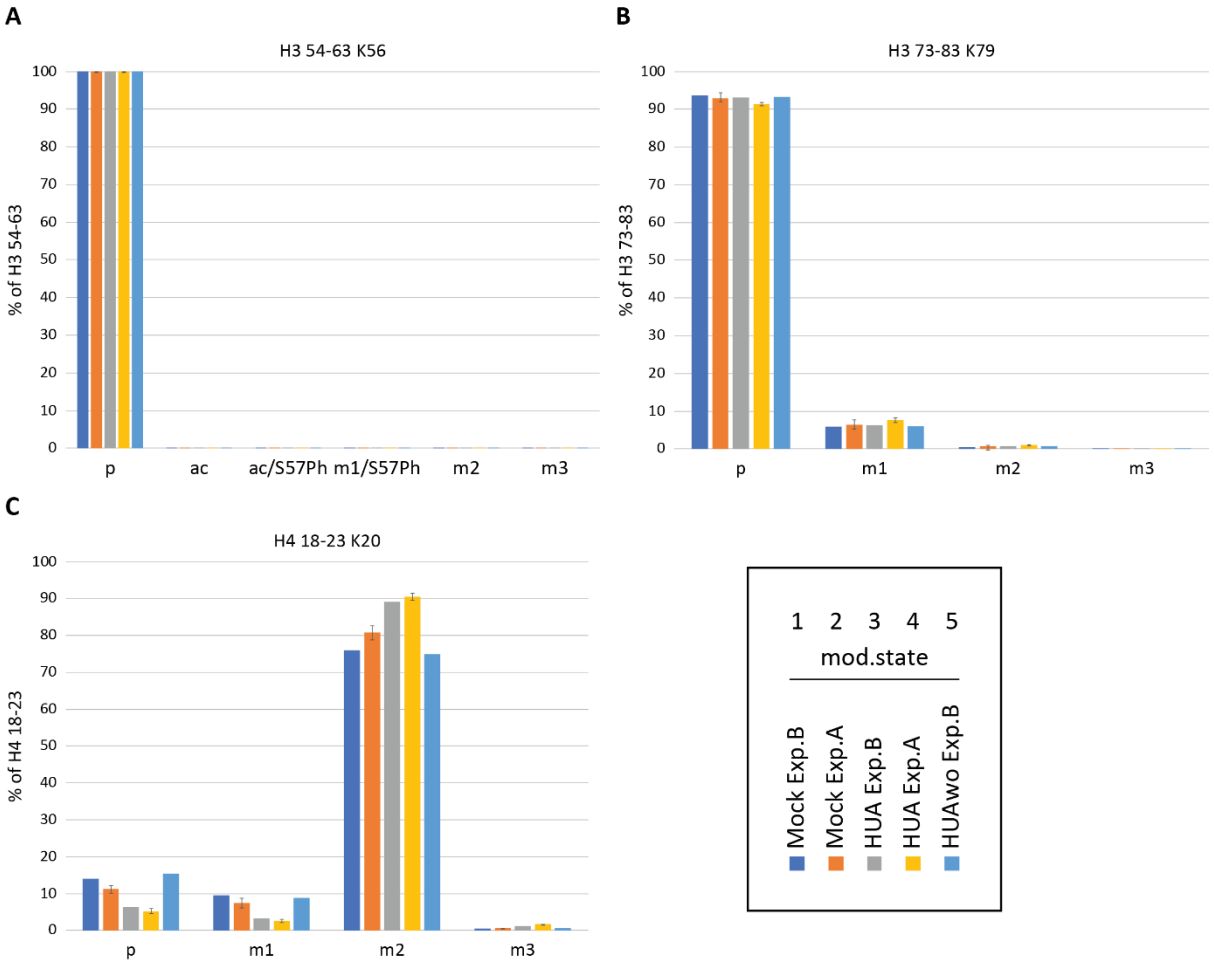

Figure 31. Comparison of relative histone PTM abundances from Experimental series type A and B. Relative PTM abundancies were calculated as described in Materials and Methods. A marked scheme illustrating the arrangement and color coding of sample types for each modification state, simplifying the evaluation of similarities and differences between the three conditions from two experimental types. In the plots are results from histone H3 tail A) aa 54-63 K56, B) aa 73-83 K79, and C) histone H4 tail aa 18-23 K20.

To estimate the extent of recovery, we decided to build up a ratio heatmap (Fig. 32). First, the relative distributions of the indicated modification states were calculated as percentages within each tryptic peptide. The relative values were presented as ratios between sample pairs indicated on top, showing the relative change for each histone modification state between the two conditions. The color key is based on Log10 scale. Numerical values in the cells indicate the fold-change. As in Figure 24, values greater 1.0 indicate an increase in HUA condition, values smaller 1.0 indicate a higher abundance in Mock condition. Color and numerical values in the cells of the first two columns illustrate the similarity between Experiment type A and B, the information in the third column shows the similarity between HUAwo and Mock samples. Notably, well known repressive chromatin marks, such as K9m3, K27m3, K20m2 and K20m3, demonstrated a tendency to revert to a

normal, Mock-like abundance, despite them having responded already to the HUA condition. This finding might suggest that the repressive marks, which play an important role in development could, maybe indirectly, prevent a normal differentiation especially of the late developing organs, such as pancreas and pronephros.

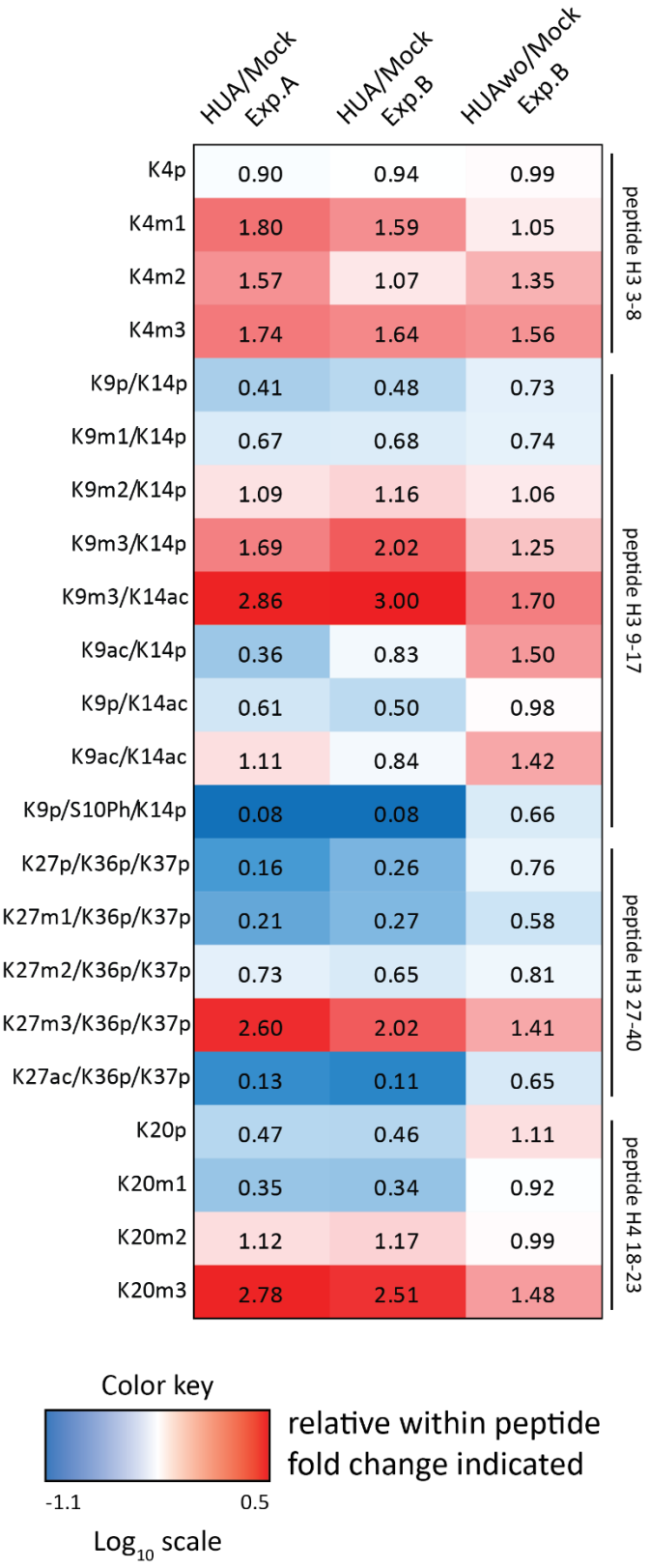

Figure 32. Recovery histone PTM abundances in HUAwo embryos. Ratio heatmap of relative histone modification abundancies for selected histone marks. First, the relative distributions of the indicated modification states are calculated as percentages within each tryptic peptide. Then, the relative values are presented as ratios between sample pairs indicated on top, showing the relative change for each histone modification state between the two conditions. Color key is based on Log10 scale. Numerical values in the cells indicate the fold-change. Values greater 1.0 indicate an increase in HUA condition, values smaller 1.0 indicate a higher abundance in Mock condition. Color and numerical values in the cells of the first two columns illustrate the similarity between Experiment type A and B, the information in the third column shows the similarity between HUAwo and Mock samples.

Conclusions on the HUAwo experiment

Overall, we demonstrated that with a transient block of the cell cycle the embryos' vitality improved. The HUAwo embryos reinitiated cell proliferation within 4 hours after the removal of HUA, which was estimated in the ICC staining on H3S10Ph mitotic mark. In contrast to embryos, treated continuously with the cell cycle inhibitors, we observed that HUAwo embryos restored to a high degree gene expression, tissue formation and sometimes, as for the heart, even organ function. This rescue is matched with a recovery of histone modification abundancies, surprisingly including repressive modifications that are considered to be epigenetically stable. Taken together, the results of the inhibitor washout experiment testify to the non-toxic nature of the HUA-dependent cell cycle arrest in *Xenopus* embryos and indicate that cell proliferation has an impact on the stage-specific histone modification profiles.

Discussion

In this study, the two small molecule inhibitors (Hydroxyurea and Aphidicolin) were applied to block the cell cycle of *X. laevis* embryos in the G1 phase. The arrested embryos were analyzed on three different levels: i) morphology — to quantitate their vitality and the overt appearance of developmental hallmarks; ii) mRNA expression — to examine their differentiation capacity and establish their "molecular age"; and iii) mass spectrometry — to measure the abundance of histone post-translational modifications (PTMs).

From a global perspective, the morphological analysis revealed that embryos were severely impacted by the treatment, lacking developmental hallmarks known to require cell proliferation such as a postanal tail, well-developed eyes, or even heartbeat, a feature that is required much later in amphibian development compared with mammals. On the other hand, morphogenetic programs like neurulation or the formation of the anteroposterior body axis did occur in a surprisingly normal manner. In total, the observations recapitulated the results reported by Harris and Hartenstein (Harris and Hartenstein, 1991), indicating that the experimental conditions achieved the maximal effect. This statement pertained even to the time point, from when on HUA treatment is compatible with embryo vitality. Application of the inhibitors before gastrulation was basically lethal, while treatment after the onset of gastrulation had nearly 40% of the embryos surviving until the end of our experiment, i.e. two-fold less than control siblings treated with DMSO only. Harris and Hartenstein had suggested that there might be a minimal number of cells required for the programming of all cell fates ("fate space model"). With HUA treatment starting before gastrulation, this number might not be reached, leading to coexistence of non-compatible gene regulatory networks in single cells, ultimately leading to cell death. With the possibility of single cell sequencing in *Xenopus* (Briggs *et al.*, 2018), this hypothesis could be tested now. An alternative explanation is provided by the finding that the early *Xenopus* embryo develops without cell cycle checkpoints, until Chk1 is activated at the beginning of gastrulation (Hensey and Gautier, 1997). HUA treatment causes stalling of replication forks. It seems a plausible assumption that the resulting replication stress can be ameliorated better in the presence of the checkpoint than without it.

The results of this work also extended the previous analysis (Harris and Hartenstein, 1991) by showing for the first time that the location and timing of gene induction events were

maintained in HUA embryos throughout embryogenesis. Although the analysis was limited in terms of gene numbers, the investigated tissue markers appeared to be expressed at stochiometric levels between control and HUA-arrested siblings (Figures 8 — 11). This is an important finding, since it attributes a near-normal molecular age to HUA arrested embryos, thereby excluding a global developmental arrest as explanation for the observed changes in chromatin modifications.

In the previous studies it has been shown that behind the morphological changes during early embryo development there are directional developmental changes in chromatin, which regule gene expression (Akkers *et al.*, 2009). The changes were detectable on the level of individual histone modifications as well as on the global scale. This observation suggested that the chromatin landscape maturates during embryo development. Here, we have set up a platform for analysis of stage-specific histone modification profiles (HMPs) in cell cycle manipulated *Xenopus* embryos. This platform can be easily adapted for other purposes. We have obtained proof of principle for a selective regulatory connection between the cell cycle and histone modification abundance, in particular for repressive trimethylation on H3K9, H3K27 and H4K20 position.

Developmental changes in histone modification landscape

At the core of organismic development lies the principle that all organs and cell types of the adult organism are derived from a single cell (the zygote). Because the genome stays largely constant during this process, most of the changes associated with cell differentiation are epigenetic in nature. In amphibians like *Xenopus*, cells start to become different from the MBT on, coincident with the onset of zygotic transcription and competence to growth factor signalling. Developmental changes in histone modification landscape, on a global level, has been shown in our lab (Schneider *et al.*, 2011). The results acquired in Mock embryos in this work partially recapitulate the previous observations. We noticed a presence of the stage-specific HMPs; and an overall trend for accumulation of the repressive marks and a decrease in the abundance of active marks during development. Recently, a cell state tree has been inferred from single-cell RNA-Seq analysis in *Xenopus* and zebrafish, illustrating the developmental decisions taken by cells as they become more and more diversified (Briggs *et al.*, 2018, Wagner *et al.*, 2018). The branchpoint structure is highly similar between the two

species, particularly during the early period. This is in line with the accepted degree of conservation for gene regulatory networks and epigenetic mechanisms among vertebrates.

The histones, used in this study, were isolated from whole embryos. In bulk, their analysis will reveal the average abundance of histone modifications at a given stage. The outcome could be strongly influenced by the relative proportion of different tissues (Fig. 33). For instance, cells with transcriptional signature “neural ectoderm” make up for 31% of the total embryo at tail bud stage (Briggs *et al.*, 2018). Given that early embryonic cells are known to be endowed with special chromatin features (Fisher and Fisher, 2011, Perino and Veenstra, 2016), the transition from toti-/pluripotency to differentiating somatic cell types will provide a vector, along which the epigenetic landscape develops.

Chromatin structure plays an important role in nuclear functions such as transcription and replication. One of the first major chromatin associated transition which happens during the early embryogenesis is an exchange of maternally deposited histone-like protein B4 to its zygotic form – linker histone H1 (Fig. 33). The maternal H1M/B4 protein is produced during oogenesis, but not in somatic cells. Zygotic linker histone proteins, predominantly the H1A isoform, are produced de novo after initiation of embryonic transcription at the MBT. Once the growing cell number, i.e. DNA amounts, are saturating the maternal H1M/B4 protein pool, newly synthesized somatic H1 proteins dilute out the maternal counterpart from MBT through neurulation (Dimitrov *et al.*, 1993). Interestingly, transplanting mammalian cell nuclei into the germinal vesicle of a *Xenopus* oocyte, leads to the opposite effect – the surplus of maternal H1M/B4 protein replaces the mammalian H1 proteins, notably in the absence of proliferation (Jullien *et al.*, 2014). Thus, at least some alterations in canonical chromatin components can be simply regulated by mass action.

Although the limitations of the HUA approach make it impossible to investigate the consequences of cell cycle arrest during the blastula/gastrula transition, we noticed that the HMP of the earliest arrested stage (i.e. early neurula, stage NF13) was the most distinct from the other analysed stages NF18 (late neurula), NF25 (tail bud) and NF32 (tadpole) (Fig. 15). Of note, the earlier stages than NF13 could not be assessed, due to the embryonic lethality caused by the HUA treatment when applied before gastrulation. This observation might suggest that the epigenome changes in a step-wise, rather than a continuous (gradual) fashion. In fact, the biggest HMP difference coincides with the gastrula-neurula transition

(Andrews *et al.*, 1991), which might be due to the H1 transition. The linker histone H1 exchange has been reported to correlate with major changes in the replicative and transcriptional activity of embryonic nuclei (Dimitrov *et al.*, 1993), that leads to the loss of mesodermal competence (Steinbach *et al.*, 1997b). Additionally, various "oocyte-type" RNA polymerase III transcribed genes (class III genes) and the vast majority of the RNA-Pol III rRNA genes were reported to be coordinately inactivated by the end of gastrulation, due to the linker histone transition. As a result, this transition from the early embryonic pattern of class III gene activity to a pattern, characteristic of adult somatic cells, might be seen on the chromatin level (Bouvet *et al.*, 1994, Vermaak *et al.*, 1998). Based on this knowledge we hypothesized that the structural changes in chromatin on a global scale might be connected to the establishment and modulation of HMPs.

Another feature to be considered is the cell cycle (Fig. 36). Early embryonic *Xenopus* development is characterized by dramatic changes in the cell cycle dynamics. It is very rapid at the beginning, approximately 25 min per cycle without G1 and G2 phases until MBT; after MBT the Gap phases are introduced, and the cell cycle becomes asynchronous and slows down. The first postmitotic cells are detectable from early neurula stage on (NF13/14), coincident with the beginning of cell differentiation in the neural plate and somitic myotomes (Hartenstein, 1989). This means, first, during initial development the embryo has very little time to write histone marks on the actually inactive genome. Second, appearance of the Gap phases in the cell cycle after MBT provides the opportunity to establish the histone PTMs (Akkers *et al.*, 2009, Bogdanovic *et al.*, 2011, Hontelez *et al.*, 2015). And third, from neurulation on proliferative and postmitotic cells are fundamentally different in one important aspect, i.e. dilution of parental histone modifications during S phase.

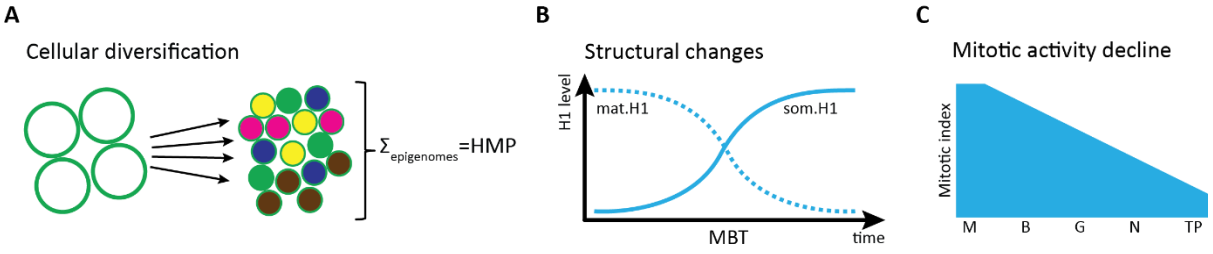

Figure 33. Models of possible mechanisms underlying chromatin maturation. A) During differentiation, a sum of all cell-specific epigenomes gives rise to acquired stage-specific histone modification profile. B) Developmental structural changes in chromatin architecture can be reflected in stage-specific HMPs. C) Decline in mitotic activity can play a role in establishment of stage-specific HMPs as a generic mechanism.

Regulatory impact of the cell cycle on the stage-specific HMPs

The epigenomes of the different developmental stages of *Xenopus laevis* can be distinguished based on the histone PTM abundancies, which gathered together form stage-specific histone modification profiles (HMPs) (Schneider *et al.*, 2011). These profiles reflect developmental changes in the epigenetic landscape of the embryo, in other words – the process of embryological chromatin maturation. As we have discussed above, the exact regulatory mechanism underlying the changes in HMPs still remains unclear. However, we assume that the stage-specific HMPs in *Xenopus* embryos are part of a developmental program, which acts in parallel to the unfolding genetic pathways. We expect this program to be controlled through broadly acting mechanisms, such as the cell cycle or growth factor signaling cascades, which may either directly regulate the activity of histone modifying enzymes or their expression.

Following the assumption, what could be a generic character of the cell cycle which mediates the regulation of the epigenome? First, the "dilution effect". With every replication round the DNA amount of a cell doubles, which leads to the necessity of doubling also the amount of nucleosomes on it. Newly synthetized histones are usually acetylated but quickly become deacetylated. It means, that newly incorporated histones are unmodified and require histone modifying enzymes and time to reestablish the pre-S phase epigenetic state. Surprisingly, the reestablishment of histone PTMs does not occur with a uniform rate. As it has been shown in synchronized human somatic cells, using metabolic labelling to distinguish new and old histones, at least two classes of histone modifications were detected (Alabert *et al.*, 2015). The first class, called "fast and finite", acquires PTMs to become identical to the parental histones within one cell cycle round. In contrast, the second class of histone modifications, called "slow and perpetual", does not reach the parental concentration of the particular histone marks on the daughter DNA after replication within one cell cycle round. Notably, famous repressive histone marks such as H3K9m3, H3K27m3 and H4K20m3 fall into the "slow and perpetual" class. We assume, that if these kinetic differences are valid for all types of cells then the length of the cell cycle becomes a limiting factor for accumulation of certain histone PTMs. Knowing that, for example, H3K27 methylation plays a crucial role in development by controlling developmental genes, we predict that the regulation of the cell

cycle plays a direct role in the maturation of chromatin landscape as an actual underlying mechanism of this process.

Second, it might be a mutual antagonism of repressive and active histone modifications (Lee and Mahadevan, 2009). That would mean that when the repressive marks (especially from the "slow and perpetual" class) are spreading, the "fast and finite" active marks will not be able to invade. Mechanistically, this process most likely involves 3D chromatin organization models within the nucleus, such as formation of the topologically associating domains (TADs) and lamina-associated domains (LADs). These domains are self-interacting genomic regions. The DNA sequences in these regions physically interact with each other or with the lamina proteins, in case of LADs, more often than with sequences outside the domains. It leads to the isolation and transcriptional inactivation of the in-domain DNA regions (Pombo and Dillon, 2015). Lamina-associated domains (LADs) are parts of the chromatin that heavily interacts with the lamina, a network-like structure at the inner membrane of the nucleus (Gonzalez-Sandoval and Gasser, 2016). The chromatin in these regions is mainly decorated with repressive marks such as H3K9m3 and H3K27m3 (Li *et al.*, 2012). Particularly in case of the LAD domains, the cell cycle can play an important role. The first rapid cleavage divisions of *Xenopus* embryos are without G1 and G2 phases, which prevents the formation of LAD domain, while somatic-like cell cycle allows their formation later during development (for more details, see introduction).

Third, theoretically, there might be a repressive threshold, caused by the local concentration of the repressive marks. There are specific histone modifications which are known to shut down transcription of the genes. However, it is not known how many repressive marks on a promoter are needed to silence a gene. That means that in rapidly proliferating cells, where writing of the histone PTMs is slower than the dilution effect, (discussed in the chapter earlier) there is a local concentration of repressive marks, which may or may not be sufficient to silence the gene. However, when the cells withdraw from cell cycle, there is no dilution effect any more, and an equilibrium between modifying and demodifying enzymes can be established. If this equilibrium crosses the theoretical functional threshold for repressive modifications, chromatin switches to a silent, sequestered or heterochromatic state. Taken together, this indicates that the cell cycle changes can affect

chromatin, subjecting the entire embryo, meaning that this can be a generic mechanism that regulates developmental changes in the epigenetic landscape on a global scale.

Another intriguing aspect was found in the ratio heatmap for selected modification states (Fig. 24). It demonstrated that the HUA treatment has left an imprint on the embryonic chromatin already at the earliest stage, immediately after the block has become active. Permanent arrest of the cell cycle showed selective effects on the stage-specific histone modification profiles, namely, repressive histone marks were the most affected ones. This raises the issue, where the surplus of repressive modifications can be found on chromatin? In principle, it is possible that they localize to the typical heterochromatic portions of the genome, but at higher local density. Alternatively, they could spread to novel sites and interfere with transcription of genomic loci. Those sites might be found among genes, which are specifically expressed in the cell types, which fail to differentiate under the HUA block (e.g. pronephros, pancreas or postanal tail). In that case, the HUA-enforced withdrawal from the cell cycle may mimic the situation of many differentiating cells, which move to the G0-phase, and thus escape the S-phase dilution of histone modifications.

Altogether, the data presented in this work provide compelling evidence for a regulatory input of the cell cycle to the stage-specific HMPs. We have shown that H3K9m3, H3K27m3 and H4K20m3 levels are significantly increased in the HUA samples. The underlying mechanism for this shift is possibly connected to the recent observation that histone PTMs are propagated by two different modes across the cell cycle (Alabert *et al.*, 2015): while most PTMs are restored quickly within one cell cycle on newly assembled histones, some others like the trimethylation of H3K9, H3K27 and H4K20 are continuously methylated with a slow rate. The observed increase of H3K9m3, H3K27m3 and H4K20m3 in HUA-arrested embryos might therefore represent an experimentally induced steady state, defined by the balance of specific KMT/KDM activities in the absence of continuous dilution of PTMs through cell divisions. Alternatively, the G1/S arrest may shift the recruitment of histone modifying enzymes to novel chromatin target sites, thus causing a net increase of the modification.

Reversibility of the cell cycle arrest effects

Under the continuous HUA treatment, the embryos demonstrated permanent cell cycle arrest from NF13 until NF32, the latest analysed stage in this study. HUA embryos at the later

stages showed largely normal differentiation, however, we detected that some late developing organs and tissues failed to form. The Experiment type B (HUAwo) revealed a recovery of the mitotic activity and a reappearance of the missing organs, such as pronephros, pancreas, postanal tail. Additionally, the heartbeat was recovered as well. These observations suggest a requirement for cell proliferation in the establishment of certain organs. Here we want to discuss why and how the cell cycle arrest could influence normal differentiation programs.

Development of many organs of the premetamorphic tadpole of *Xenopus laevis* is initiated at quite early stages of the embryogenesis. For example, specification of the pronephros anlage occurs between NF12.5 and NF14 (by overcoming the expression of activators for pax8 and hnf1b through odd-skipped related osr1/2), however, it fully develops at NF37 (Lienkamp, 2016, Nieuwkoop and Faber, 1994, McCoy *et al.*, 2011). Therefore, it is very likely that if the organ initiation was perturbed by the cell cycle block at early stages, then it can not differentiate to its final state. This is exactly what we could verify by performing the HUAwo experiment. However, the exact mechanisms, by which the HUA block has ablated late organs formation, remain unknown.

Firstly, perhaps, Hydroxyurea and Aphidicolin could have a toxic effect on the cells. In this case, however, we would have observed an increased level in cell death and apoptosis, which was not detected. Additionally, continuous treatment allowed about 50% survival of the HUA embryos up to NF32. Moreover, the HUA embryos demonstrated an overall normal differentiation, arguing against a toxic effect of the HUA treatment. Secondly, another possible underlying mechanism of not forming organs upon HUA could be a certain specific impact of the drugs to the cell signaling. Hydroxyurea and Aphidicolin are frequently used in experiments with cells of different origin: drosophila, human, mouse and plant. In these studies researchers do not report of any other side effect of the drugs apart from the cell cycle block at the G1/S phase. Given that, it is unlikely that in *Xenopus laevis* embryos HUA can have an impact on signaling events for late developing organs. Finally, we hypothesized that missing organ phenomenon is directly due to the arrested cell proliferation. There are pools of stem cells which give rise to a variety of organs and tissues. In theory, some cell types may get lost as consequence of blocking the cell cycle too early, so that the remaining cell pool can not accommodate all the different cell types (“Fate space” model; (Harris and

Hartenstein, 1991)). Alternatively, these phenotypes may arise from epigenetic misregulation that we have discussed in the chapter above. Shortly, repressive histone modifications, which accumulate in excess in HUA embryos, could extinguish cellular competence for organ-specific gene expression programs. Notably, this hypothesis can be supported by our findings in the HUAwo experiment, where we observed a normalization of histone PTM abundances and organ differentiation.

In the Experiment type B (HUAwo) we observed a recovery of the histone PTM abundance at the stage NF32 (Fig. 26). The extent of the recovery is visible in the ratio heatmap (Fig. 27). Interestingly, not all histone modifications reverted their abundances to the Mock-like state. This might be due to the time window being too short for the complete recovery, which, in theory, might be seen if the histones were extracted from a later time point than NF32 (the end-point of the HUAwo analysis). In addition, this finding argues against a ratchet mechanism, in which an increase of a factor stays at the elevated level even after removal of the treatment (Gurdon *et al.*, 1995).

Altogether, in this work we investigated histone modifications at discrete developmental timepoints and assessed in parallel the impact of the experimental conditions on the developmental programs. We conclude that the cell cycle plays a role in the process of chromatin maturation. Additionally, we provide compelling evidence for the impact of stage-specific HMPs on embryonic development and their regulation by the cell cycle activity.

Opportunities (outlook)

Early embryogenesis is a complex sophisticated process that relies on many different mechanisms. Based on the diversity of these underlying mechanisms one could study embryo development from different angles. In this work we tried to find a link between two individually well studied mechanisms: cell cycle and epigenetic regulation. Specifically, we have focused on a possible role for the cell cycle in the dynamics of the epigenetic landscape. As a result, the scope and overall results of this study have opened novel opportunities to deepen our knowledge in early embryogenesis.

Reappearance of the missing organs and tissues in the HUAwo experiment suggests a critical time window, during which the cell cycle is crucial for the organ development. As an elaboration of the experimental scheme, one could apply HUA at different developmental

timepoints for equal duration, thereby identifying time windows, in which specific organs or tissues are susceptible to the cell cycle regulation.

Mass spectrometry is a fast-developing technology widely spread in many scientific fields, from chemistry and biology to space studies (Bakaikina *et al.*, 2018). It proved itself as a reliable technique in molecular biology regarding identification and quantification different protein complexes (Schmidt and Urlaub, 2017), individual peptides or small metabolites (Gillet *et al.*, 2016). Due to its diverse applications, it was not complicated to find a type of MS analysis that would fulfill the needed criteria of this study, however, an adjustment of the method was required. optimization process could be divided into three steps: MS sample preparation, the MS machine method and analysis of the raw data.

The MS sample preparation was extensively studied and specifically modified to the use of *Xenopus* embryos by T. Schneider from our group (Schneider *et al.*, 2011). The MS machine operated in the regular scheduled PRM mode (Bourmaud *et al.*, 2016) with specifically set retention time windows. However, the MS raw data analysis underwent considerable adjustments. Initially, the MS raw data analysis was done in Xcalibur, the default analysis program developed and supported by the MS vendor ThermoFisher. It required many manual adjustments during the analysis that sometimes could introduce unpredicted inaccuracies with peak identification and biases in quantification. Switching from Xcalibur to the Skyline software has eased the MS raw data analysis dramatically. Skyline was developed by a group of scientists from the University of Washington, USA with a purpose to provide a functional platform for MS raw data analysis derived from different MS methods from different vendors. The program allows to treat the data in the same way with a very diverse functionality. During this study I developed Skyline layouts for the histone PTM analysis, which can be recycled in the future for other purposes.

References

ABDI, H. & WILLIAMS, L. J. 2010. Principal component analysis. *WIREs Computational Statistics*.

ABSHIRU, N., IPPERSIEL, K., TANG, Y., YUAN, H., MARMORSTEIN, R., VERREAULT, A. & THIBAULT, P. 2013. Chaperone-mediated acetylation of histones by Rtt109 identified by quantitative proteomics. *J Proteomics,* 81**,** 80-90.

AFELIK, S., CHEN, Y. & PIELER, T. 2006. Combined ectopic expression of Pdx1 and Ptf1a/p48 results in the stable conversion of posterior endoderm into endocrine and exocrine pancreatic tissue. *Genes Dev,* 20**,** 1441-6.

AGALIOTI, T., CHEN, G. & THANOS, D. 2002. Deciphering the transcriptional histone acetylation code for a human gene. *Cell,* 111**,** 381-92.

AHMED, K., DEHGHANI, H., RUGG-GUNN, P., FUSSNER, E., ROSSANT, J. & BAZETT-JONES, D. P. 2010. Global chromatin architecture reflects pluripotency and lineage commitment in the early mouse embryo. *PLoS One,* 5**,** e10531.

AKKERS, R. C., VAN HEERINGEN, S. J., JACOBI, U. G., JANSSEN-MEGENS, E. M., FRANCOIJS, K. J., STUNNENBERG, H. G. & VEENSTRA, G. J. 2009. A hierarchy of H3K4me3 and H3K27me3 acquisition in spatial gene regulation in Xenopus embryos. *Dev Cell,* 17**,** 425-34.

ALABERT, C., BARTH, T. K., REVERÓN-GÓMEZ, N., SIDOLI, S., SCHMIDT, A., JENSEN, O., IMHOF, A. & GROTH, A. 2015. Two distinct modes for propagation of histone PTMs across the cell cycle. *Genes and Development,* 29**,** 585-590.

ALLFREY, V. G., FAULKNER, R. & MIRSKY, A. E. 1964. Acetylation and Methylation of Histones and Their Possible Role in the Regulation of RNA Synthesis. *Proc Natl Acad Sci U S A,* 51**,** 786-94.

ALLIS, C. D., JENUWEIN, T. & REINBERG, D. 2006. Epigenetics. *Cold Spring Harbor Laboratory Press*.

ALLISON, S. J. & MILNER, J. 2003. Loss of p53 has site-specific effects on histone H3 modification, including serine 10 phosphorylation important for maintenance of ploidy. *Cancer Res,* 63**,** 6674-9.

ALMOUZNI, G. & CEDAR, H. 2016. Maintenance of Epigenetic Information. *Cold Spring Harb Perspect Biol,* 8.

ANDREWS, M. T., LOO, S. & WILSON, L. R. 1991. Coordinate inactivation of class III genes during the Gastrula-Neurula Transition in Xenopus. *Dev Biol,* 146**,** 250-4.

ASENSIO-JUAN, E., GALLEGO, C. & MARTINEZ-BALBAS, M. A. 2012. The histone demethylase PHF8 is essential for cytoskeleton dynamics. *Nucleic Acids Res,* 40**,** 9429-40.

AZUARA, V., PERRY, P., SAUER, S., SPIVAKOV, M., JORGENSEN, H. F., JOHN, R. M., GOUTI, M., CASANOVA, M., WARNES, G., MERKENSCHLAGER, M. & FISHER, A. G. 2006. Chromatin signatures of pluripotent cell lines. *Nat Cell Biol,* 8**,** 532-8.

BAKAIKINA, N. V., KENESSOV, B., UL'YANOVSKII, N. V. & KOSYAKOV, D. S. 2018. Quantification of transformation products of rocket fuel unsymmetrical dimethylhydrazine in soils using SPME and GC-MS. *Talanta,* 184**,** 332-337.

BARBER, M. F., MICHISHITA-KIOI, E., XI, Y., TASSELLI, L., KIOI, M., MOQTADERI, Z., TENNEN, R. I., PAREDES, S., YOUNG, N. L., CHEN, K., STRUHL, K., GARCIA, B. A., GOZANI, O., LI, W. & CHUA, K. F. 2012. SIRT7 links H3K18 deacetylation to maintenance of oncogenic transformation. *Nature,* 487**,** 114-8.

BARSKI, A., CUDDAPAH, S., CUI, K., ROH, T. Y., SCHONES, D. E., WANG, Z., WEI, G., CHEPELEV, I. & ZHAO, K. 2007. High-resolution profiling of histone methylations in the human genome. *Cell,* 129**,** 823-37.

BECK, C. W. & SLACK, J. M. 1998. Analysis of the developing Xenopus tail bud reveals separate phases of gene expression during determination and outgrowth. *Mech Dev,* 72**,** 41-52.

BECK, D. B., ODA, H., SHEN, S. S. & REINBERG, D. 2012. PR-Set7 and H4K20me1: at the crossroads of genome integrity, cell cycle, chromosome condensation, and transcription. *Genes Dev,* 26**,** 325-37.

BECKER, J. S., NICETTO, D. & ZARET, K. S. 2016. H3K9me3-Dependent Heterochromatin: Barrier to Cell Fate Changes. *Trends Genet,* 32**,** 29-41.

BENAZERAF, B. & POURQUIE, O. 2013. Formation and segmentation of the vertebrate body axis. *Annu Rev Cell Dev Biol,* 29**,** 1-26.

BERGHOLZ, J. & XIAO, Z. X. 2012. Role of p63 in Development, Tumorigenesis and Cancer Progression. *Cancer Microenviron,* 5**,** 311-22.

BERNIER, M., LUO, Y., NWOKELO, K. C., GOODWIN, M., DREHER, S. J., ZHANG, P., PARTHUN, M. R., FONDUFE-MITTENDORF, Y., OTTESEN, J. J. & POIRIER, M. G. 2015. Linker histone H1 and H3K56 acetylation are antagonistic regulators of nucleosome dynamics. *Nat Commun,* 6**,** 10152.

BERNSTEIN, B. E., MIKKELSEN, T. S., XIE, X., KAMAL, M., HUEBERT, D. J., CUFF, J., FRY, B., MEISSNER, A., WERNIG, M., PLATH, K., JAENISCH, R., WAGSCHAL, A., FEIL, R., SCHREIBER, S. L. & LANDER, E. S. 2006. A bivalent chromatin structure marks key developmental genes in embryonic stem cells. *Cell,* 125**,** 315-26.

BHATTACHARYA, D., TALWAR, S., MAZUMDER, A. & SHIVASHANKAR, G. V. 2009. Spatio-temporal plasticity in chromatin organization in mouse cell differentiation and during Drosophila embryogenesis. *Biophys J,* 96**,** 3832-9.

BICKMORE, W. A. & VAN STEENSEL, B. 2013. Genome architecture: domain organization of interphase chromosomes. *Cell,* 152**,** 1270-84.

BIECHELE, S., LIN, C. J., RINAUDO, P. F. & RAMALHO-SANTOS, M. 2015. Unwind and transcribe: chromatin reprogramming in the early mammalian embryo. *Curr Opin Genet Dev,* 34**,** 17-23.

BOGDANOVIC, O., VAN HEERINGEN, S. J. & VEENSTRA, G. J. 2011. The epigenome in early vertebrate development. *Genesis,* 50**,** 192-206.

BOIJA, A. & MANNERVIK, M. 2015. A time of change: Dynamics of chromatin and transcriptional regulation during nuclear programming in early Drosophila development. *Mol Reprod Dev,* 82**,** 735-46.

BONE, J. R., LAVENDER, J., RICHMAN, R., PALMER, M. J., TURNER, B. M. & KURODA, M. I. 1994. Acetylated histone H4 on the male X chromosome is associated with dosage compensation in Drosophila. *Genes Dev,* 8**,** 96-104.

BOTUYAN, M. V., LEE, J., WARD, I. M., KIM, J. E., THOMPSON, J. R., CHEN, J. & MER, G. 2006. Structural basis for the methylation state-specific recognition of histone H4-K20 by 53BP1 and Crb2 in DNA repair. *Cell,* 127**,** 1361-73.

BOURMAUD, A., GALLIEN, S. & DOMON, B. 2016. Parallel reaction monitoring using quadrupole-Orbitrap mass spectrometer: Principle and applications. *Proteomics,* 16**,** 2146-59.

BOURQUE, G., BURNS, K. H., GEHRING, M., GORBUNOVA, V., SELUANOV, A., HAMMELL, M., IMBEAULT, M., IZSVAK, Z., LEVIN, H. L., MACFARLAN, T. S., MAGER, D. L. & FESCHOTTE, C. 2018. Ten things you should know about transposable elements. *Genome Biol,* 19**,** 199.

BOUVET, P., DIMITROV, S. & WOLFFE, A. P. 1994. Specific regulation of Xenopus chromosomal 5S rRNA gene transcription in vivo by histone H1. *Genes Dev,* 8**,** 1147-59.

BOYER, L. A., PLATH, K., ZEITLINGER, J., BRAMBRINK, T., MEDEIROS, L. A., LEE, T. I., LEVINE, S. S., WERNIG, M., TAJONAR, A., RAY, M. K., BELL, G. W., OTTE, A. P., VIDAL, M., GIFFORD, D. K., YOUNG, R. A. & JAENISCH, R. 2006. Polycomb complexes repress developmental regulators in murine embryonic stem cells. *Nature,* 441**,** 349-53.

BRACKEN, A. P., DIETRICH, N., PASINI, D., HANSEN, K. H. & HELIN, K. 2006. Genome-wide mapping of Polycomb target genes unravels their roles in cell fate transitions. *Genes Dev,* 20**,** 1123-36.

BRIGGS, J. A., WEINREB, C., WAGNER, D. E., MEGASON, S., PESHKIN, L., KIRSCHNER, M. W. & KLEIN, A. M. 2018. The dynamics of gene expression in vertebrate embryogenesis at single-cell resolution. *Science,* 360.

BROOKE, N. M., GARCIA-FERNANDEZ, J. & HOLLAND, P. W. 1998. The ParaHox gene cluster is an evolutionary sister of the Hox gene cluster. *Nature,* 392**,** 920-2.

CANELLA, D., HOCK, S. J., HILTNER, O., HERDTWECK, E., HERRMANN, W. A. & KUHN, F. E. 2012. Synthesis and characterization of propylene and butylene bridged fac-tricarbonylrhenium(I) biscarbene complexes. *Dalton Trans,* 41**,** 2110-21.

CAO, R., WANG, L., WANG, H., XIA, L., ERDJUMENT-BROMAGE, H., TEMPST, P., JONES, R. S. & ZHANG, Y. 2002. Role of histone H3 lysine 27 methylation in Polycomb-group silencing. *Science,* 298**,** 1039-43.

CAO, Y., KNOCHEL, S., DONOW, C., MIETHE, J., KAUFMANN, E. & KNOCHEL, W. 2004. The POU factor Oct-25 regulates the Xvent-2B gene and counteracts terminal differentiation in Xenopus embryos. *J Biol Chem,* 279**,** 43735-43.

CASTILLO-AGUILERA, O., DEPREUX, P., HALBY, L., ARIMONDO, P. B. & GOOSSENS, L. 2017. DNA Methylation Targeting: The DNMT/HMT Crosstalk Challenge. *Biomolecules,* 7.

CEDAR, H. & BERGMAN, Y. 2009. Linking DNA methylation and histone modification: patterns and paradigms. *Nat Rev Genet,* 10**,** 295-304.

CHAL, J. & POURQUIE, O. 2017. Making muscle: skeletal myogenesis in vivo and in vitro. *Development,* 144**,** 2104-2122.

CHEN, G. & DENG, X. 2018. Cell Synchronization by Double Thymidine Block. *Bio Protoc,* 8.

CIAU-UITZ, A., LIU, F. & PATIENT, R. 2010. Genetic control of hematopoietic development in Xenopus and zebrafish. *Int J Dev Biol,* 54**,** 1139-49.

CIAU-UITZ, A. & PATIENT, R. 2016. The embryonic origins and genetic programming of emerging haematopoietic stem cells. *FEBS Lett,* 590**,** 4002-4015.

CLARKE, H. J., MCLAY, D. W. & MOHAMED, O. A. 1998. Linker histone transitions during mammalian oogenesis and embryogenesis. *Dev Genet,* 22**,** 17-30.

COLLART, C., SMITH, J. C. & ZEGERMAN, P. 2017. Chk1 Inhibition of the Replication Factor Drf1 Guarantees Cell-Cycle Elongation at the Xenopus laevis Mid-blastula Transition. *Dev Cell,* 42**,** 82-96 e3.

COSGROVE, M. S. 2007. Histone proteomics and the epigenetic regulation of nucleosome mobility. *Expert Rev Proteomics,* 4**,** 465-78.

CREYGHTON, M. P., CHENG, A. W., WELSTEAD, G. G., KOOISTRA, T., CAREY, B. W., STEINE, E. J., HANNA, J., LODATO, M. A., FRAMPTON, G. M., SHARP, P. A., BOYER, L. A., YOUNG, R. A. & JAENISCH, R. 2010. Histone H3K27ac separates active from poised enhancers and predicts developmental state. *Proceedings of the National Academy of Sciences,* 107**,** 21931-21936.

CZERMIN, B., MELFI, R., MCCABE, D., SEITZ, V., IMHOF, A. & PIRROTTA, V. 2002. Drosophila enhancer of Zeste/ESC complexes have a histone H3 methyltransferase activity that marks chromosomal Polycomb sites. *Cell,* 111**,** 185-96.

DAVIS, P. K., HO, A. & DOWDY, S. F. 2001. Biological methods for cell-cycle synchronization of mammalian cells. *Biotechniques,* 30**,** 1322-6, 1328, 1330-1.

DE ROBERTIS, E. M. 2008. Evo-devo: variations on ancestral themes. *Cell,* 132**,** 185-95.

DI LORENZO, A. & BEDFORD, M. T. 2011. Histone arginine methylation. *FEBS Lett,* 585**,** 2024-31.

DIMITROV, S., ALMOUZNI, G., DASSO, M. & WOLFFE, A. P. 1993. Chromatin transitions during early Xenopus embryogenesis: changes in histone H4 acetylation and in linker histone type. *Dev Biol,* 160**,** 214-27.

DOI, A., PARK, I. H., WEN, B., MURAKAMI, P., ARYEE, M. J., IRIZARRY, R., HERB, B., LADD-ACOSTA, C., RHO, J., LOEWER, S., MILLER, J., SCHLAEGER, T., DALEY, G. Q. & FEINBERG, A. P. 2009. Differential methylation of tissue- and cancer-specific CpG island shores distinguishes human induced pluripotent stem cells, embryonic stem cells and fibroblasts. *Nat Genet,* 41**,** 1350-3.

DROST, H. G., JANITZA, P., GROSSE, I. & QUINT, M. 2017. Cross-kingdom comparison of the developmental hourglass. *Curr Opin Genet Dev,* 45**,** 69-75.

DUBAISSI, E. & PAPALOPULU, N. 2011. Embryonic frog epidermis: a model for the study of cell-cell interactions in the development of mucociliary disease. *Dis Model Mech,* 4**,** 179-92.

EGELHOFER, T. A., MINODA, A., KLUGMAN, S., LEE, K., KOLASINSKA-ZWIERZ, P., ALEKSEYENKO, A. A., CHEUNG, M. S., DAY, D. S., GADEL, S., GORCHAKOV, A. A., GU, T., KHARCHENKO, P. V., KUAN, S., LATORRE, I., LINDER-BASSO, D., LUU, Y., NGO, Q., PERRY, M., RECHTSTEINER, A., RIDDLE, N. C., SCHWARTZ, Y. B., SHANOWER, G. A., VIELLE, A., AHRINGER, J., ELGIN, S. C., KURODA, M. I., PIRROTTA, V., REN, B., STROME, S., PARK, P. J., KARPEN, G. H., HAWKINS, R. D. & LIEB, J. D. 2011. An assessment of histone-modification antibody quality. *Nat Struct Mol Biol,* 18**,** 91-3.

FAN, Y., NIKITINA, T., MORIN-KENSICKI, E. M., ZHAO, J., MAGNUSON, T. R., WOODCOCK, C. L. & SKOULTCHI, A. I. 2003. H1 linker histones are essential for mouse development and affect nucleosome spacing in vivo. *Mol Cell Biol,* 23**,** 4559-72.

FAN, Y., NIKITINA, T., ZHAO, J., FLEURY, T. J., BHATTACHARYYA, R., BOUHASSIRA, E. E., STEIN, A., WOODCOCK, C. L. & SKOULTCHI, A. I. 2005. Histone H1 depletion in mammals alters global chromatin structure but causes specific changes in gene regulation. *Cell,* 123**,** 1199-212.

FAROOQ, Z., BANDAY, S., PANDITA, T. K. & ALTAF, M. 2016. The many faces of histone H3K79 methylation. *Mutat Res Rev Mutat Res,* 768**,** 46-52.

FENG, Y., VLASSIS, A., ROQUES, C., LALONDE, M. E., GONZALEZ-AGUILERA, C., LAMBERT, J. P., LEE, S. B., ZHAO, X., ALABERT, C., JOHANSEN, J. V., PAQUET, E., YANG, X. J., GINGRAS, A. C., COTE, J. & GROTH, A. 2016. BRPF3-HBO1 regulates replication origin activation and histone H3K14 acetylation. *EMBO J,* 35**,** 176-92.

FERRARI, K. J., SCELFO, A., JAMMULA, S., CUOMO, A., BAROZZI, I., STUTZER, A., FISCHLE, W., BONALDI, T. & PASINI, D. 2014. Polycomb-dependent H3K27me1 and H3K27me2 regulate active transcription and enhancer fidelity. *Mol Cell,* 53**,** 49-62.

FISHER, C. L. & FISHER, A. G. 2011. Chromatin states in pluripotent, differentiated, and reprogrammed cells. *Curr Opin Genet Dev,* 21**,** 140-6.

FLANAGAN, J. F., MI, L. Z., CHRUSZCZ, M., CYMBOROWSKI, M., CLINES, K. L., KIM, Y., MINOR, W., RASTINEJAD, F. & KHORASANIZADEH, S. 2005. Double chromodomains cooperate to recognize the methylated histone H3 tail. *Nature,* 438**,** 1181-5.

FNU, S., WILLIAMSON, E. A., DE HARO, L. P., BRENNEMAN, M., WRAY, J., SHAHEEN, M., RADHAKRISHNAN, K., LEE, S. H., NICKOLOFF, J. A. & HROMAS, R. 2011. Methylation of histone H3 lysine 36 enhances DNA repair by nonhomologous end-joining. *Proc Natl Acad Sci U S A,* 108**,** 540-5.

FREITAS, M. A., SKLENAR, A. R. & PARTHUN, M. R. 2004. Application of mass spectrometry to the identification and quantification of histone post-translational modifications. *J Cell Biochem,* 92**,** 691-700.

FU, H., MAUNAKEA, A. K., MARTIN, M. M., HUANG, L., ZHANG, Y., RYAN, M., KIM, R., LIN, C. M., ZHAO, K. & ALADJEM, M. I. 2013. Methylation of histone H3 on lysine 79 associates with a group of replication origins and helps limit DNA replication once per cell cycle. *PLoS Genet,* 9**,** e1003542.

GARCIA-BLANCO, N. & MORENO, S. 2019. Down-regulation of Cdk1 activity in G1 coordinates the G1/S gene expression programme with genome replication. *Curr Genet*.

GILLET, L. C., LEITNER, A. & AEBERSOLD, R. 2016. Mass Spectrometry Applied to Bottom-Up Proteomics: Entering the High-Throughput Era for Hypothesis Testing. *Annu Rev Anal Chem (Palo Alto Calif),* 9**,** 449-72.

GONZALEZ-SANDOVAL, A. & GASSER, S. M. 2016. On TADs and LADs: Spatial Control Over Gene Expression. *Trends Genet,* 32**,** 485-495.

GRAHAM, C. F. & MORGAN, R. W. 1966. Changes in the cell cycle during early amphibian development. *Developmental Biology,* 14**,** 439-460.

GREESON, N. T., SENGUPTA, R., ARIDA, A. R., JENUWEIN, T. & SANDERS, S. L. 2008. Di-methyl H4 lysine 20 targets the checkpoint protein Crb2 to sites of DNA damage. *J Biol Chem,* 283**,** 33168-74.

GURDON, J. B. 1962. The developmental capacity of nuclei taken from intestinal epithelium cells of feeding tadpoles. *J Embryol Exp Morphol,* 10**,** 622-40.

GURDON, J. B., MITCHELL, A. & MAHONY, D. 1995. Direct and continuous assessment by cells of their position in a morphogen gradient. *Nature,* 376**,** 520-1.

HAKE, S. B. & ALLIS, C. D. 2006. Histone H3 variants and their potential role in indexing mammalian genomes: the "H3 barcode hypothesis". *Proc Natl Acad Sci U S A,* 103**,** 6428-35.

HARRIS, W. A. & HARTENSTEIN, V. 1991. Neuronal Determination in Xenopus Embryos without Cell Division. *Neuron,* 6**,** 499-515.

HARTENSTEIN, V. 1989. Early neurogenesis in Xenopus: the spatio-temporal pattern of proliferation and cell lineages in the embryonic spinal cord. *Neuron,* 3**,** 399-411.

HAYASHI-TAKANAKA, Y., MAEHARA, K., HARADA, A., UMEHARA, T., YOKOYAMA, S., OBUSE, C., OHKAWA, Y., NOZAKI, N. & KIMURA, H. 2015. Distribution of histone H4 modifications as revealed by a panel of specific monoclonal antibodies. *Chromosome Res,* 23**,** 753-66.

HEMBERGER, M., DEAN, W. & REIK, W. 2009. Epigenetic dynamics of stem cells and cell lineage commitment: Digging Waddington's canal. *Nature Reviews Molecular Cell Biology,* 10**,** 526-537.

HENDZEL, M. J., WEI, Y., MANCINI, M. A., VAN HOOSER, A., RANALLI, T., BRINKLEY, B. R., BAZETT-JONES, D. P. & ALLIS, C. D. 1997. Mitosis-specific phosphorylation of histone H3 initiates primarily within pericentromeric heterochromatin during G2 and spreads in an ordered fashion coincident with mitotic chromosome condensation. *Chromosoma,* 106**,** 348-60.

HENSEY, C. & GAUTIER, J. 1997. A developmental timer that regulates apoptosis at the onset of gastrulation. *Mech Dev,* 69**,** 183-95.

HERGETH, S. P. & SCHNEIDER, R. 2015. The H1 linker histones: multifunctional proteins beyond the nucleosomal core particle. *EMBO Rep,* 16**,** 1439-53.

HONTELEZ, S., VAN KRUIJSBERGEN, I., GEORGIOU, G., VAN HEERINGEN, S. J., BOGDANOVIC, O., LISTER, R. & VEENSTRA, G. J. 2015. Embryonic transcription is controlled by maternally defined chromatin state. *Nat Commun,* 6**,** 10148.

HORB, M. E., SHEN, C. N., TOSH, D. & SLACK, J. M. 2003. Experimental conversion of liver to pancreas. *Curr Biol,* 13**,** 105-15.

HORB, M. E. & SLACK, J. M. 2002. Expression of amylase and other pancreatic genes in Xenopus. *Mech Dev,* 113**,** 153-7.

HORMANSEDER, E., SIMEONE, A., ALLEN, G. E., BRADSHAW, C. R., FIGLMULLER, M., GURDON, J. & JULLIEN, J. 2017. H3K4 Methylation-Dependent Memory of Somatic Cell Identity Inhibits Reprogramming and Development of Nuclear Transfer Embryos. *Cell Stem Cell,* 21**,** 135-143 e6.

IKEGAMI, R., RIVERA-BENNETTS, A. K., BROOKER, D. L. & YAGER, T. D. 1997. Effect of inhibitors of DNA replication on early zebrafish embryos: evidence for coordinate activation of multiple intrinsic cell-cycle checkpoints at the mid-blastula transition. *Zygote,* 5**,** 153-75.

IKEGAMI, S., TAGUCHI, T., OHASHI, M., OGURO, M., NAGANO, H. & MANO, Y. 1978. Aphidicolin prevents mitotic cell division by interfering with the activity of DNA polymerase-alpha. *Nature,* 275**,** 458-60.

ISAACS, H. V., POWNALL, M. E. & SLACK, J. M. 1998. Regulation of Hox gene expression and posterior development by the Xenopus caudal homologue Xcad3. *EMBO J,* 17**,** 3413-27.

IZZO, A. & SCHNEIDER, R. 2016. The role of linker histone H1 modifications in the regulation of gene expression and chromatin dynamics. *Biochim Biophys Acta,* 1859**,** 486-95.

JARIKJI, Z. H., VANAMALA, S., BECK, C. W., WRIGHT, C. V., LEACH, S. D. & HORB, M. E. 2007. Differential ability of Ptf1a and Ptf1a-VP16 to convert stomach, duodenum and liver to pancreas. *Dev Biol,* 304**,** 786-99.

JENSEN, L. M. 1987. Phenotypic differentiation of aphidicolin-selected human neuroblastoma cultures after long-term exposure to nerve growth factor. *Dev Biol,* 120**,** 56-64.

JENUWEIN, T. & ALLIS, C. D. 2001. Translating the histone code. *Science,* 293**,** 1074-80.

JEVTIC, P. & LEVY, D. L. 2015. Nuclear size scaling during Xenopus early development contributes to midblastula transition timing. *Curr Biol,* 25**,** 45-52.

JORGENSEN, S., SCHOTTA, G. & SORENSEN, C. S. 2013. Histone H4 lysine 20 methylation: key player in epigenetic regulation of genomic integrity. *Nucleic Acids Res,* 41**,** 2797-806.

JUAN, A. H., WANG, S., KO, K. D., ZARE, H., TSAI, P. F., FENG, X., VIVANCO, K. O., ASCOLI, A. M., GUTIERREZ-CRUZ, G., KREBS, J., SIDOLI, S., KNIGHT, A. L., PEDERSEN, R. A., GARCIA, B.

A., CASELLAS, R., ZOU, J. & SARTORELLI, V. 2016. Roles of H3K27me2 and H3K27me3 Examined during Fate Specification of Embryonic Stem Cells. *Cell Rep,* 17**,** 1369-1382.

JULLIEN, J., MIYAMOTO, K., PASQUE, V., ALLEN, G. E., BRADSHAW, C. R., GARRETT, N. J., HALLEY-STOTT, R. P., KIMURA, H., OHSUMI, K. & GURDON, J. B. 2014. Hierarchical molecular events driven by oocyte-specific factors lead to rapid and extensive reprogramming. *Mol Cell,* 55**,** 524-36.

KANDOLF, H. 1994. The H1A histone variant is an in vivo repressor of oocyte-type 5S gene transcription in Xenopus laevis embryos. *Proc Natl Acad Sci U S A,* 91**,** 7257-61.

KANE, D. A. & KIMMEL, C. B. 1993. The zebrafish midblastula transition. *Development (Cambridge, England),* 119**,** 447-56.

KARMODIYA, K., KREBS, A. R., OULAD-ABDELGHANI, M., KIMURA, H. & TORA, L. 2012. H3K9 and H3K14 acetylation co-occur at many gene regulatory elements, while H3K14ac marks a subset of inactive inducible promoters in mouse embryonic stem cells. *BMC Genomics,* 13**,** 424.

KEBEDE, A. F., SCHNEIDER, R. & DAUJAT, S. 2015. Novel types and sites of histone modifications emerge as players in the transcriptional regulation contest. *FEBS J,* 282**,** 1658-74.

KIM, J. M., KIM, K., PUNJ, V., LIANG, G., ULMER, T. S., LU, W. & AN, W. 2015. Linker histone H1.2 establishes chromatin compaction and gene silencing through recognition of H3K27me3. *Sci Rep,* 5**,** 16714.

KIMELMAN, D., KIRSCHNER, M. & SCHERSON, T. 1987. The events of the midblastula transition in Xenopus are regulated by changes in the cell cycle. *Cell,* 48**,** 399-407.

KOC, A., WHEELER, L. J., MATHEWS, C. K. & MERRILL, G. F. 2004. Hydroxyurea arrests DNA replication by a mechanism that preserves basal dNTP pools. *J Biol Chem,* 279**,** 223-30.

KORNBERG, R. D. 1974. Chromatin structure: a repeating unit of histones and DNA. *Science,* 184**,** 868-71.

KUO, A. J., SONG, J., CHEUNG, P., ISHIBE-MURAKAMI, S., YAMAZOE, S., CHEN, J. K., PATEL, D. J. & GOZANI, O. 2012. The BAH domain of ORC1 links H4K20me2 to DNA replication licensing and Meier-Gorlin syndrome. *Nature,* 484**,** 115-9.

KUZMICHEV, A., NISHIOKA, K., EDRJUMENT-BROMAGE, H., TEMPST, P. & REINBERG, D. 2002. Histone methyltransferase activity associated with a human multiprotein complex containing the Enhancer of Zeste protein. *Genes & …***,** 2893-2905.

LACOSTE, N., UTLEY, R. T., HUNTER, J. M., POIRIER, G. G. & COTE, J. 2002. Disruptor of telomeric silencing-1 is a chromatin-specific histone H3 methyltransferase. *J Biol Chem,* 277**,** 30421-4.

LANGE, C. & CALEGARI, F. 2010. Cdks and cyclins link G1 length and differentiation of embryonic, neural and hematopoietic stem cells. *Cell Cycle,* 9**,** 1893-900.

LAUBERTH, S. M., NAKAYAMA, T., WU, X., FERRIS, A. L., TANG, Z., HUGHES, S. H. & ROEDER, R. G. 2013. H3K4me3 interactions with TAF3 regulate preinitiation complex assembly and selective gene activation. *Cell,* 152**,** 1021-36.

LEE, B. M. & MAHADEVAN, L. C. 2009. Stability of histone modifications across mammalian genomes: Implications for 'epigenetic' marking. *Journal of Cellular Biochemistry,* 108**,** 22-34.

LEE, H., HABAS, R. & ABATE-SHEN, C. 2004. MSX1 cooperates with histone H1b for inhibition of transcription and myogenesis. *Science,* 304**,** 1675-8.

LEHNERTZ, B., UEDA, Y., DERIJCK, A. A., BRAUNSCHWEIG, U., PEREZ-BURGOS, L., KUBICEK, S., CHEN, T., LI, E., JENUWEIN, T. & PETERS, A. H. 2003. Suv39h-mediated histone H3 lysine 9 methylation directs DNA methylation to major satellite repeats at pericentric heterochromatin. *Curr Biol,* 13**,** 1192-200.

LEISE, W. F., 3RD & MUELLER, P. R. 2004. Inhibition of the cell cycle is required for convergent extension of the paraxial mesoderm during Xenopus neurulation. *Development,* 131**,** 1703-15.

LEVY, V., MAROM, K., ZINS, S., KOUTSIA, N., YELIN, R. & FAINSOD, A. 2002. The competence of marginal zone cells to become Spemann's organizer is controlled by Xcad2. *Dev Biol,* 248**,** 40-51.

LI, H., ILIN, S., WANG, W., DUNCAN, E. M., WYSOCKA, J., ALLIS, C. D. & PATEL, D. J. 2006. Molecular basis for site-specific read-out of histone H3K4me3 by the BPTF PHD finger of NURF. *Nature,* 442**,** 91-5.

LI, M., LIU, G. H. & IZPISUA BELMONTE, J. C. 2012. Navigating the epigenetic landscape of pluripotent stem cells. *Nat Rev Mol Cell Biol,* 13**,** 524-35.

LIEBLER, D. C. & ZIMMERMAN, L. J. 2013. Targeted quantitation of proteins by mass spectrometry. *Biochemistry,* 52**,** 3797-806.

LIENKAMP, S. S. 2016. Using Xenopus to study genetic kidney diseases. *Semin Cell Dev Biol,* 51**,** 117-24.

LIM, J. W., HUMMERT, P., MILLS, J. C. & KROLL, K. L. 2011. Geminin cooperates with Polycomb to restrain multi-lineage commitment in the early embryo. *Development,* 138**,** 33-44.

LIU, P. K., CHANG, C. C. & TROSKO, J. E. 1984. Evidence for mutagenic repair in V79 cell mutant with aphidicolin-resistant DNA polymerase-alpha. *Somat Cell Mol Genet,* 10**,** 235-45.

LUCO, R. F., PAN, Q., TOMINAGA, K., BLENCOWE, B. J., PEREIRA-SMITH, O. M. & MISTELI, T. 2010. Regulation of alternative splicing by histone modifications. *Science,* 327**,** 996-1000.

LUGER, K., MADER, A. W., RICHMOND, R. K., SARGENT, D. F. & RICHMOND, T. J. 1997. Crystal structure of the nucleosome core particle at 2.8 A resolution. *Nature,* 389**,** 251-60.

MACALPINE, D. M. & ALMOUZNI, G. 2013. Chromatin and DNA replication. *Cold Spring Harb Perspect Biol,* 5**,** a010207.

MACLEAN, B., TOMAZELA, D. M., SHULMAN, N., CHAMBERS, M., FINNEY, G. L., FREWEN, B., KERN, R., TABB, D. L., LIEBLER, D. C. & MACCOSS, M. J. 2010. Skyline: an open source document editor for creating and analyzing targeted proteomics experiments. *Bioinformatics,* 26**,** 966-8.

MANANDHAR, D., SONG, L., KABADI, A., KWON, J. B., EDSALL, L. E., EHRLICH, M., TSUMAGARI, K., GERSBACH, C. A., CRAWFORD, G. E. & GORDAN, R. 2017. Incomplete MyoD-induced transdifferentiation is associated with chromatin remodeling deficiencies. *Nucleic Acids Res,* 45**,** 11684-11699.

MATMATI, N., METELLI, A., TRIPATHI, K., YAN, S., MOHANTY, B. K. & HANNUN, Y. A. 2013. Identification of C18:1-phytoceramide as the candidate lipid mediator for hydroxyurea resistance in yeast. *J Biol Chem,* 288**,** 17272-84.

MAURER-SCHULTZE, B., SIEBERT, M. & BASSUKAS, I. D. 1988. An in vivo study on the synchronizing effect of hydroxyurea. *Exp Cell Res,* 174**,** 230-43.

MCCOY, K. E., ZHOU, X. & VIZE, P. D. 2011. Non-canonical wnt signals antagonize and canonical wnt signals promote cell proliferation in early kidney development. *Dev Dyn,* 240**,** 1558-66.

MESHORER, E. & MISTELI, T. 2006. Chromatin in pluripotent embryonic stem cells and differentiation. *Nat Rev Mol Cell Biol,* 7**,** 540-6.

MIKKELSEN, T. S., KU, M., JAFFE, D. B., ISSAC, B., LIEBERMAN, E., GIANNOUKOS, G., ALVAREZ, P., BROCKMAN, W., KIM, T. K., KOCHE, R. P., LEE, W., MENDENHALL, E., O'DONOVAN, A., PRESSER, A., RUSS, C., XIE, X., MEISSNER, A., WERNIG, M., JAENISCH, R., NUSBAUM, C., LANDER, E. S. & BERNSTEIN, B. E. 2007. Genome-wide maps of chromatin state in pluripotent and lineage-committed cells. *Nature,* 448**,** 553-60.

MORRIS, S. A., RAO, B., GARCIA, B. A., HAKE, S. B., DIAZ, R. L., SHABANOWITZ, J., HUNT, D. F., ALLIS, C. D., LIEB, J. D. & STRAHL, B. D. 2007. Identification of histone H3 lysine 36 acetylation as a highly conserved histone modification. *J Biol Chem,* 282**,** 7632-40.

NEWPORT, J. & DASSO, M. 1989. On the coupling between DNA replication and mitosis. *J Cell Sci Suppl,* 12**,** 149-60.

NEWPORT, J. & KIRSCHNER, M. 1982. A major developmental transition in early xenopus embryos: I. characterization and timing of cellular changes at the midblastula stage. *Cell,* 30**,** 675-686.

NEWPORT, J. W. & KIRSCHNER, M. W. 1984. Regulation of the cell cycle during early Xenopus development. *Cell,* 37**,** 731-742.

NICETTO, D., DONAHUE, G., JAIN, T., PENG, T., SIDOLI, S., SHENG, L., MONTAVON, T., BECKER, J. S., GRINDHEIM, J. M., BLAHNIK, K., GARCIA, B. A., TAN, K., BONASIO, R., JENUWEIN, T. & ZARET, K. S. 2019. H3K9me3-heterochromatin loss at protein-coding genes enables developmental lineage specification. *Science,* 363**,** 294-297.

NICETTO, D., HAHN, M., JUNG, J., SCHNEIDER, T. D., STRAUB, T., DAVID, R., SCHOTTA, G. & RUPP, R. A. 2013. Suv4-20h histone methyltransferases promote neuroectodermal differentiation by silencing the pluripotency-associated Oct-25 gene. *PLoS Genet,* 9**,** e1003188.

NICKLAY, J. J., SHECHTER, D., CHITTA, R. K., GARCIA, B. A., SHABANOWITZ, J., ALLIS, C. D. & HUNT, D. F. 2009. Analysis of histones in Xenopus laevis. II. mass spectrometry reveals an index of cell type-specific modifications on H3 and H4. *J Biol Chem,* 284**,** 1075-85.

NIEUWKOOP, P. D. & FABER, J. 1994. Normal Table of Xenopus laevis (Daudin). *Garland Publishing, Inc.*

NISHIOKA, K., CHUIKOV, S., SARMA, K., ERDJUMENT-BROMAGE, H., ALLIS, C. D., TEMPST, P. & REINBERG, D. 2002. Set9, a novel histone H3 methyltransferase that facilitates transcription by precluding histone tail modifications required for heterochromatin formation. *Genes Dev,* 16**,** 479-89.

NISHITANI, E., LI, C., LEE, J., HOTTA, H., KATAYAMA, Y., YAMAGUCHI, M. & KINOSHITA, T. 2015. Pou5f3.2-induced proliferative state of embryonic cells during gastrulation of Xenopus laevis embryo. *Dev Growth Differ,* 57**,** 591-600.

ODA, H., OKAMOTO, I., MURPHY, N., CHU, J., PRICE, S. M., SHEN, M. M., TORRES-PADILLA, M. E., HEARD, E. & REINBERG, D. 2009. Monomethylation of histone H4-lysine 20 is involved in chromosome structure and stability and is essential for mouse development. *Mol Cell Biol,* 29**,** 2278-95.

OTSUKI, L. & BRAND, A. H. 2018. Cell cycle heterogeneity directs the timing of neural stem cell activation from quiescence. *Science,* 360**,** 99-102.

PAN, C. & FAN, Y. 2016. Role of H1 linker histones in mammalian development and stem cell differentiation. *Biochim Biophys Acta,* 1859**,** 496-509.

PEARL, E. J., BILOGAN, C. K., MUKHI, S., BROWN, D. D. & HORB, M. E. 2009. Xenopus pancreas development. *Dev Dyn,* 238**,** 1271-86.

PERINO, M. & VEENSTRA, G. J. 2016. Chromatin Control of Developmental Dynamics and Plasticity. *Dev Cell,* 38**,** 610-20.

PESAVENTO, J. J., YANG, H., KELLEHER, N. L. & MIZZEN, C. A. 2008. Certain and progressive methylation of histone H4 at lysine 20 during the cell cycle. *Mol Cell Biol,* 28**,** 468-86.

POMBO, A. & DILLON, N. 2015. Three-dimensional genome architecture: players and mechanisms. *Nat Rev Mol Cell Biol,* 16**,** 245-57.

RAPPSILBER, J., MANN, M. & ISHIHAMA, Y. 2007. Protocol for micro-purification, enrichment, pre-fractionation and storage of peptides for proteomics using StageTips. *Nat Protoc,* 2**,** 1896-906.

REGGIANI, L., RACITI, D., AIRIK, R., KISPERT, A. & BRANDLI, A. W. 2007. The prepattern transcription factor Irx3 directs nephron segment identity. *Genes Dev,* 21**,** 2358-70.

RICHARD-PARPAILLON, L., COSGROVE, R. A., DEVINE, C., VERNON, A. E. & PHILPOTT, A. 2004. G1/S phase cyclin-dependent kinase overexpression perturbs early development and delays tissue-specific differentiation in Xenopus. *Development,* 131**,** 2577-86.

ROBERTS, A., SOFFE, S. R., WOLF, E. S., YOSHIDA, M. & ZHAO, F. Y. 1998. Central circuits controlling locomotion in young frog tadpoles. *Ann N Y Acad Sci,* 860**,** 19-34.

ROQUE, A., PONTE, I. & SUAU, P. 2016. Interplay between histone H1 structure and function. *Biochim Biophys Acta,* 1859**,** 444-54.

ROUGEULLE, C., CHAUMEIL, J., SARMA, K., ALLIS, C. D., REINBERG, D., AVNER, P. & HEARD, E. 2004. Differential histone H3 Lys-9 and Lys-27 methylation profiles on the X chromosome. *Mol Cell Biol,* 24**,** 5475-84.

RUDNICKI, M. A., SCHNEGELSBERG, P. N., STEAD, R. H., BRAUN, T., ARNOLD, H. H. & JAENISCH, R. 1993. MyoD or Myf-5 is required for the formation of skeletal muscle. *Cell,* 75**,** 1351-9.

SADAKIERSKA-CHUDY, A. & FILIP, M. 2014. A Comprehensive View of the Epigenetic Landscape. Part II: Histone Post-translational Modification, Nucleosome Level, and Chromatin Regulation by ncRNAs. *Neurotoxicity Research*.

SAKSOUK, N., SIMBOECK, E. & DEJARDIN, J. 2015. Constitutive heterochromatin formation and transcription in mammals. *Epigenetics Chromatin,* 8**,** 3.

SAWICKA, A. & SEISER, C. 2014. Sensing core histone phosphorylation - a matter of perfect timing. *Biochim Biophys Acta,* 1839**,** 711-8.

SCHMIDT, C. & URLAUB, H. 2017. Combining cryo-electron microscopy (cryo-EM) and cross-linking mass spectrometry (CX-MS) for structural elucidation of large protein assemblies. *Curr Opin Struct Biol,* 46**,** 157-168.

SCHNEIDER, R., BANNISTER, A. J., WEISE, C. & KOUZARIDES, T. 2004. Direct binding of INHAT to H3 tails disrupted by modifications. *J Biol Chem,* 279**,** 23859-62.

SCHNEIDER, T. D., ARTEAGA-SALAS, J. M., MENTELE, E., DAVID, R., NICETTO, D., IMHOF, A. & RUPP, R. A. W. 2011. Stage-Specific histone modification profiles reveal global transitions in the Xenopus embryonic epigenome. *PLoS ONE,* 6.

SCHOTTA, G., LACHNER, M., SARMA, K., EBERT, A., SENGUPTA, R., REUTER, G., REINBERG, D. & JENUWEIN, T. 2004. A silencing pathway to induce H3-K9 and H4-K20 trimethylation at constitutive heterochromatin. *Genes Dev,* 18**,** 1251-62.

SCHOTTA, G., SENGUPTA, R., KUBICEK, S., MALIN, S., KAUER, M., CALLEN, E., CELESTE, A., PAGANI, M., OPRAVIL, S., DE LA ROSA-VELAZQUEZ, I. A., ESPEJO, A., BEDFORD, M. T., NUSSENZWEIG, A., BUSSLINGER, M. & JENUWEIN, T. 2008. A chromatin-wide transition to H4K20 monomethylation impairs genome integrity and programmed DNA rearrangements in the mouse. *Genes Dev,* 22**,** 2048-61.

SCHUETTENGRUBER, B., BOURBON, H. M., DI CROCE, L. & CAVALLI, G. 2017. Genome Regulation by Polycomb and Trithorax: 70 Years and Counting. *Cell,* 171**,** 34-57.

SCHVARTZMAN, J. B., KRIMER, D. B. & VAN'T HOF, J. 1984. The effects of different thymidine concentrations on DNA replication in pea-root cells synchronized by a protracted 5-fluorodeoxyuridine treatment. *Exp Cell Res,* 150**,** 379-89.

SERRA-CARDONA, A. & ZHANG, Z. 2018. Replication-Coupled Nucleosome Assembly in the Passage of Epigenetic Information and Cell Identity. *Trends Biochem Sci,* 43**,** 136-148.

SHECHTER, D., NICKLAY, J. J., CHITTA, R. K., SHABANOWITZ, J., HUNT, D. F. & ALLIS, C. D. 2009. Analysis of histones in Xenopus laevis. I. A distinct index of enriched variants and modifications exists in each cell type and is remodeled during developmental transitions. *J Biol Chem,* 284**,** 1064-74.

SIMS, R. J., 3RD, BELOTSERKOVSKAYA, R. & REINBERG, D. 2004. Elongation by RNA polymerase II: the short and long of it. *Genes Dev,* 18**,** 2437-68.

SMITH, Z. D. & MEISSNER, A. 2013. DNA methylation: roles in mammalian development. *Nat Rev Genet,* 14**,** 204-20.

STALDER, J., LARSEN, A., ENGEL, J. D., DOLAN, M., GROUDINE, M. & WEINTRAUB, H. 1980. Tissue-specific DNA cleavages in the globin chromatin domain introduced by DNAase I. *Cell,* 20**,** 451-60.

STEGER, D. J., LEFTEROVA, M. I., YING, L., STONESTROM, A. J., SCHUPP, M., ZHUO, D., VAKOC, A. L., KIM, J. E., CHEN, J., LAZAR, M. A., BLOBEL, G. A. & VAKOC, C. R. 2008. DOT1L/KMT4 recruitment and H3K79 methylation are ubiquitously coupled with gene transcription in mammalian cells. *Mol Cell Biol,* 28**,** 2825-39.

STEINBACH, O. C., WOLFFE, A. P. & RUPP, R. A. 1997a. Somatic linker histones cause loss of mesodermal competence in Xenopus. *Nature,* 389**,** 395-9.

STEINBACH, O. C., WOLFFE, A. P. & RUPP, R. A. W. 1997b. Mesodermal competence in Xenopus is regulated by somatic linker histone variants. *Developmental Biology,* 186**,** B38-B38.

STRAHL, B. D. & ALLIS, C. D. 2000. The language of covalent histone modifications. *Nature,* 403**,** 41-5.

STUBBS, J. L., DAVIDSON, L., KELLER, R. & KINTNER, C. 2006. Radial intercalation of ciliated cells during Xenopus skin development. *Development,* 133**,** 2507-15.

SURANI, M. A., HAYASHI, K. & HAJKOVA, P. 2007. Genetic and epigenetic regulators of pluripotency. *Cell,* 128**,** 747-62.

TADROS, W. & LIPSHITZ, H. D. 2009. The maternal-to-zygotic transition: a play in two acts. *Development,* 136**,** 3033-42.

TAKAHASHI, K. & YAMANAKA, S. 2006. Induction of pluripotent stem cells from mouse embryonic and adult fibroblast cultures by defined factors. *Cell,* 126**,** 663-76.

TIE, F., BANERJEE, R., STRATTON, C. A., PRASAD-SINHA, J., STEPANIK, V., ZLOBIN, A., DIAZ, M. O., SCACHERI, P. C. & HARTE, P. J. 2009. CBP-mediated acetylation of histone H3 lysine 27 antagonizes Drosophila Polycomb silencing. *Development,* 136**,** 3131-41.

TONG, J., SUN, D., YANG, C., WANG, Y., SUN, S., LI, Q., BAO, J. & LIU, Y. 2016. Serum starvation and thymidine double blocking achieved efficient cell cycle synchronization and altered the expression of p27, p53, bcl-2 in canine breast cancer cells. *Res Vet Sci,* 105**,** 10-4.

TRIBULO, C., GUADALUPE BARRIONUEVO, M., AGUERO, T. H., SANCHEZ, S. S., CALCATERRA, N. B. & AYBAR, M. J. 2012. DeltaNp63 is regulated by BMP4 signaling and is required for early epidermal development in Xenopus. *Dev Dyn,* 241**,** 257-69.

TURNER, B. M. 1993. Decoding the nucleosome. *Cell,* 75**,** 5-8.

VAN DEN AKKER, E., FORLANI, S., CHAWENGSAKSOPHAK, K., DE GRAAFF, W., BECK, F., MEYER, B. I. & DESCHAMPS, J. 2002. Cdx1 and Cdx2 have overlapping functions in anteroposterior patterning and posterior axis elongation. *Development,* 129**,** 2181-93.

VAN HOOSER, A., GOODRICH, D. W., ALLIS, C. D., BRINKLEY, B. R. & MANCINI, M. A. 1998. Histone H3 phosphorylation is required for the initiation, but not maintenance, of mammalian chromosome condensation. *J Cell Sci,* 111 (Pt 23)**,** 3497-506.

VAN KRUIJSBERGEN, I., HONTELEZ, S., ELURBE, D. M., VAN HEERINGEN, S. J., HUYNEN, M. A. & VEENSTRA, G. J. C. 2017. Heterochromatic histone modifications at transposons in Xenopus tropicalis embryos. *Dev Biol,* 426**,** 460-471.

VAN STEENSEL, B. 2011. Chromatin: Constructing the big picture. *EMBO Journal,* 30**,** 1885-1895.

VASTENHOUW, N. L., ZHANG, Y., WOODS, I. G., IMAM, F., REGEV, A., LIU, X. S., RINN, J. & SCHIER, A. F. 2010. Chromatin signature of embryonic pluripotency is established during genome activation. *Nature,* 464**,** 922-926.

VERMAAK, D., STEINBACH, O. C., DIMITROV, S., RUPP, R. A. & WOLFFE, A. P. 1998. The globular domain of histone H1 is sufficient to direct specific gene repression in early Xenopus embryos. *Curr Biol,* 8**,** 533-6.

VILLAR-GAREA, A., FORNE, I., VETTER, I., KREMMER, E., THOMAE, A. & IMHOF, A. 2012. Developmental regulation of N-terminal H2B methylation in Drosophila melanogaster. *Nucleic Acids Res,* 40**,** 1536-49.

VILLAR-GAREA, A., ISRAEL, L. & IMHOF, A. 2008. Analysis of histone modifications by mass spectrometry. *Curr Protoc Protein Sci,* Chapter 14**,** Unit 14 10.

VOIGT, P., TEE, W. W. & REINBERG, D. 2013. A double take on bivalent promoters. *Genes Dev,* 27**,** 1318-38.

WADDINGTON, C. H. 1957. *The Strategy of the Genes: A Discussion of Some Aspects of Theoretical Biology,* London, George Allen & Unwin Ltd.

WAGNER, D. E., WEINREB, C., COLLINS, Z. M., BRIGGS, J. A., MEGASON, S. G. & KLEIN, A. M. 2018. Single-cell mapping of gene expression landscapes and lineage in the zebrafish embryo. *Science,* 360**,** 981-987.

WANG, F. & HIGGINS, J. M. 2013. Histone modifications and mitosis: countermarks, landmarks, and bookmarks. *Trends Cell Biol,* 23**,** 175-84.

WANG, J., LIN, X., WANG, S., WANG, C., WANG, Q., DUAN, X., LU, P., WANG, Q., WANG, C., LIU, X. S. & HUANG, J. 2014. PHF8 and REST/NRSF co-occupy gene promoters to regulate proximal gene expression. *Sci Rep,* 4**,** 5008.

WANG, L., JOSHI, P., MILLER, E. L., HIGGINS, L., SLATTERY, M. & SIMON, J. A. 2018. A Role for Monomethylation of Histone H3-K27 in Gene Activity in Drosophila. *Genetics,* 208**,** 1023-1036.

WANG, Z., ZANG, C., ROSENFELD, J. A., SCHONES, D. E., BARSKI, A., CUDDAPAH, S., CUI, K., ROH, T. Y., PENG, W., ZHANG, M. Q. & ZHAO, K. 2008. Combinatorial patterns of histone acetylations and methylations in the human genome. *Nat Genet,* 40**,** 897-903.

WEINTRAUB, H., DAVIS, R., TAPSCOTT, S., THAYER, M., KRAUSE, M., BENEZRA, R., BLACKWELL, T. K., TURNER, D., RUPP, R., HOLLENBERG, S. & ET AL. 1991. The myoD gene family: nodal point during specification of the muscle cell lineage. *Science,* 251**,** 761-6.

WU, C., BINGHAM, P. M., LIVAK, K. J., HOLMGREN, R. & ELGIN, S. C. 1979. The chromatin structure of specific genes: I. Evidence for higher order domains of defined DNA sequence. *Cell,* 16**,** 797-806.

WU, S. & RICE, J. C. 2011. A new regulator of the cell cycle: the PR-Set7 histone methyltransferase. *Cell Cycle,* 10**,** 68-72.

XUE, K., SONG, J., WEI, H., CHEN, L., MA, Y., LIU, S., LI, Y., DAI, Y., ZHAO, Y. & LI, N. 2010. Synchronous behaviors of CBP and acetylations of lysine 18 and lysine 23 on histone H3 during porcine oocyte first meiotic division. *Mol Reprod Dev,* 77**,** 605-14.

YANG, P., WU, W. & MACFARLAN, T. S. 2015. Maternal histone variants and their chaperones promote paternal genome activation and boost somatic cell reprogramming. *Bioessays,* 37**,** 52-9.

ZHANG, R., ERLER, J. & LANGOWSKI, J. 2017. Histone Acetylation Regulates Chromatin Accessibility: Role of H4K16 in Inter-nucleosome Interaction. *Biophys J,* 112**,** 450-459.

Acknowledgements

I would like to express my deepest gratitude to Ralph Rupp, Axel Imhof, Ignasi Forné Anne-Kathrin Classen, Peter Becker and Viktoria Korzhova. Ralph, being a group leader of the lab, has helped me a lot in the project development, generating new cool ideas and keeping the lab spirit and enthusiasm up. Axel and Ignasi have invested a lot of time and effort teaching me the mass spec magic. Together with my native Russian magic it turned out very well. Anne was a group leader in the lab where I did a summer school practice in 2012. That time was a milestone for me which showed the bright side of the wet-lab work and reassured my intention to do a PhD. Peter established the fist connection between Ralph and me, basically opening the door to the LMU. Vika has supported me during the whole PhD life and more. She was there when it was needed and always knew when to help and when not to disturb.

A huge portion of thankfulness goes to the current and former lab members: Edith Mentele, Barbara Hölscher, Gabriele Wagner, Alessandro Angerilli, Julian Berges and Claudia Rauch. They have taught and helped me a lot during the work time, and we shared a lot of fun outside of the lab.

Special thanks go to the BMC coffee group: Andrea Lukacs, Magdalini Serefidou, Lisa Harpprecht, Irina Shcherbakova, Nadiya Prayitno, Belén Casalini, Rodaria Roussou, Sophia Groh and all others. Thank you for the lunches, coffees, international dinners, “thank God, it´s Friday” and cocktail parties.

Особая благодарность (по-русски) Русскому ланчу. Женя, Андрей, Варя, Илья, Даша, Артём и все-все-все, спасибо большое за весёлые обеды, поддержку и сохранение языка на рабочем уровне.

Finita la comedia.